Quantum Monte Carlo Methods on Lattices: The Determinantal Approach

Fakher F. Assaad

Quantum Monte Carlo Methods on Lattices: The Determinantal Approach

Fakher F. Assaad

[1] Institut für Theoretische Physik III, Universität Stuttgart
Pfaffenwaldring 57, 70550 Stuttgart, Germany

[2] Max Planck Institute for Solid State Research
Heisenbergstr. 1, 70569, Stuttgart, Germany
E-mail: assaad@theo3.physik.uni-stuttgart.de

We present a review of the auxiliary field (i.e. determinantal) Quantum Monte Carlo method applied to various problems of correlated electron systems. The ground state projector method, the finite temperature approach as well as the Hirsch-Fye impurity algorithm are described in details. It is shown how to apply those methods to a variety of models: Hubbard Hamiltonians, periodic Anderson model, Kondo lattice and impurity problems, as well as hard core bosons and the Heisenberg model. An introduction to the world-line method with loop upgrades as well as an appendix on the Monte Carlo method is provided.

1   Introduction

The correlated electron problem remains one of the central challenges in solid state physics. Given the complexity of the problem numerical simulations provide an essential source of information to test ideas and develop intuition. In particular for a given model describing a particular material we would ultimately like to be able to carry out efficient numerical simulations so as to provide *exact* results on thermodynamic, dynamical, transport and ground state properties. If the model shows a continuous quantum phase transition we would like to characterize it by computing the critical exponents. Without restriction on the type of model, this is an extremely challenging goal.

The are however a set of problems for which numerical techniques have and will provided invaluable insight. Here we list a few which are *exact*, capable of reaching large system sizes (the computational effort scales as a power of the volume), and provide ground state, dynamical as well as thermodynamic quantities. i) Density matrix renormalization group applied to general one-dimensional systems[1] ii) world-line loop Quantum Monte Carlo (QMC) applied to non-frustrated spin systems in arbitrary dimensions[2] and iii) auxiliary field QMC methods[3]. The latter method is the only algorithm capable of handling a class of models with spin and charge degrees of freedom in dimensions larger than unity. This class contains fermionic lattice models with an attractive interactions (e.g. attractive Hubbard model), models invariant under a particle-hole transformation, as well as impurity problems modeled by Kondo or Anderson Hamiltonians.

Here we will concentrate primarily on the auxiliary field QMC method and introduce briefly the world line method with loop updates. Both algorithms are based on a path integral formulation of the imaginary time propagator which maps a d-dimensional quantum system on a $d + 1$-dimensional classical system. The additional dimension is nothing but the imaginary time. For example, within the World Line QMC algorithm[4], this mapping

relates the one-dimensional XYZ quantum spin chain to an eight vertex model[5] or the one-dimensional t-J model to the 15-vertex model[6]. The classical models may then be solved exactly as in the case of the eight vertex model[7] or simulated very efficiently by means of cluster Monte Carlo methods[2]. The latter approach has proved to be extremely efficient for the investigation of non-frustrated quantum spin systems[8] in arbitrary dimensions. The efficiency lies in the fact that i) the computational time scales as the volume of the $d+1$ dimensional classical system so that very large system sizes may be achieved and ii) the autocorrelation times are small. In the next section we will briefly, by way of introduction, review the World Line approach and thereby show how the XXZ chain maps onto the 6-vertex model. The attractive feature of the World Line approach is it's simplicity. It will also allow us to aquire some insight into the so called sign problem. This is a major, open, issue in QMC methods applied to correlated systems. When it occurs the computational effort scales exponentially with system size and inverse temperature.

In spacial dimensions larger than unity, the World Line approach often fails (i.e. the occurrence of a sign problem) already at the *mean-field* level. That is: consider the paramagnetic mean-field solution of the two dimensional Hubbard model which boils down to solving a free electron problem in a tight binding approximation. This simple model, already leads to a severe sign problem when formulated within the World Line approach. The auxiliary field QMC method[3] relies on a different formulation which solves the mean-field problem exactly. With the use of a Hubbard Stratonovich transformation the partition function of a Hamiltonian H at temperature $T = 1/\beta$ and chemical potential μ is written as:

$$Z = \text{Tr}\left[e^{-\beta(H-\mu N)}\right] = \int D\Phi e^{-S(\Phi)}. \tag{1}$$

$S(\Phi)$ is the action of a one-body problem in a imaginary time and space dependent field Φ. As we will see for a given field Φ the computational cost required to compute the action scales as the product of the volume to the cubed and inverse temperature. [a] The functional integral is carried by means of Monte Carlo sampling. In this approach the mean-field solution is given by the saddle point approximation: the functional integral over Φ is replaced by a single field Φ^* for which $\left.\frac{\partial S(\Phi)}{\partial \Phi}\right|_{\Phi=\Phi^*} = 0$. The nature of the mean-field solution depends on the choice of the Hubbard Stratonovich decoupling. Thus, in the auxiliary field QMC mean-field Hamiltonians are solved exactly, the price being the above mentioned scaling of the computational effort. In the above framework, the Monte Carlo integration over the field Φ may be seen as a means of taking into account all fluctuations around the mean-field solution. This will in many cases introduce a sign problem. Nevertheless the method has the advantage that symmetries of the model, such as particle-hole symmetry, may be put to use to avoid the sign problem in many non-trivial cases. Other classes of models where the sign problem does not occur include models with attractive interactions which couple independently to an internal symmetry with an even number of states. The attractive Hubbard model is a member of this class. It is also worth mentioning that when the sign problem occurs in the auxiliary field QMC it is often less severe than in World Line approach so that at least high temperature properties may be investigated.

---

[a] For the Hirsch-Fye impurity algorithm computational effort scales as the cubed of the inverse temperature.

The auxiliary field quantum Monte-Carlo method is the central topic of this article. In section 3 we will review in all details both the finite temperature[9–11] and ground state[12–14] formulation of the method. The application of the method to various models (Hubbard model, periodic Anderson model, Kondo lattice model, hard core boson systems and Heisenberg models) will be discussed in section 4. Since the computational effort scales as the cube of the volume, it is important to control size effects. A simple method to reduce size effects by an order of magnitude in temperature will also be discussed in section 4. In section 5 we review a very much related algorithm, the Hirsch-Fye impurity algorithm, which has been used extensively in the context of dynamical mean-field theories[15,16]. We will apply this algorithm to the single impurity Kondo problem.

Finally, we provide an Appendix for the Monte Carlo method and error analysis.

2   The World Line Approach for the XXZ Model and Relation to the 6-Vertex Model

To illustrate with on a simple example the World Line quantum Monte Carlo method, we consider the XXZ quantum spin chain defined as:

$$H = J_X \sum_i \left(S_i^x S_{i+1}^x + S_i^y S_{i+1}^y \right) + J_Z \sum_i S_i^z S_{i+1}^z \tag{2}$$

where $\vec{S}_i$ are the spin $1/2$ operators on site i satisfying the commutation relations:

$$\left[S_i^\eta, S_j^\nu \right] = \delta_{i,j} i \epsilon^{\eta,\nu,\gamma} S_i^\gamma. \tag{3}$$

In the above, $\epsilon^{\eta,\nu,\gamma}$ is the antisymmetric tensor and the sum over repeated indices is understood. Our aim is to compute observables:

$$\langle O \rangle = \frac{\mathrm{Tr}\left[e^{-\beta H} O \right]}{\mathrm{Tr}\left[e^{-\beta H} \right]}. \tag{4}$$

The basic idea of the World Line algorithm is to split the above Hamiltonian into a set of independent - in this case - two site problems. The way to achieve this decoupling is with the use of a path integral and the Trotter decomposition. First we write

$$H = \underbrace{\sum_n H^{(2n+1)}}_{H_1} + \underbrace{\sum_n H^{(2n+2)}}_{H_2} \tag{5}$$

with

$$H^{(i)} = J_X \left(S_i^x S_{i+1}^x + S_i^y S_{i+1}^y \right) + J_Z S_i^z S_{i+1}^z$$

One may verify that H_1 and H_2 are sums of commuting (i.e. independent) two site problems. Hence, on their own H_1 and H_2 are trivially solvable problems. However, H is not.

To put to use this fact, we wish split the imaginary propagation $e^{-\beta H}$ into successive infinitesimal propagations of H_1 and H_2. This is achieved with the Trotter decomposition[17]:

$$\left(e^{-\Delta\tau H_1}e^{-\Delta\tau H_2}\right)^m = \left(e^{-\Delta\tau H} + \frac{\Delta\tau^2}{2}[H_1, H_2] + \mathcal{O}(\Delta\tau^3)\right)^m \tag{6}$$

$$= \left(e^{-\Delta\tau(H-\Delta\tau[H_1,H_2]/2)} + O(\Delta\tau^3)\right)^m = e^{-\beta(H-\Delta\tau[H_1,H_2]/2)} + \mathcal{O}(\Delta\tau^2)$$

$$= e^{-\beta H} + \frac{\Delta\tau}{2}\int_0^\beta d\tau e^{-(\beta-\tau)H}[H_1, H_2]e^{-\tau H} + \mathcal{O}(\Delta\tau^2)$$

where $m\Delta\tau = \beta$ and $\mathcal{O}(\Delta\tau^n)$ means that for fixed values of β the error scales as $\Delta\tau^n$. In many cases, we will not take the limit $\Delta\tau \to 0$ and is important to understand the order of the systematic error produced by the above decomposition. [b] A priori, it is of the oder $\Delta\tau$. However, in many non-trivial cases, the prefactor of the error of order $\Delta\tau$ vanishes. In the World line approach we compute:

$$\frac{\mathrm{Tr}\left[\left(e^{-\Delta\tau H_1}e^{-\Delta\tau H_2}\right)^m O\right]}{\mathrm{Tr}\left[\left(e^{-\Delta\tau H_1}e^{-\Delta\tau H_2}\right)^m\right]} = \frac{\mathrm{Tr}\left[e^{-\beta H}O\right] + \frac{\Delta\tau}{2}\mathrm{Tr}\left[AO\right]}{\mathrm{Tr}\left[e^{-\beta H}\right] + \frac{\Delta\tau}{2}\mathrm{Tr}\left[A\right]} + O(\Delta\tau^2). \tag{7}$$

Here $A = \int_0^\beta d\tau e^{-(\beta-\tau)H}[H_1, H_2]e^{-\tau H}$ and $m\Delta\tau = \beta$. Since A is an antihermetian operator, $A^\dagger = -A$, it follows that $\overline{\mathrm{Tr}\left[A\right]} = \mathrm{Tr}\left[A^\dagger\right] = -\mathrm{Tr}\left[A\right]$ as well as $\overline{\mathrm{Tr}\left[AO\right]} = -\mathrm{Tr}\left[AO\right]$. Note that the observable O is a hermitian operator. Thus, if O, H_1 and H_2 are simultaneously real representable in a given basis, the systematic error proportional to $\Delta\tau$ vanishes since in this case the trace is real. Hence the systematic error is of order $\Delta\tau^2$.

With the above, the estimation of the partition function reads:

$$\mathrm{Tr}\left[e^{-\beta H}\right] = \mathrm{Tr}\left[\left(e^{-\Delta\tau H}\right)^m\right] = \mathrm{Tr}\left[\left(e^{-\Delta\tau H_1}e^{-\Delta\tau H_2}\right)^m\right] + \mathcal{O}(\Delta\tau^2) = \tag{8}$$

$$\sum_{n_1\cdots n_{2m}} \langle n_1|e^{-\Delta\tau H_1}|n_{2m}\rangle \cdots \langle n_3|e^{-\Delta\tau H_1}|n_2\rangle\langle n_2|e^{-\Delta\tau H_2}|n_1\rangle + \mathcal{O}(\Delta\tau^2)$$

where $m\Delta\tau = \beta$ and the states $|n_\tau\rangle$ span the Hilbert space. We choose the states $|n_\tau\rangle$ to be eigenstates of S_i^z. For each set of states $|n_1\rangle \cdots |n_{2m}\rangle$ with non-vanishing contribution to the partition function we have a simple graphical representation in terms of world lines as shown in Fig. 1. Observables are now given by:

$$\langle O\rangle = \frac{\sum_w \Omega(w)O(w)}{\sum_w \Omega(w)} \tag{9}$$

where $\Omega(w)$ corresponds to the weight of a given world line configuration as obtained through multiplication of the weights of the individual plaquettes listed in Fig. 1. Note that although spin-flip processes have negative weight, no sign problem occurs. One can for example carry out the transformation: $S_i^x \to (-1)^i S_i^x, S_i^y \to (-1)^i S_i^y, S_i^z \to S_i^z$ which leaves the commutations relation unaltered (i.e. is canonical) but changes the sign of J_x. Observables O which locally conserve the z-component of the spin are easy to compute. If we decide to measure on time slice τ then $O|n_\tau\rangle = O(w)|n_\tau\rangle$. [c]

---

[b]Within the loop algorithm a continuous time formulation may be achieved[18]
[c]In practice, one will measure on all time slices so as to reduce statistical fluctuations
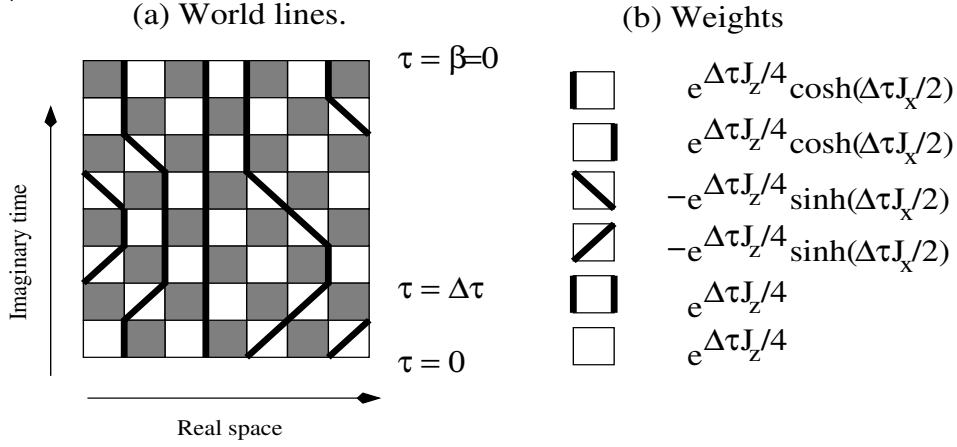
(a) World lines. (b) Weights

Figure 1. (a) World line configuration for the XXZ model of Eq. (2). Here, $m = 4$ and the system size is $L = 8$. The bold lines follow the time evolution of the up spins and empty sites, with respect to the world lines, correspond to the down spins. A full time step $\Delta\tau$ corresponds to the propagation with H_1 followed by H_2. Periodic boundary conditions are chosen in the spacial direction. In the time direction, periodic boundary conditions follow from the fact that we are evaluating a trace. (b) The weights for a given world line configuration is the product of the weights of plaquettes listed in the figure. Note that, although the spin-flip processes come with a minus sign the overall weight for the world line configuration is positive since each world line configuration contains an even number of spin flips.
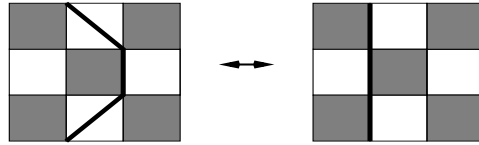

Figure 2. Local updates. A shaded plaquette is chosen randomly and a Word Line is shifted from left to right or vice versa across the shaded plaquette.

The problem is now cast into one which may be solved with classical Monte Carlo methods (see Appendix). To generate a Markov chain through the space of World Lines we need to devise an updating mechanism. Local updates where one locally deforms a World Line configuration have been used successfully (see Fig. 2). The local updates conserve the z-component of the total spin (i.e. canonical in the hard core boson notation introduced in Section 4.4) and are ergodic only in the case of open boundary conditions. Choosing periodic boundary conditions and starting with a configuration with zero winding one will remain in this sector. That is: the configuration of Fig. 4e will not be generated starting from the configuration of Fig. 4a with local updates. Note however, that this is a boundary problem so that when the thermodynamic limit is taken with the above local updates the correct thermodynamic result is obtained[6].

That the XXZ quantum spin chain is equivalent to the classical two-dimensional 6-vertex model follows from a one to one mapping of a World Line configuration to one of the 6-vertex model. The identification of single plaquettes is shown in Fig. 3(a). The
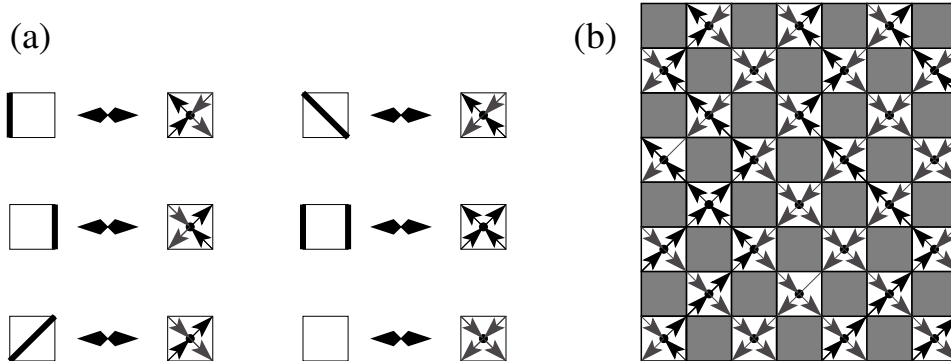
Figure 3. (a) Identification of world lines configurations on plaquettes with the vertices of the 6-vertex model. (b) The World Line configuration of Fig. 1 in the language of the 6-vertex model.

world line configuration of Fig. 1 is plotted in the language of the 6-vertex mode in Fig. 3(b). The vertex model lies on a 45 degrees rotated lattice denoted by bullets in Fig. 1(b). At each vertex (bullets in Fig. 1(b)) the number of incoming arrows equals the number of outgoing arrows. In the case of the XYZ chain, source and drain terms have to be added to yield the 8-vertex model.

The identification of the XXZ model to the 6-vertex model gives us an intuitive picture of loop upgrades[2]. Consider the World Line configuration in Fig.4a and it's corresponding vertex formulation (Fig.4b). One can pick a palquette at random and follow the arrows of the vertex configuration. At each plaquette there are two possible arrow paths to follow. One is chosen, appropriately, and the arrows are followed to arrive to the next plaquette. The procedure is then repeated until one returns to the starting point. Such a loop is shown in Fig. 4c. Along the loop, changing the direction of the arrows generates another valid vertex configuration (see Fig. 4d). The corresponding World Line configuration (after *flipping* the loop) is shown in Fig. 4e. As apparent, this is a global update which changes the winding number and is not achievable with local moves. To gain further insight into the loop algorithm the reader is referred to the review article of H.G. Evertz[19] and references therein. Let us however mention that the loop algorithm has been applied with great success to non-frustrated spin systems. Critical exponents of the order-disorder transition for a two dimensional depleted Heisenberg model were pinned down to show that the transition belongs to the universality class of the three dimensional classical $O(3)$ model[8]. Furthermore this algorithm has been used to study single particle dynamics in non-frustrated quantum antiferromagnets on various topologies[20,21].

2.1 The Sign Problem in the World Line Approach

The Quantum Monte Carlo approach is often plagued by the so-called sign problem. Since the origin of this problem is easily understood in the framework of the World Line algorithm we will briefly discuss it in this section on a specific model. Consider spinless
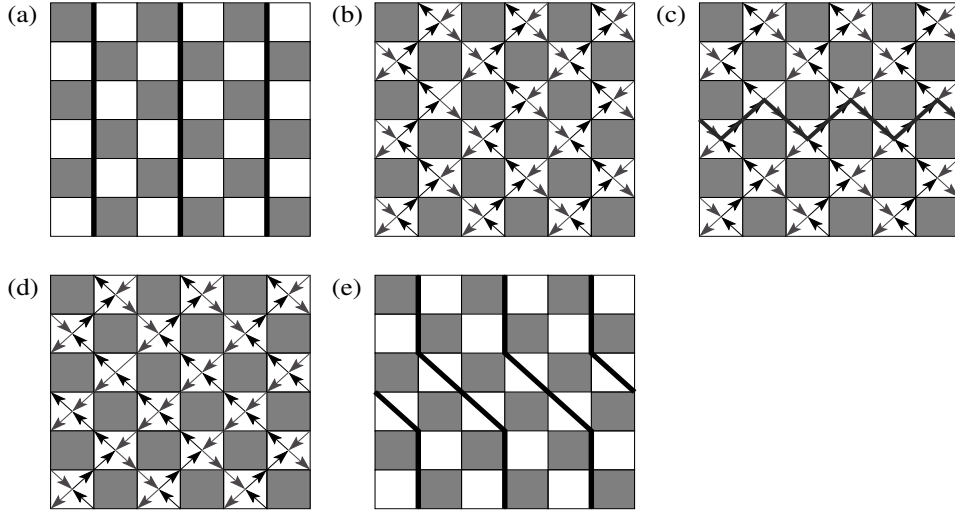
104

Figure 4. Example of a loop update.

electrons on an L-site linear chain

$$H = -t \sum_i c_i^\dagger (c_{i+1} + c_{i+2}) + \text{H.c.} \quad \text{with} \quad \left\{ c_i^\dagger, c_j^\dagger \right\} = \left\{ c_i, c_j \right\} = 0, \left\{ c_i^\dagger, c_j \right\} = \delta_{i,j}.$$
(10)

Here, we consider periodic boundary conditions, $c_{i+L} = c_i$ and $t > 0$. To apply the World Line algorithm to the above Hamiltonian we split it into a set of independent four site problems:

$$H = \underbrace{\sum_{n=0}^{L/4-1} H^{(4n+1)}}_{H_1} + \underbrace{\sum_{n=0}^{L/4-1} H^{(4n+3)}}_{H_2}$$
(11)

with

$$H^{(i)} = -t c_i^\dagger \left(\frac{1}{2} c_{i+1} + c_{i+2} \right) - t c_{i+1}^\dagger (c_{i+2} + c_{i+3}) - \frac{t}{2} c_{i+2}^\dagger c_{i+3} + \text{H.c.}$$

With this decomposition one obtains the graphical representation of Fig. 5.[22].

The sign problem occurs from the fact that the weights $\Omega(w)$ are not necessarily positive. An example is shown in Fig. 10. In this case the origin of negative signs lies in Fermi statistics. To *solve* the problem, one decides to carry out the sampling with an auxiliary probability distribution:

$$\overline{Pr}(\omega) = \frac{|\Omega(w)|}{\sum_w |\Omega(w)|}$$
(12)

which in the limit of small values of $\Delta\tau$ corresponds to the partition function of the Hamiltonian of Eq. (10) but with fermions replaced by hard-core bosons. Thus, we can now
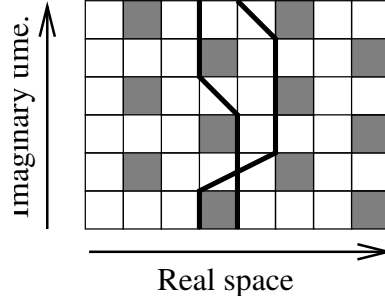
Figure 5. World line configuration for the model of Eq. (10). Here, $m = 3$. Since the two electrons exchange their positions during the imaginary time propagation, this world line configuration has a negative weight.

evaluate Eq. 9 with:

$$\langle O \rangle = \frac{\sum_w \overline{Pr}(\omega)\text{sign}(w)O(w)}{\sum_w \overline{Pr}(\omega)\text{sign}(w)} \tag{13}$$

where both the numerator and denominator are evaluated with MC methods. Let us first consider the denominator:

$$\langle \text{sign} \rangle = \sum_w \overline{Pr}(\omega)\text{sign}(w) = \frac{\sum_w \Omega(w)}{\sum_w |\Omega(w)|} = \frac{\text{Tr}\left[e^{-\beta H}\right]}{\text{Tr}\left[e^{-\beta H_B}\right]} \tag{14}$$

Here, H_B corresponds to the Hamiltonian of Eq. (10) but with fermions replaced by hard-core bosons. In the limit of large inverse temperatures, β, the partition functions is dominated by the ground state. Thus in this limit

$$\langle \text{sign} \rangle \sim e^{-\beta\left(E_0 - E_0^B\right)} = e^{-\beta L \Delta} \tag{15}$$

where $\Delta = \left(E_0 - E_0^B\right)/L$ is an intensive, in general positive, quantity. The above equation corresponds to the sign problem. When the temperature is small or system size large, the average sign becomes exponentially small. Hence, the observable $\langle O \rangle$ is given by the quotient of two exponentially small values which are determined stochastically. When the error-bars become comparable to the average sign, uncontrolled fluctuations in the evaluation of $\langle O \rangle$ will occur. Two comments are in order. (i) In this simple example the sign problem occurs due to Fermi statistics. However, sign problems occur equally in frustrated spin-1/2 systems which are nothing but hard core boson models. Note that replacing the fermions by hard core bosons in Eq. (10) and considering hopping matrix elements of different signs between nearest and next nearest neighbors will generate a sign problem in the above formulation. (ii) The sign problem is formulation dependent. In the World Line algorithm, we decide to work in real space. Had we chosen Fourier space, the Hamiltonian would have been diagonal and hence no sign problem occurs. In the auxiliary field approach discussed in the next section the sign problem would not occur for this non-interacting problem since as mentioned in the introduction one body operators are treated exactly. That is, the sum over all World Lines is carried out exactly.

3 Auxiliary Field Quantum Monte Carlo Algorithms

In the remaining, we will concentrate on auxiliary field Quantum Monte Carlo algorithms which we will describe in detail. Consider the Hamiltonian

$$H = H_t + H_I \tag{16}$$

where H_t is the kinetic energy and H_I a two-body interaction term. The ground state expectation value of an observable O is at best obtained by projecting a trial wave function $|\Psi_T\rangle$ along the imaginary time axis:

$$\frac{\langle\Psi_0|O|\Psi_0\rangle}{\langle\Psi_0|\Psi_0\rangle} = \lim_{\Theta\to\infty}\frac{\langle\Psi_T|e^{-\Theta H}Oe^{-\Theta H}|\Psi_T\rangle}{\langle\Psi_T|e^{-2\Theta H}|\Psi_T\rangle}. \tag{17}$$

The above equation is readily verified by writing $|\Psi_T\rangle = \sum_n|\Psi_n\rangle\langle\Psi_n|\Psi_0\rangle$ with $H|\Psi_n\rangle = E_n|\Psi_n\rangle$. The assumptions that $\langle\Psi_T|\Psi_0\rangle \neq 0$ and that the ground state is non-degenerate are however required. The algorithm based on Eq. (17) is known as the projector quantum Monte Carlo (PQMC) algorithm[12–14].

Finite temperature properties in the grand canonical ensemble are obtained by evaluating

$$\langle O\rangle = \frac{\mathrm{Tr}\left[e^{-\beta(H-\mu N)}O\right]}{\mathrm{Tr}\left[e^{-\beta(H-\mu N)}\right]} \tag{18}$$

where the trace runs over the Fock space, $\beta = 1/k_B T$ and μ is the chemical potential. The algorithm based on Eq. (18) will be referred to as finite temperature QMC (FTQMC) method[9, 10]. Comparison of both algorithms are shown in Fig. (6) for the Hubbard model in standard notation.

$$H_U = -t\sum_{\langle\vec{i},\vec{j}\rangle,\sigma}e^{\frac{2\pi i}{\Phi_0}\int_{\vec{i}}^{\vec{j}}\vec{A}\cdot d\vec{l}}c^\dagger_{\vec{i},\sigma}c_{\vec{j},\sigma} + U\sum_{\vec{i}}n_{\vec{i},\uparrow}n_{\vec{i},\downarrow}. \tag{19}$$

Here, and for future use, we have included a magnetic field $\vec{B} = \nabla\times\vec{A}$. At half-filling, the ground state is insulating so that charge fluctuations are absent in the low temperature limit on finite lattices. Hence, in this limit both grand canonical and canonical approaches yield identical results. It is however clear that if one is interested solely in ground state properties the PQMC is more efficient. As we will see, this lies in the choice of the trial wave function which is chosen to be a spin singlet.

3.1 Trotter Decomposition and Hubbard Stratonovich Transformation

As in the World Line approach we wish to evaluate the imaginary time propagation which we will split into infenitesimal successive propagations with H_t followed by H_I. This is again achieved with the Trotter decomposition

$$\left(e^{-\Delta\tau H_I}e^{-\Delta\tau H_t}\right)^m = e^{-\Theta H} + \frac{\Delta\tau}{2}\int_0^\Theta d\tau e^{-(\Theta-\tau)H}[H_I,H_t]e^{-\tau H} + \mathcal{O}(\Delta\tau^2) \tag{20}$$

or a symmetric variant

$$\left(e^{-\Delta\tau H_t/2}e^{-\Delta\tau H_I}e^{-\Delta\tau H_t/2}\right)^m = e^{-\Theta H} + \mathcal{O}(\Delta\tau^2) \tag{21}$$
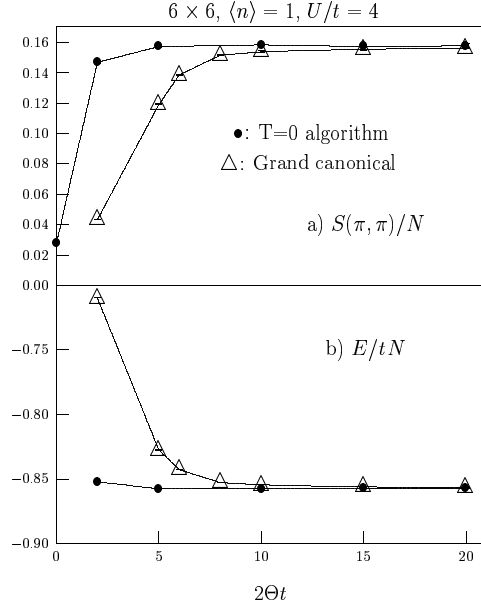
Figure 6. Fourier transform of the spin-spin correlation functions at $\vec{Q} = (\pi, \pi)$ (a) and energy (b) for the half-filled Hubbard model in the absence of magnetic field (19). ●: PQMC algorithm. △: FTQMC algorithm at $\beta = 2\Theta$.

where $m\Delta\tau = \Theta$. As mentioned previously and for the FTQMC if O, H_I and H_t are simultaneously real representable in a given basis, the systematic error proportional to $\Delta\tau$ in Eq. (20) vanishes. To achieve this in the PQMC some care has to be taken. To reduce fluctuations one wishes to measure an observable over several time slices. In the QMC evaluation of O based on the Trotter decomposition of Eq. (20) we hence compute:

$$\frac{1}{2N+1} \sum_{n=-N}^{N} \frac{\langle\Psi_T| \left(e^{-\Delta\tau H_I}e^{-\Delta\tau H_t}\right)^{m-n} O \left(e^{-\Delta\tau H_I}e^{-\Delta\tau H_t}\right)^{m+n} |\Psi_T\rangle}{\langle\Psi_T| \left(e^{-\Delta\tau H_I}e^{-\Delta\tau H_t}\right)^{2m} |\Psi_T\rangle}. \quad (22)$$

If $[O, H] = 0$, then one can set $N = m$ and the effective projection parameter is 2Θ. On the other hand, if $[O, H] \neq 0$ one has to choose $N < m$ since the effective projection parameter is $(m-N)\Delta\tau$. It is however crucial to measure symmetrically around the central time slice, since only then can show that the systematic error proportional to $\Delta\tau$ vanishes. This is of course valid provided that O, H_I, H_t as well as $|\Psi_T\rangle$ are simultaneously real representable.

Fig. 7 compares both choices of Trotter decompositions (Eqn. (20) and (21)) for the Hubbard model of Eq. (19). Here we use the PQMC algorithm. As apparent the symmetric decomposition of Eq. (21) is much more accurate and due to the variational principle provides an upper bound to the exact energy. It is however often cumbersome to implement.

Having isolated the interaction term H_I with the Trotter decomposition, we may now proceed with the Hubbard-Stratonovich (HS) transformation. The choice of the HS is
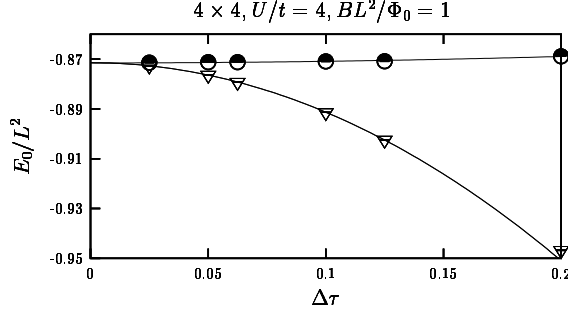
Figure 7. Ground state energy of the Half-filled Hubbard model on a 4×4 lattice, $U/t = 4$, $\langle n \rangle = 1$ and $BL^2/\Phi_0 = 1$ as a function of $\Delta\tau$ as obtained with the PQMC. The Trotter decompositions of Eqn. (20) ($\bigtriangledown$) and (21) ($\bigcirc$) are considered. Note that due to the variational principle the the Trotter decomposition of Eq. (21) yields an upper bound to the energy. The solid lines correspond to least square fits to the form $a + b\Delta\tau^2$.

important. For Hubbard interactions,

$$H_I = U \sum_{\vec{i}} \left(n_{\vec{i},\uparrow} - 1/2 \right) \left(n_{\vec{i},\downarrow} - 1/2 \right), \tag{23}$$

with $U > 0$ one usually chooses Hirsch's discrete transformation[23]

$$\exp\left(-\Delta\tau U \sum_{\vec{i}} \left(n_{\vec{i},\uparrow} - 1/2 \right) \left(n_{\vec{i},\downarrow} - 1/2 \right) \right) \tag{24}$$

$$= \tilde{C} \sum_{s_1,\dots,s_N = \pm 1} \exp\left(\tilde{\alpha} \sum_{\vec{i}} s_{\vec{i}} \left(n_{\vec{i},\uparrow} - n_{\vec{i},\downarrow} \right) \right).$$

where $\cosh(\tilde{\alpha}) = \exp\left(\Delta\tau U/2 \right)$. On an N-site lattice, the constant $\tilde{C} = \exp\left(\Delta\tau U N/4 \right)/2^N$. As apparent from the above equation, for a fixed set of HS fields, $s_1 \dots s_N$, $SU(2)$-spin symmetry is broken since the field couples to the z-component of the magnetization. This symmetry is of course restored after summation over the HS fields with the Monte Carlo method. Alternatively, one may consider[23]

$$\exp\left(-\Delta\tau U \sum_{\vec{i}} \left(n_{\vec{i},\uparrow} - 1/2 \right) \left(n_{\vec{i},\downarrow} - 1/2 \right) \right) \tag{25}$$

$$= C \sum_{s_1,\dots,s_N = \pm 1} \exp\left(i\alpha \sum_{\vec{i}} s_{\vec{i}} \left(n_{\vec{i},\uparrow} + n_{\vec{i},\downarrow} - 1 \right) \right).$$

where $\cos(\alpha) = \exp\left(-\Delta\tau U/2 \right)$ and $C = \exp\left(\Delta\tau U N/4 \right)/2^N$. With this choice of the HS transformation $SU(2)$ spin invariance is retained for any given HS configuration since the field couples to the density. Even taking into account the overhead of working with complex numbers, it is more convenient to work with this transformation[24] since it is often hard to restore the full $SU(2)$ spin symmetry via Monte Carlo sampling of the HS field. When $U < 0$ the transformation (25) may readily be used and involves only real numbers.

109

We now consider interaction terms of the form:

$$H_I = -W \sum_{\vec{i}} \left(O^{(\vec{i})} \right)^2 \tag{26}$$

where $O^{(\vec{i})}$ is a one-body operator. In general, $\left[O^{(\vec{i})}, O^{(\vec{j})} \right] \neq 0$ so that the sum in the above equation has to be split into sums of commuting terms: $H_I = \sum_r H_I^r$, $H_I^r = -W \sum_{\vec{i} \epsilon S_r} \left(O^{(\vec{i})} \right)^2$. For $\vec{i}$ and $\vec{j}$ in the set S_r one requires $\left[O^{(\vec{i})}, O^{(\vec{j})} \right] = 0$. The imaginary time evolution may be written as $e^{-\Delta\tau H_t} \approx \prod_r e^{-\Delta\tau H_t^r}$. Thus we are left with the problem of decoupling $e^{\Delta\tau W O^2}$ where we have omitted the index $\vec{i}$. In principle, one can decouple a perfect square with the canonical HS transformation:

$$e^{\Delta\tau W O^2} = \frac{1}{\sqrt{2\pi}} \int d\Phi e^{-\frac{\Phi^2}{2} + \sqrt{2\Delta\tau W}\Phi O} \tag{27}$$

However, this involves a continuous field which renders the sampling hard. An alternative formulation is given by[25]:

$$e^{\Delta\tau W O^2} = \sum_{l=\pm1,\pm2} \gamma(l) e^{\sqrt{\Delta\tau W}\eta(l)O} + \mathcal{O}(\Delta\tau^4) \tag{28}$$

where the fields η and γ take the values:

$$\gamma(\pm1) = 1 + \sqrt{6}/3, \quad \gamma(\pm2) = 1 - \sqrt{6}/3$$
$$\eta(\pm1) = \pm\sqrt{2\left(3 - \sqrt{6}\right)}, \quad \eta(\pm2) = \pm\sqrt{2\left(3 + \sqrt{6}\right)}.$$

This transformation is not exact and produces an overall systematic error proportional to $\Delta\tau^3$. However, since we already have a systematic error proportional to $\Delta\tau^2$ from the Trotter decomposition, the transformation is as good as exact. It also has the great advantage of being discrete thus allowing efficient sampling.

Thus, the HS transformation has enabled us to split the two-body interaction term into a one-body operator interacting with an external field. We may now write the imaginary time propagator as:

$$\prod_{n=1}^{m} \left[e^{-\Delta\tau H_I} e^{-\Delta\tau H_t} \right] = \prod_{n=1}^{m} \left[\sum_{\vec{s}} C(\vec{s}) e^{H_I(\vec{s})} e^{-\Delta\tau H_t} \right] \tag{29}$$

$$\sum_{\vec{s}_1 \cdots \vec{s}_m} C(\vec{s}_1 \cdots \vec{s}_m) \prod_{n=1}^{m} \left[e^{H_I(\vec{s}_n)} e^{-\Delta\tau H_t} \right]$$

Here, $H_I(\vec{s}_n)$ is a single body operator. The HS fields have a lattice site, $\vec{i}$ and imaginary time, n, index. We will adopt the notation: $\vec{s} = \left\{ s_{\vec{i},n} \right\} \vec{i} = 1 \cdots N$ and $n = 1 \cdots m$, and $\vec{s}_n$ denotes the HS fields on time slice n. In the special case of the Hubbard model with the HS transformation of Eq. (25),

$$H_I(\vec{s}_n) = i\alpha \sum_{\vec{j},\sigma} s_{\vec{j},n} c^\dagger_{\vec{j},\sigma} c_{\vec{j},\sigma}, \quad C(\vec{s}_1 \cdots \vec{s}_m) = \exp\left(\Theta U N/4\right) \exp\left(-i\alpha \sum_{\vec{j},n} s_{\vec{j},n}\right). \tag{30}$$

For an interaction term of the form in Eq. (26) $e^{H_I(\vec{s}_n)}$ has to be replaced by

$$\prod_r \exp\left(\sqrt{\Delta\tau W} \sum_{\vec{i}\epsilon S_r} \eta(l_{\vec{i},n}) O^{(\vec{i})}\right) \tag{31}$$

and $C(\{s_{\vec{i},n}\})$ by $C(\{l_{\vec{i},n}\}) = \prod_{\vec{i},n} \gamma(l_{\vec{i},n})$.

At this stage, the fermionic degrees of freedom may be integrated out. In the framework of the PQMC, we will require the trial wave function to be a Slater determinant:

$$|\Psi_T\rangle = \prod_{y=1}^{N_p}\left(\sum_x c_x^\dagger P_{x,y}\right)|0\rangle = \prod_{y=1}^{N_p}\left(\vec{c}^\dagger P\right)_y|0\rangle \tag{32}$$

where we have introduced the indices $\vec{x} = (\vec{i},\sigma)$, which run from $1\cdots 2N$, N_p is the number of particles and $\vec{c}^\dagger = \left(c_1^\dagger,\cdots,c_{2N}^\dagger\right)$. For a Hermitian or anti-hermitian matrix T, one may show that:

$$e^{\vec{c}^\dagger T \vec{c}} \prod_{y=1}^{N_p}\left(\vec{c}^\dagger P\right)_y|0\rangle = \prod_{y=1}^{N_p}\left(\vec{c}^\dagger e^T P\right)_y|0\rangle. \tag{33}$$

To derive the above equation, it is useful to go into a basis where T is diagonal: $U^\dagger T U = D$. U is a unitary matrix and D a real (purely imaginary) diagonal matrix provided that T is hermitian (anti-hermetian). Thus we can define the fermionic operators $\vec{\gamma}^\dagger = \vec{c}^\dagger U$ to obtain:

$$e^{\vec{c}^\dagger T \vec{c}} \prod_{y=1}^{N_p}\left(\vec{c}^\dagger P\right)_y|0\rangle = e^{\vec{\gamma}^\dagger D \vec{\gamma}} \prod_{y=1}^{N_p}\left(\vec{\gamma}^\dagger U P\right)_y|0\rangle =$$

$$\sum_{y_1,\cdots,y_{N_p}} e^{\sum_x D_{x,x} \vec{\gamma}_x^\dagger \vec{\gamma}_x} \gamma_{y_1}^\dagger \cdots \gamma_{y_{N_p}}^\dagger |0\rangle \left(UP\right)_{y_1,1} \cdots \left(UP\right)_{y_{N_p},N_p} =$$

$$\sum_{y_1,\cdots,y_{N_p}} e^{D_{y_1,y_1}} \gamma_{y_1}^\dagger \cdots e^{D_{y_{N_p},y_{N_p}}} \gamma_{y_{N_p}}^\dagger |0\rangle \left(UP\right)_{y_1,1} \cdots \left(UP\right)_{y_{N_p},N_p} =$$

$$\prod_{y=1}^{N_p}\left(\vec{\gamma}^\dagger e^D U P\right)_y|0\rangle = \prod_{y=1}^{N_p}\left(\vec{c}^\dagger U^\dagger e^D U P\right)_y|0\rangle = \prod_{y=1}^{N_p}\left(\vec{c}^\dagger e^T P\right)_y|0\rangle.$$

We can now evaluate the imaginary time propagator. It is convenient to define the notation:

$$H_I = \vec{c}^\dagger h_I(\vec{s}_\tau)\vec{c}, \quad H_t = \vec{c}^\dagger h_t \vec{c}$$

$$U_{\vec{s}}(\tau_2,\tau_1) = \prod_{n=n_1+1}^{n_2} e^{H_I(\vec{s}_n)} e^{-\Delta\tau H_t} \tag{34}$$

$$\text{and } B_{\vec{s}}(\tau_2,\tau_1) = \prod_{n=n_1+1}^{n_2} e^{h_I(\vec{s}_n)} e^{-\Delta\tau h_t} \tag{35}$$

where, $n_1\Delta\tau = \tau_1$ and $n_2\Delta\tau = \tau_2$, h_t is a $2N \times 2N$ hermetian matrix and $h_I(\vec{s}_n)$ a $2N \times 2N$ hermetian or anti-hermetian matrix depending upon the choice of the HS

transformation. One can then derive:

$$\langle \Psi_T | U_{\vec{s}}(2\Theta, 0) | \Psi_T \rangle = \det \left(P^\dagger B(2\Theta, 0) P \right). \tag{36}$$

The above follows from:

$$\langle \Psi_T | U_{\vec{s}}(2\Theta, 0) | \Psi_T \rangle = \langle \Psi_T | \prod_{y=1}^{N_p} \left(\vec{c}^\dagger B_{\vec{s}}(2\Theta, 0) P \right)_y | 0 \rangle =$$

$$\sum_{\substack{x_1 \cdots x_{N_p} \\ y_1 \cdots y_{N_p}}} P^\dagger_{1,y_{N_p}} \cdots P^\dagger_{1,y_1} \langle 0 | c_{y_1} \cdots c_{y_{N_p}} c^\dagger_{x_{N_p}} \cdots c^\dagger_{x_1} | 0 \rangle \times$$

$$\left(B_{\vec{s}}(2\Theta, 0) P \right)_{x_1, 1} \cdots \left(B_{\vec{s}}(2\Theta, 0) P \right)_{x_{N_p}, N_p}.$$

The matrix element $\langle 0 | c_{y_1} \cdots c_{y_{N_p}} c^\dagger_{x_{N_p}} \cdots c^\dagger_{x_1} | 0 \rangle$ does not vanish provided that
i) $x_1 \neq x_2 \neq \cdots \neq x_{N_p}$ and
ii) the indices $y_1 \cdots y_{N_p}$ are a permutation (π) of the indices $x_1 \cdots x_{N_p}$:
$y_1 = x_{\pi(1)} \cdots y_{N_p} = x_{\pi(N_p)}$.
The matrix element is then equal to the sign of permutation: $(-1)^\pi$. Hence,

$$\langle \Psi_T | U_{\vec{s}}(2\Theta, 0) | \Psi_T \rangle =$$
$$\sum_{\substack{x_1 \cdots x_{N_p} \\ \pi \epsilon S_{N_p}}} (-1)^\pi P^\dagger_{1, x_{\pi(1)}} \left(B_{\vec{s}}(2\Theta, 0) P \right)_{x_1, 1} \cdots P^\dagger_{N_p, x_{\pi(N_p)}} \left(B_{\vec{s}}(2\Theta, 0) P \right)_{x_{N_p}, N_p} =$$
$$\sum_{\pi \epsilon S_{N_p}} (-1)^\pi \left(P^\dagger B_{\vec{s}}(2\Theta, 0) P \right)_{\pi(1), 1} \cdots \left(P^\dagger B_{\vec{s}}(2\Theta, 0) P \right)_{\pi(N_p), N_p} =$$
$$\det \left(P^\dagger B_{\vec{s}}(2\Theta, 0) P \right)$$

where the last sum runs over the space S_{N_p} consisting of the $N_p!$ permutations of the integers $[1 \cdots N_p]$.

For the FTQMC, we have to evaluate evaluate the trace over the Fock space.

$$\mathrm{Tr} \left(U_{\vec{s}}(\beta, 0) \right) = \det \left(1 + B_{\vec{s}}(\beta, 0) \right) \tag{37}$$

where $m\Delta\tau = \beta$. The above equation is readily verified:

$$\det \left(1 + B_{\vec{s}}(\beta, 0)\right)$$

$$= \sum_{\pi\epsilon\mathcal{S}_{2N}} (-1)^\pi \left(1 + B_{\vec{s}}(\beta,0)\right)_{\pi(1),1} \cdots \left(1 + B_{\vec{s}}(\beta,0)\right)_{\pi(2N),2N}$$

$$= \sum_{\pi\epsilon\mathcal{S}_{2N}} (-1)^\pi \delta_{1,\pi(1)} \cdots \delta_{2N,\pi(2N)} +$$

$$\sum_x \sum_{\pi\epsilon\mathcal{S}_{2N}} (-1)^\pi B_{\vec{s}}(\beta,0)_{\pi(x),x} \delta_{1,\pi(1)} \cdots \widehat{\delta_{x,\pi(x)}} \cdots \delta_{2N,\pi(2N)} +$$

$$\sum_{y>x} \sum_{\pi\epsilon\mathcal{S}_{2N}} (-1)^\pi B_{\vec{s}}(\beta,0)_{\pi(x),x} B_{\vec{s}}(\beta,0)_{\pi(y),y} \times$$

$$\delta_{1,\pi(1)} \cdots \widehat{\delta_{x,\pi(x)}} \cdots \widehat{\delta_{y,\pi(y)}} \cdots \delta_{2N,\pi(2N)} +$$

$$\sum_{y>x>z} \sum_{\pi\epsilon\mathcal{S}_{2N}} (-1)^\pi B_{\vec{s}}(\beta,0)_{\pi(x),x} B_{\vec{s}}(\beta,0)_{\pi(y),y} B_{\vec{s}}(\beta,0)_{\pi(z),z} \times$$

$$\delta_{1,\pi(1)} \cdots \widehat{\delta_{x,\pi(x)}} \cdots \widehat{\delta_{y,\pi(y)}} \cdots \widehat{\delta_{z,\pi(z)}} \cdots \delta_{2N,\pi(2N)} + \cdots$$

$$= 1 + \sum_x \langle 0|c_x U_{\vec{s}}(\beta,0) c_x^\dagger|0\rangle + \sum_{y>x} \langle 0|c_x c_y U_{\vec{s}}(\beta,0) c_y^\dagger c_x^\dagger|0\rangle +$$

$$\sum_{y>x>z} \langle 0|c_x c_y c_z U_{\vec{s}}(\beta,0) c_z^\dagger c_y^\dagger c_x^\dagger|0\rangle + \cdots$$

$$= \text{Tr}\left(U_{\vec{s}}(\beta,0)\right).$$

Here, $\widehat{\delta_{y,\pi(y)}}$ means that this term is omitted in the product: $\prod_{x=1}^{2N} \delta_{x,\pi(x)}$. We have used Eq. (36) to derive the third equality.

3.2 Observables and Wick's Theorem

In the last section, we have shown how to carry out the HS transformation and integrate out the fermionic degrees of freedom. Here, we show both for the PQMC and FTQMC how to compute observables as well as the validity of Wick's theorem for a fixed configuration of HS fields.

3.2.1 PQMC

In the PQMC algorithm we compute:

$$\frac{\langle \Psi_T|e^{-\Theta H} O e^{-\Theta H}|\Psi_T\rangle}{\langle \Psi_T|e^{-2\Theta H}|\Psi_T\rangle} = \sum_{\vec{s}} \text{Pr}_{\vec{s}} \langle O\rangle_{\vec{s}} + O(\Delta\tau^2). \tag{38}$$

For each lattice site, $\vec{i}$, time slice, n, we have introduced an independent HS field, $\vec{s} = \left\{ s_{\vec{i},n} \right\}$ and

$$\mathrm{Pr}_{\vec{s}} = \frac{C_{\vec{s}} \det \left(P^\dagger B_{\vec{s}}(2\Theta, 0) P \right)}{\sum_{\vec{s}} C_{\vec{s}} \det \left(P^\dagger B_{\vec{s}}(2\Theta, 0) P \right)}$$

$$\langle O \rangle_{\vec{s}} = \frac{\langle \Psi_T | U_{\vec{s}}(2\Theta, \Theta) O U_{\vec{s}}(\Theta, 0) | \Psi_T \rangle}{\langle \Psi_T | U_{\vec{s}}(2\Theta, 0) | \Psi_T \rangle}$$

We start by computing the equal time Green function: $O = c_x c_y^\dagger = \delta_{x,y} - \vec{c}^\dagger A^{(y,x)} \vec{c}$ with $A^{(y,x)}_{x_1,x_2} = \delta_{x_1,y} \delta_{x_2,y}$. Inserting a source term, we obtain:

$$\langle c_x c_y^\dagger \rangle_{\vec{s}} = \delta_{x,y} - \frac{\partial}{\partial \eta} \ln \langle \Psi_T | U_{\vec{s}}(2\Theta, \Theta) e^{\eta \vec{c}^\dagger A^{(y,x)} \vec{c}} U_{\vec{s}}(\Theta, 0) | \Psi_T \rangle \mid_{\eta=0} =$$

$$\delta_{x,y} - \frac{\partial}{\partial \eta} \ln \det \left(P^\dagger B_{\vec{s}}(2\Theta, \Theta) e^{\eta A^{(y,x)}} B_{\vec{s}}(\Theta, 0) P \right) \mid_{\eta=0} =$$

$$\delta_{x,y} - \frac{\partial}{\partial \eta} \mathrm{Tr} \ln \left(P^\dagger B_{\vec{s}}(2\Theta, \Theta) e^{\eta A^{(y,x)}} B_{\vec{s}}(\Theta, 0) P \right) \mid_{\eta=0} = \qquad (39)$$

$$\delta_{x,y} - \mathrm{Tr} \left[\left(P^\dagger B_{\vec{s}}(2\Theta, 0) P \right)^{-1} P^\dagger B_{\vec{s}}(2\Theta, \Theta) A^{(y,x)} B_{\vec{s}}(\Theta, 0) P \right]$$

$$\left(1 - B_{\vec{s}}(\Theta, 0) P \left(P^\dagger B_{\vec{s}}(2\Theta, 0) P \right)^{-1} P^\dagger B_{\vec{s}}(2\Theta, \Theta) \right)_{x,y} \equiv (G_{\vec{s}}(\Theta))_{x,y}$$

We have used Eq. (36) to go from the second to third equality. The attentive reader will have noticed that Eq. (36) was shown to be valid only in the case of hermetian or anti-hermetian matrices which is certainly not the case of $A^{(y,x)}$. However, since only terms of order η are relevant in the calculation, we may replace $e^{\eta A}$ by $e^{\eta(A+A^\dagger)/2} e^{\eta(A-A^\dagger)/2}$ which is exact up to order η^2. For the latter form, one may use Eq. (36). To obtain the fourth equality we have used the relation: $\det A = \exp \mathrm{Tr} \ln A$.

We now show that any multi-point correlation function decouples into a sum of products of the above defined Green functions. First, we define the cummulants:

$$\langle\langle O_n \cdots O_1 \rangle\rangle_{\vec{s}} = \frac{\partial^n \ln \langle \Psi_T | U_{\vec{s}}(2\Theta, \Theta) e^{\eta_n O_n} \cdots e^{\eta_1 O_1} U_{\vec{s}}(\Theta, 0) | \Psi_T \rangle}{\partial \eta_n \cdots \partial \eta_1} \Bigg|_{\eta_1 \cdots \eta_n = 0}$$

with $O_i = \vec{c}^\dagger A^{(i)} \vec{c}$. $\qquad (40)$

Differentiating the above definition we obtain:

$$\langle\langle O_1 \rangle\rangle_{\vec{s}} = \langle O_1 \rangle_{\vec{s}}$$

$$\langle\langle O_2 O_1 \rangle\rangle_{\vec{s}} = \langle O_2 O_1 \rangle_{\vec{s}} - \langle O_2 \rangle_{\vec{s}} \langle O_1 \rangle_{\vec{s}}$$

$$\langle\langle O_3 O_2 O_1 \rangle\rangle_{\vec{s}} = \langle O_3 O_2 O_1 \rangle_{\vec{s}} -$$

$$\langle O_3 \rangle_{\vec{s}} \langle\langle O_2 O_1 \rangle\rangle_{\vec{s}} - \langle O_2 \rangle_{\vec{s}} \langle\langle O_3 O_1 \rangle\rangle_{\vec{s}} - \langle O_1 \rangle_{\vec{s}} \langle\langle O_3 O_2 \rangle\rangle_{\vec{s}} -$$

$$\langle O_1 \rangle_{\vec{s}} \langle O_2 \rangle_{\vec{s}} \langle O_3 \rangle_{\vec{s}}. \qquad (41)$$

The following rule, which may be proven by induction, emerges:

$$
\langle O_n \cdots O_1 \rangle_{\vec{s}} = \langle\langle O_n \cdots O_1 \rangle\rangle_{\vec{s}} + \sum_{j=1}^{n} \langle\langle O_n \cdots \widehat{O_j} \cdots O_1 \rangle\rangle_{\vec{s}} \langle\langle O_j \rangle\rangle_{\vec{s}} +
$$

$$
\sum_{j>i} \langle\langle O_n \cdots \widehat{O_j} \cdots \widehat{O_i} \cdots O_1 \rangle\rangle_{\vec{s}} \langle\langle O_j O_i \rangle\rangle_{\vec{s}} + \cdots +
$$

$$
\langle\langle O_n \rangle\rangle_{\vec{s}} \cdots \langle\langle O_1 \rangle\rangle_{\vec{s}} \tag{42}
$$

where $\widehat{O_j}$ means that the operator O_j has been omitted from the product.

The cumulants may now be computed order by order. We concentrate on the form $\langle\langle c_{x_n}^\dagger c_{y_n} \cdots c_{x_1}^\dagger c_{y_1} \rangle\rangle$ so that $A_{x,y}^{(i)} = \delta_{x,x_i} \delta_{y,y_i}$. To simplify notation in the next calculation we introduce:

$$
B^\rangle = B_{\vec{s}}(\Theta, 0) P, \quad \text{and} \quad B^\langle = P^\dagger B_{\vec{s}}(2\Theta, \Theta) \tag{43}
$$

We have already computed $\langle\langle O_1 \rangle\rangle_{\vec{s}}$ (see Eq. (39)):

$$
\langle\langle O_1 \rangle\rangle_{\vec{s}} = \langle\langle c_{x_1}^\dagger c_{y_1} \rangle\rangle = \text{Tr}\left((1 - G_{\vec{s}}(\Theta)) A^{(1)}\right) = (1 - G_{\vec{s}}(\Theta))_{y_1, x_1} \tag{44}
$$

For $n = 2$ we have:

$$
\begin{aligned}
\langle\langle O_2 O_1 \rangle\rangle_{\vec{s}} &= \langle\langle c_{x_2}^\dagger c_{y_2} c_{x_1}^\dagger c_{y_1} \rangle\rangle_{\vec{s}} \\
&= \frac{\partial^2 \text{Tr} \ln \left(P^\dagger B_{\vec{s}}(2\Theta, \Theta) e^{\eta_2 A^{(2)}} e^{\eta_1 A^{(1)}} B_{\vec{s}}(\Theta, 0) P \right)}{\partial \eta_2 \partial \eta_1} \Bigg|_{\eta_2, \eta_1 = 0} \\
&= \frac{\partial}{\partial \eta_2} \text{Tr}\left[\left(B^\langle e^{\eta_2 A^{(2)}} B^\rangle \right)^{-1} B^\langle e^{\eta_2 A^{(2)}} A^{(1)} B^\rangle \right] \Bigg|_{\eta_2 = 0} \\
&= -\text{Tr}\left[\left(B^\langle B^\rangle \right)^{-1} B^\langle A^{(2)} B^\rangle \left(B^\langle B^\rangle \right)^{-1} B^\langle A^{(1)} B^\rangle \right] \\
&\quad + \text{Tr}\left[\left(B^\langle B^\rangle \right)^{-1} B^\langle A^{(2)} A^{(1)} B^\rangle \right] \\
&= \text{Tr}\left(\overline{G_{\vec{s}}(\Theta)} A^{(2)} G_{\vec{s}}(\Theta) A^{(1)} \right) \\
&= \langle c_{x_2}^\dagger c_{y_1} \rangle_{\vec{s}} \langle c_{y_2} c_{x_1}^\dagger \rangle_{\vec{s}}, \quad \text{with } \overline{G} = 1 - G \tag{45}
\end{aligned}
$$

To derive the above, we have used the cyclic properties of the trace as well as the relation $G = 1 - B^\rangle \left(B^\langle B^\rangle \right)^{-1} B^\langle$. Note that for a matrix $A(\eta)$, $\frac{\partial}{\partial \eta} A^{-1}(\eta) = -A^{-1}(\eta) \left(\frac{\partial}{\partial \eta} A(\eta) \right) A^{-1}(\eta)$. There is a simple rule to obtain the third cumulant given the second. In the above expression for the second cumulant, one replaces $B^\rangle$ with $B^\langle e^{\eta_3 A^{(3)}}$. This amounts in redefining the Green function as

115

$$G(\eta_3) = 1 - B^{\rangle} \left(B^{\langle} e^{\eta_3 A^{(3)}} B^{\rangle} \right)^{-1} B^{\langle} e^{\eta_3 A^{(3)}}. \text{ Thus,}$$

$$
\begin{aligned}
\langle\langle O_3 O_2 O_1 \rangle\rangle_{\vec{s}} &= \langle\langle c^\dagger_{x_3} c_{y_3} c^\dagger_{x_2} c_{y_2} c^\dagger_{x_1} c_{y_1} \rangle\rangle_{\vec{s}} \\
&= \frac{\partial}{\partial \eta_3} \text{Tr} \left(\overline{G_{\vec{s}}(\Theta, \eta_3)} A^{(2)} G_{\vec{s}}(\Theta, \eta_3) A^{(1)} \right) \Big|_{\eta_3 = 0} \\
&= \text{Tr} \left(\overline{G_{\vec{s}}(\Theta)} A^{(3)} G_{\vec{s}}(\Theta) A^{(2)} G_{\vec{s}}(\Theta) A^{(1)} \right) - \\
&\quad \text{Tr} \left(\overline{G_{\vec{s}}(\Theta)} A^{(3)} G_{\vec{s}}(\Theta) A^{(1)} \overline{G_{\vec{s}}(\Theta)} A^{(2)} \right) \\
&= \langle c^\dagger_{x_3} c_{y_1} \rangle_{\vec{s}} \langle c_{y_3} c^\dagger_{x_2} \rangle_{\vec{s}} \langle c_{y_2} c^\dagger_{x_1} \rangle_{\vec{s}} - \\
&\quad \langle c^\dagger_{x_3} c_{y_2} \rangle_{\vec{s}} \langle c_{y_3} c^\dagger_{x_1} \rangle_{\vec{s}} \langle c_{y_2} c^\dagger_{y_1} \rangle_{\vec{s}}
\end{aligned}
\tag{46}
$$

since

$$\frac{\partial}{\partial \eta_3} G_{\vec{s}}(\Theta, \eta_3)\big|_{\eta_3=0} = -\overline{G_{\vec{s}}(\Theta)} A^{(3)} G_{\vec{s}}(\Theta) = -\frac{\partial}{\partial \eta_3} \overline{G_{\vec{s}}(\Theta, \eta_3)}\Big|_{\eta_3=0}.$$

Clearly the same procedure may be applied to obtain the $n^{th}+1$ cumulant given the nth one. It is also clear that the nth cumulant is a sum of products of Green functions. Thus with equation (42) we have shown that any multi-point correlation function may be reduced into a sum of products of Green functions: Wicks theorem. Useful relations include:

$$\langle c^\dagger_{x_2} c_{y_2} c^\dagger_{x_1} c_{y_1} \rangle_{\vec{s}} = \langle c^\dagger_{x_2} c_{y_1} \rangle_{\vec{s}} \langle c_{y_2} c^\dagger_{x_1} \rangle_{\vec{s}} + \langle c^\dagger_{x_2} c_{y_2} \rangle_{\vec{s}} \langle c^\dagger_{x_1} c_{y_1} \rangle_{\vec{s}}. \tag{47}$$

3.2.2 FTQMC

For the FTQMC we wish to evaluate:

$$\frac{\text{Tr}\left[e^{-\beta H} O \right]}{\text{Tr}\left[e^{-\beta H} O \right]} = \sum_{\vec{s}} \text{Pr}_{\vec{s}} \langle O \rangle_{\vec{s}} + O(\Delta \tau^2). \tag{48}$$

where

$$\text{Pr}_{\vec{s}} = \frac{C_{\vec{s}} \det \left(1 + B_{\vec{s}}(\beta, 0) \right)}{\sum_{\vec{s}} C_{\vec{s}} \det \left(1 + B_{\vec{s}}(\beta, 0) \right)}, \quad \langle O \rangle_{\vec{s}} = \frac{\text{Tr}\left[U_{\vec{s}}(\beta, \tau) O U_{\vec{s}}(\tau, 0) \right]}{\text{Tr}\left[U_{\vec{s}}(\beta, 0) \right]}.$$

Here, we measure the observable on time slice τ. Single body observables, $O = \vec{c}^\dagger A \vec{c}$ are evaluated as:

$$
\begin{aligned}
\langle O \rangle_{\vec{s}} &= \frac{\partial \ln \text{Tr}\left[U_{\vec{s}}(\beta, \tau) e^{\eta O} U_{\vec{s}}(\tau, 0) \right]}{\partial \eta} \bigg|_{\eta=0} \\
&= \frac{\partial \ln \det \left[1 + B_{\vec{s}}(\beta, \tau) e^{\eta A} B_{\vec{s}}(\tau, 0) \right]}{\partial \eta} \bigg|_{\eta=0} \\
&= \frac{\partial \ln \text{Tr}\left[1 + B_{\vec{s}}(\beta, \tau) e^{\eta A} B_{\vec{s}}(\tau, 0) \right]}{\partial \eta} \bigg|_{\eta=0} \\
&= \text{Tr}\left[B_{\vec{s}}(\tau, 0)(1 + B_{\vec{s}}(\beta, 0))^{-1} B_{\vec{s}}(\beta, \tau) A \right] \\
&= \text{Tr}\left[\left(1 - (1 + B_{\vec{s}}(\tau, 0) B_{\vec{s}}(\beta, \tau))^{-1} \right) A \right]
\end{aligned}
\tag{49}
$$

In particular the Green function is given by:

$$\langle c_x c_y^\dagger \rangle_{\vec{s}} = (1 + B_{\vec{s}}(\tau,0)B_{\vec{s}}(\beta,\tau))_{x,y}^{-1} \tag{50}$$

Defining the cumulants as

$$\langle\langle O_n \cdots O_1 \rangle\rangle_{\vec{s}} = \left. \frac{\partial^n \ln \text{Tr}\left[U_{\vec{s}}(\beta,\tau)e^{\eta_n O_n}\cdots e^{\eta_1 O_1}U_{\vec{s}}(\tau,0)\right]}{\partial\eta_n \cdots \partial\eta_1} \right|_{\eta_1\cdots\eta_n=0}$$

$$\text{with} \quad O_i = \vec{c}^\dagger A^{(i)}\vec{c}, \tag{51}$$

one can derive Wicks theorem in precisely the same manner as shown for the PQMC. Thus both in the PQMC and FTQMC, it suffices to compute the equal time Green functions to evaluate any equal time observable.

3.3 The Monte Carlo Sampling

We now have to sum over the HS fields. The lowest temperature results in Fig. 6 require summing over 2^{5760} Ising field configurations. An exact summation is thus clearly not possible. We will thus use the Monte Carlo method (see Appendix) and use a single site upgrading method which requires the calculation of the ratio

$$R = \frac{\text{Pr}_{\vec{s}'}}{\text{Pr}_{\vec{s}}} \tag{52}$$

where $\vec{s}$ and $\vec{s}'$ differ only at one point in space and imaginary time, $\vec{i}, n$. For the Ising field required to decouple the Hubbard interaction (Eqn. (24) and (25)):

$$s'_{\vec{i}',n'} = \begin{cases} s_{\vec{i}',n'} & \text{if } \vec{i}' \neq \vec{i} \text{ and } n' \neq n \\ -s_{\vec{i},n} & \text{if } \vec{i}' = \vec{i} \text{ and } n' = n \end{cases} \tag{53}$$

For HS fields $\vec{l}$ required to decouple perfect square terms (Eq. (28)):

$$l'_{\vec{i}',n'} = \begin{cases} l_{\vec{i}',n'} & \text{if } \vec{i}' \neq \vec{i} \text{ and } n' \neq n \\ \mathcal{F}\left(l_{\vec{i},n}\right) & \text{if } \vec{i}' = \vec{i} \text{ and } n' = n \end{cases} \tag{54}$$

where $\mathcal{F}\left(l_{\vec{i},n}\right)$ flips the HS field $l_{\vec{i},n}$ into one of the three other choices with probability $1/3$. The calculation of R boils down to computing the ration of two determinants:

$$\frac{\det[1+B_{\vec{s}'}(\beta,0)]}{\det[1+B_{\vec{s}}(\beta,0)]} \quad \text{for the FTQMC}$$

$$\frac{\det\left[P^\dagger B_{\vec{s}'}(2\Theta,0)P\right]}{\det[P^\dagger B_{\vec{s}}(2\Theta,0)P]} \quad \text{for the PQMC.} \tag{55}$$

For the Hubbard interaction with HS transformation of Eq. (25) only $h_I(\vec{s}_n)$ will be affected by the move.

$$e^{h_I(\vec{s}'_n)} = e^{i\alpha \sum_{\vec{j}} s'_{\vec{j},n} A^{(\vec{j})}} = e^{i\alpha s'_{\vec{i},n} A^{(\vec{i})}} e^{i\alpha \sum_{\vec{j}\neq\vec{i}} s_{\vec{i},n} A^{(\vec{i})}}$$

$$= e^{-i\alpha s_{\vec{i},n} A^{(\vec{i})}} e^{i\alpha \sum_{\vec{j}\neq\vec{i}} s_{\vec{i},n} A^{(\vec{i})}} = e^{-2i\alpha s_{\vec{i},n} A^{(\vec{i})}} e^{i\alpha \sum_{\vec{j}} s_{\vec{i},n} A^{(\vec{i})}}$$

$$= (1 + \underbrace{\left(e^{-2i\alpha s_{\vec{i},n} A^{(\vec{i})}} - 1\right)}_{=\Delta^{(\vec{i})}})e^{h_I(\vec{s}_n)}. \tag{56}$$

117

Here $A^{(\vec{i})}_{x,y} = \delta_{x,y}\delta_{x,(\vec{i},\sigma)}$ so that $\left[A^{(\vec{i})}, A^{(\vec{j})}\right] = 0 \ \forall \vec{i}, \vec{j}$. The matrix $\Delta^{(\vec{i})}$ is diagonal and has only two non-zero entries at $x = (\vec{i}, \sigma)$. Thus, for the Hubbard model:

$$B_{\vec{s}'}(\bullet, 0) = B_{\vec{s}}(\bullet, \tau)\left(1 + \Delta^{(\vec{i})}\right)B_{\vec{s}}(\tau, 0) \tag{57}$$

where the $\bullet$ stands for 2Θ or β and $\tau = n\Delta\tau$. For interaction term in the form of perfect squares isolating the HS filed $l_{\vec{i},n}$ is a bit more cumbersome. First let us assume that $\vec{i}$ is in the set S_r (see paragraph after Eq. (26)) and that $O^{(\vec{i})} = \vec{c}^\dagger A^{(\vec{i})}\vec{c}$. We will work in a basis where $A^{(\vec{i})}$ is diagonal: $U^{(\vec{i}),\dagger}A^{(\vec{i})}U^{(\vec{i})} = D^{(\vec{i})}$.

$$e^{h_I^r(\vec{l}_n)} = e^{\sqrt{\Delta\tau W}\sum_{\vec{j}\epsilon S_r}\eta(l'_{\vec{j},n})A^{(\vec{j})}} = e^{\sqrt{\Delta\tau W}(\eta(l'_{\vec{i},n})-\eta(l_{\vec{i},n}))A^{(\vec{i})}}e^{h_I^r(\vec{l}_n)}$$

$$= U^{(\vec{i})}\left(1 + \underbrace{\left(e^{\sqrt{\Delta\tau W}(\eta(l'_{\vec{i},n})-\eta(l_{\vec{i},n}))D^{(\vec{i})}} - 1\right)}_{=\Delta^{(\vec{i})}}\right)U^{(\vec{i}),\dagger}e^{h_I^r(\vec{l}_n)}. \tag{58}$$

Thus, $B_{\vec{i}'}(\bullet, 0)$ takes the form:

$$B_{\vec{i}'}(\bullet, 0) = \overbrace{B_{\vec{i}}(\bullet, \tau)\left[\prod_{r'=1}^{r-1}e^{h_I^{r'}(\vec{l}_n)}\right]U^{(\vec{i})}}^{\tilde{B}_{\vec{i}}(\bullet, \tau)}\left(1 + \Delta^{(\vec{i})}\right)$$

$$\underbrace{U^{(\vec{i}),\dagger}\left[\prod_{r'\geq r}e^{h_I^{r'}(\vec{l}_n)}\right]B_{\vec{i}}(\tau, 0)}_{\tilde{B}_{\vec{i}}(\tau, 0)} \tag{59}$$

After a redefinition of the B matrices as shown in the above equation, a similar form to that for the Hubbard model is obtained. Note that $\tilde{B}$ matrices satisfy: $\tilde{B}_{\vec{i}}(\bullet, \tau)\tilde{B}_{\vec{i}}(\tau, 0) = B_{\vec{i}}(\bullet, 0)$. It is often important to work in a basis where the $A^{(\vec{i})}$ matrices are diagonal since computer time is saved if some of the eigenvalues vanish. In the the so-called t-U-W model[26,25] a factor 6 in CPU time in the upgrading is saved.

Concentrating first on the PQMC, and again introducing the notation $B_{\vec{s}}^\langle = P^\dagger B_{\vec{s}}(2\Theta, \tau)$ and $B_{\vec{s}}^\rangle = B_{\vec{s}}(\tau, 0)P$ we have to evaluate:

$$\frac{\det\left[B_{\vec{s}}^\langle\left(1 + \Delta^{(\vec{i})}\right)B_{\vec{s}}^\rangle\right]}{\det\left[B_{\vec{s}}^\langle B_{\vec{s}}^\rangle\right]} = \det\left[B_{\vec{s}}^\langle\left(1 + \Delta^{(\vec{i})}\right)B_{\vec{s}}^\rangle\left(B_{\vec{s}}^\langle B_{\vec{s}}^\rangle\right)^{-1}\right] \tag{60}$$

$$= \det\left[1 + B_{\vec{s}}^\langle\Delta^{(\vec{i})}B_{\vec{s}}^\rangle\left(B_{\vec{s}}^\langle B_{\vec{s}}^\rangle\right)^{-1}\right] = \det\left[1 + \Delta^{(\vec{i})}B_{\vec{s}}^\rangle\left(B_{\vec{s}}^\langle B_{\vec{s}}^\rangle\right)^{-1}B_{\vec{s}}^\langle\right]$$

where the last equation follows from the identity $\det\left[1 + AB\right] = \det\left[1 + BA\right]$ for arbitrary rectangular matrices. [d] We can recognize the Green function

---

[d]This identity may be formally shown by using the relation $\det(1 + AB) = \exp\operatorname{Tr}\log(1 + AB)$, expanding the logarithm and using the cyclic properties of the trace.

$B_{\vec{s}}^{\rangle} \left(B_{\vec{s}}^{\langle} B_{\vec{s}}^{\rangle} \right)^{-1} B_{\vec{s}}^{\langle} = 1 - G_{\vec{s}}(\tau) \equiv \bar{G}_{\vec{s}}(\tau)$. By construction, $\Delta^{(\vec{i})}$ is diagonal. For a form with Q non vanishing entries,

$$(\Delta^{(\vec{i})})_{z,z_1} = \delta_{z,z_1} \sum_{q=1}^{Q} \Delta_{x_q}^{(\vec{i})} \delta_{x_q,z} \tag{61}$$

one has,

$$\det \left[1 + \Delta^{(\vec{i})} \bar{G}_{\vec{s}}(\tau) \right] =$$
$$\det \begin{pmatrix} (1 + \Delta^{(\vec{i})} \bar{G}_{\vec{s}}(\tau))_{x_1,x_1} & \cdots & (1 + \Delta^{(\vec{i})} \bar{G}_{\vec{s}}(\tau))_{x_1,x_Q} \\ & \cdot & \\ & \cdot & \\ (1 + \Delta^{(\vec{i})} \bar{G}_{\vec{s}}(\tau))_{x_Q,x_1} & \cdots & (1 + \Delta^{(\vec{i})} \bar{G}_{\vec{s}}(\tau))_{x_Q,x_Q} \end{pmatrix}. \tag{62}$$

For the FTQMC, we have to evaluate:

$$\frac{\det \left[1 + B_{\vec{s}}(\beta,\tau)(1 + \Delta^{(\vec{i})}) B_{\vec{s}}(\tau,0) \right]}{\det \left[1 + B_{\vec{s}}(\beta,0) \right]} =$$
$$\det \left[1 + \Delta^{(\vec{i})} B_{\vec{s}}(\tau,0) \left(1 + B_{\vec{s}}(\beta,0) \right)^{-1} B_{\vec{s}}(\beta,\tau) \right] =$$
$$\det \left[1 + \Delta^{(\vec{i})} \left(1 - (1 + B_{\vec{s}}(\tau,0) B_{\vec{s}}(\beta,\tau))^{-1} \right) \right]. \tag{63}$$

Since the finite temperature equal time Green function is given by: $G_{\vec{s}}(\tau) = (1 + B_{\vec{s}}(\tau,0) B_{\vec{s}}(\beta,\tau))^{-1}$ so that precisely same form as in the PQMC is obtained.

Having calculated the ratio R for a single spin-flip one may now decide stochastically if the move is accepted or not. In case of acceptance, the Green function is to be upgraded since this quantity will be requires for the next spin-flip. The upgrading of the Green function is based on the Sherman-Morrison formula[27]:

$$(A + \vec{u} \otimes \vec{v})^{-1} = A^{-1} - \frac{\left(A^{-1}\vec{u} \right) \otimes \left(\vec{v} A^{-1} \right)}{1 + \vec{v} \bullet A^{-1}\vec{u}} \tag{64}$$

where the outer product is defined by $(\vec{u} \otimes \vec{v})_{x,y} = \vec{u}_x \vec{v}_y$. In the case of the FTQMC and $\Delta^{(\vec{i})}$ given by Eq. (61),

$$G_{\vec{s}'}(\tau) = \left(1 + B_{\vec{s}}(\tau,0)(1 + \Delta^{(\vec{i})}) B_{\vec{s}}(\beta,\tau) \right)^{-1}$$
$$= \left(1 + B_{\vec{s}}(\tau,0) B_{\vec{s}}(\beta,\tau) + \sum_q \vec{u}^{(q)} \otimes \vec{v}^{(q)} \right)^{-1} \tag{65}$$

where

$$(\vec{u}^{(q)})_x = (B_{\vec{s}}(\tau,0))_{x,x_q} \Delta_{x_q}^{(\vec{i})} \quad \text{and} \quad (\vec{v}^{(q)})_x = (B_{\vec{s}}(\beta,\tau))_{x_q,x}.$$

Identifying A to $(G_{\vec{s}}(\tau))^{-1} = 1 + B_{\vec{s}}(\tau,0) B_{\vec{s}}(\beta,\tau)$, Eq. (64) may now be applied Q times to upgrade the Green function.

For the PQMC, the upgrading of the Green function is equivalent to the upgrading of $(B_{\vec{s}'}^{\langle} B_{\vec{s}'}^{\rangle})^{-1}$, which is achieved with the Sherman-Morrison formula:

$$(B_{\vec{s}'}^{\langle} B_{\vec{s}'}^{\rangle})^{-1} = \left(B_{\vec{s}}^{\langle}(1 + \Delta^{(\vec{i})})B_{\vec{s}}^{\rangle} \right)^{-1} = \left(B_{\vec{s}}^{\langle} B_{\vec{s}}^{\rangle} + \sum_q \vec{u}^{(q)} \otimes \vec{v}^{(q)} \right)^{-1} \qquad (66)$$

with $(\vec{u}^{(q)})_x = (B_{\vec{s}}^{\langle})_{x,x_q} \Delta_{x_q}^{(\vec{i})}$ and $(\vec{v}^{(q)})_x = (B_{\vec{s}}^{\rangle})_{x_q,x}$. Here x runs from $1 \cdots N_p$ where N_p corresponds to the number of particles contained in the trial wave function.

In principle, we now have all elements required to carry out the simulations. The equal time Green function is the central quantity. On one hand it is used to compute any observables. On the other hand, it determines the Monte Carlo dynamics. It is convenient to adopt a sequential upgrading scheme. Given the Green function at imaginary time $\tau = \Delta\tau$, one upgrades the HS fields on this time slice deterministically or randomly. In case of acceptance, the Green function is upgraded after each single spin flip. To reach the next time slice, the relation:

$$G_{\vec{s}}(\tau + 1) = B_{\vec{s}}(\tau + 1, \tau) G_{\vec{s}}(\tau) \left(B_{\vec{s}}(\tau + 1, \tau) \right)^{-1} \qquad (67)$$

is used and the procedure is repeated till $\tau = \beta$ (FTQMC) or $\tau = 2\Theta$ (PQMC). Having reached $\tau = \beta$ or $\tau = 2\Theta$ we propagate the Green function to back $\tau = 1$ and on the way upgrade the HS fields. The whole procedure may then be repeated. We note that for interactions of the form (26) the propagation of the Green function from time slice τ to time slice $\tau + 1$ is split into intermediate steps according to (59) so as to upgrade the HS fields in the the sets S_r successively.

The above corresponds precisely to the procedure adopted in the case of the FTQMC. For the PQMC, it is more efficient to keep track of $(P^\dagger B_{\vec{s}}(2\Theta, 0)P)^{-1}$ since (i) it is of dimension $N_p \times N_p$ in contrast to the Green function which is a $N \times N$ matrix and (ii) it is τ independent. When Green functions are required - to compute R, or observables - they are computed from scratch.

3.4 Numerical Stabilization

In the previous section, we have assumed that we are able to compute the Green functions. On finite precision machines this is unfortunately not the case. To understand the sources of numerical instabilities, it is convenient to consider the PQMC. The rectangular matrix P is just a set of column orthonormal vectors. Typically for a Hubbard model, at weak couplings, the extremal scales in the matrix $B_{\vec{s}}(2\Theta, 0)$ are determined by the kinetic energy and range from $e^{8t\Theta}$ to $e^{-8t\Theta}$ in the two-dimensional case. When the set of orthonormal vectors in P are propagated, the large scales will wash out the small scales yielding an numerically ill defined inversion of the matrix $P^\dagger B_{\vec{s}}(2\Theta, 0)P$. To be more precise consider a two electron problem. The matrix P then consists of two column orthonormal vectors, $\vec{v}(0)_1$ and $\vec{v}(0)_2$. After propagation along the imaginary time axis, will be dominated by the largest scales in $B_{\vec{s}}(2\Theta, 0)$ so that $\vec{v}(2\Theta)_1 = \vec{v}(2\Theta)_2 + \vec{\epsilon}$, where $\vec{v}(2\Theta)_1 = B_{\vec{s}}(2\Theta, 0)\vec{v}_1$. It is the information contained in $\vec{\epsilon}$ which renders the matrix $P^\dagger B_{\vec{s}}(2\Theta, 0)P$ non-singular. For large values of Θ this information is lost in round-off errors.

To circumvent this problem a set of matrix decomposition techniques were developed[13, 14, 10]. Those matrix decomposition techniques are best introduced with the Gram-Schmidt orthonormalization method of N_p linearly independent vectors. At imaginary

time τ, $B_{\vec{s}}(\tau,0)P \equiv B^{\rangle}$ is given by the N_p vectors $\vec{v}_1 \cdots \vec{v}_{N_p}$. Orthogonalizing those vectors yields:

$$\vec{v}_1' = \vec{v}_1$$
$$\vec{v}_2' = \vec{v}_2 - \frac{\vec{v}_2 \cdot \vec{v}_1'}{\vec{v}_1' \cdot \vec{v}_1'} \vec{v}_1'$$
$$\cdot$$
$$\cdot$$
$$\vec{v}_{N_p}' = \vec{v}_{N_p} - \sum_{i=1}^{N_p-1} \frac{\vec{v}_{N_p} \cdot \vec{v}_i'}{\vec{v}_i' \cdot \vec{v}_i'} \vec{v}_i'. \tag{68}$$

Since $\vec{v}_n'$ depends only on the vectors $\vec{v}_n \cdots \vec{v}_1$ we can write,

$$\left(\vec{v}_1', \cdots, \vec{v}_{N_p}' \right) = \left(\vec{v}_1, \cdots, \vec{v}_{N_p} \right) V_R^{-1} \tag{69}$$

where V_R is an upper unit triangular $N_p \times N_p$ matrix, that is the diagonal matrix elements are equal to unity. One can furthermore normalize the vectors $\vec{v}_1', \cdots, \vec{v}_{N_p}'$ to obtain:

$$B^{\rangle} \equiv \left(\vec{v}_1, \cdots, \vec{v}_{N_p} \right) = \underbrace{\left(\frac{\vec{v}_1'}{|\vec{v}_1'|}, \cdots, \frac{\vec{v}_{N_p}'}{|\vec{v}_{N_p}'|} \right)}_{\equiv U^{\rangle}} D_R V_R \tag{70}$$

where D is a diagonal matrix containing the scales. One can repeat the procedure to obtain: $B^{\langle} \equiv P^{\dagger} B_{\vec{s}}(2\Theta, \tau) = V_L D_L U^{\langle}$. The Green function for the PQMC is now particularly easy to compute:

$$\begin{aligned}
1 - G_{\vec{s}}(\tau) &= B^{\rangle} \left(B^{\langle} B^{\rangle} \right)^{-1} B^{\langle} \\
&= U^{\rangle} D_R V_R \left(V_L D_L U^{\langle} U^{\rangle} D_R V_R \right)^{-1} V_L D_L U^{\langle} \\
&= U^{\rangle} D_R V_R \left(D_R V_R \right)^{-1} \left(U^{\langle} U^{\rangle} \right)^{-1} \left(V_L D_L \right)^{-1} V_L D_L U^{\langle} \\
&= U^{\rangle} \left(U^{\langle} U^{\rangle} \right)^{-1} U^{\langle} \tag{71}
\end{aligned}$$

Thus, in the PQMC, all scales which are at the origin of the numerical instabilities disappear from the problem when computing Green functions. Since the entire algorithm relies solely on the knowledge of the Green function, the above stabilization procedure leaves the physical results invariant. Note that although appealing, the Gram-Schmidt orthonormalization is itself unstable, and hence is is more appropriate to use singular value decompositions based on Housholder's method to obtain the above UDV form for the B matrices[27]. In practice the frequency at which the stabilization is carried out is problem dependent. Typically, for the Hubbard model with $\Delta\tau t = 0.125$ stabilization at every 10th time slice produces excellent accuracy.

The stabilization procedure for the finite temperature algorithm is more subtle since scales may not be doped in the calculation of the Green function. Below, we provide two ways of computing the Green function.

The first approach relies on the identity:

$$\begin{pmatrix} A & B \\ C & D \end{pmatrix}^{-1} = \begin{pmatrix} (A - BD^{-1}C)^{-1} & (C - DB^{-1}A)^{-1} \\ (B - AC^{-1}D)^{-1} & (D - CA^{-1}B)^{-1} \end{pmatrix} \tag{72}$$

where A, B, C and D are matrices. Using the above, we obtain:

$$\begin{pmatrix} 1 & B_{\vec{s}}(\tau, 0) \\ -B_{\vec{s}}(\beta, \tau) & 1 \end{pmatrix}^{-1} = \begin{pmatrix} G_{\vec{s}}(0) & -(1 - G_{\vec{s}}(0))B_{\vec{s}}^{-1}(\tau, 0) \\ B_{\vec{s}}(\tau, 0)G_{\vec{s}}(0) & G_{\vec{s}}(\tau) \end{pmatrix} \tag{73}$$

The diagonal terms on the right hand side of the above equation correspond to the desired equal time Green functions. The off-diagonal terms are nothing but the time displaced Green functions which will be discussed in the next section. To evaluate the left hand side of the above equation, we first have to bring $B_{\vec{s}}(\tau, 0)$ and $B_{\vec{s}}(\beta, \tau)$ in UDV forms. This has to be done step by step so as to avoid mixing large and small scales. Consider the propagation $B_{\vec{s}}(\tau, 0)$, and a time interval τ_1, with $n\tau_1 = \tau$, for which the different scales in $B_{\vec{s}}(n\tau_1, (n-1)\tau_1)$ do not exceed machine precision. Since $B_{\vec{s}}(\tau, 0) = B_{\vec{s}}(n\tau_1, (n-1)\tau_1) \cdots B_{\vec{s}}(\tau_1, 0)$ we can evaluate $B_{\vec{s}}(\tau, 0)$ for $n = 2$ with:

$$B_{\vec{s}}(2\tau_1, \tau_1) \underbrace{B_{\vec{s}}(\tau_1, 0)}_{U_1 D_1 V_1} = \underbrace{((B_{\vec{s}}(2\tau_1, \tau_1)U_1)D_1)}_{U_2 D_2 V} V_1 = U_2 D_2 V_2 \tag{74}$$

where $V_2 = VV_1$. The parenthesis determine the order in which the matrix multiplication are to be done. In all operations, mixing of scales are avoided. After the multiplication with diagonal matrix D_1 scales are again separated with the used of the singular value decomposition.

Thus, for $B_{\vec{s}}(\tau, 0) = U_R D_R V_R$ and $B_{\vec{s}}(\beta, \tau) = V_L D_L U_L$ we have to invert:

$$\begin{pmatrix} I & V_L D_L U_L \\ -U_R D_R V_R & I \end{pmatrix}^{-1} =$$

$$\left[\begin{pmatrix} V_L & 0 \\ 0 & U_R \end{pmatrix} \underbrace{\begin{pmatrix} (V_R V_L)^{-1} & D_L \\ -D_R & (U_L U_R)^{-1} \end{pmatrix}}_{UDV} \begin{pmatrix} V_R & 0 \\ 0 & U_L \end{pmatrix} \right]^{-1} =$$

$$\left[\begin{pmatrix} (V_R)^{-1} & 0 \\ 0 & (U_L)^{-1} \end{pmatrix} V^{-1} \right] D^{-1} \left[U^{-1} \begin{pmatrix} (V_L)^{-1} & 0 \\ 0 & (U_R)^{-1} \end{pmatrix} \right] \tag{75}$$

In the above, all matrix multiplications are well defined. In particular, the matrix D contains only large scales since the matrices $(V_R V_L)^{-1}$ and $(U_L U_R)^{-1}$ act as a cutoff to the exponentially small scales in D_L and D_R. This method to compute Green functions is very stable and has the advantage of producing time displaced Green functions. However, it is numerically expensive since the matrices involved are twice as big as the B matrices.

Alternative methods to compute $G_{\vec{s}}(\tau)$ which involve matrix manipulations only of the size of B include:

$$\begin{aligned} (1 + B_{\vec{s}}(\tau, 0)B_{\vec{s}}(\beta, \tau))^{-1} &= (1 + U_R D_R V_R V_L D_L U_L)^{-1} \\ &= (U_L)^{-1} (\underbrace{(U_L U_R)^{-1} + D_R(V_R V_L)D_L}_{UDV})^{-1} U_R^{-1} \\ &= (VU_L)^{-1} D^{-1} (U_R U^{-1}). \end{aligned} \tag{76}$$

Again, $(U_L U_R)^{-1}$ acts as a cutoff to the small scales in $D_R(V_R V_L)D_L$ so that D contains only large scales.

The accuracy of both presented methods may be tested by in the following way. Given the Green function at time τ we can can upgrade and wrap (see Eq. (67)) this Green function to time slice $\tau + \tau_1$. Of course, for the time interval τ_1 the involved scales should lie within the accuracy of the the computer, $\sim 1^{-12}$ for double precision numbers. The thus obtained Green function at time $\tau + \tau_1$ may be compared to the one computed from scratch using Eq. (75) or Eq. (76). For a 4×4 half-filled Hubbard model at $U/t = 4$, $\beta t = 20$, $\Delta \tau t = 0.1$ and $\tau_1 = 10\Delta\tau$ we obtain an average (maximal) difference between the matrix elements of both Green functions of 1^{-10} (1^{-6}) which is orders of magnitude smaller than the statistical uncertainty. Had we chosen $\tau_1 = 50\Delta\tau$ the accuracy drops to 0.01 and 100.0 for the average and maximal differences.

3.5 Imaginary Time Displaced Green Functions

Imaginary time displaced correlation yield important information. On one hand they may be used to obtain spin and charge gaps[28, 29], as well quasiparticle weights[20]. On the other hand, with the use of the Maximum Entropy method[30, 31] dynamical properties such as spin and charge dynamical structure factors, optical conductivity, and single particle spectral functions may be computed. Those quantities offer the possibility of direct comparison with experiments, such as photoemission, neutron scattering and optical measurements.

Since there is again a Wick's theorem for time displaced correlation functions. it suffices to compute the single particle Green function for a given HS configuration. We will first start with the FTQMC and then concentrate on the PQMC.

3.5.1 FTQMC

For a given HS field, we wish to evaluate:

$$G_{\vec{s}}(\tau_1, \tau_2)_{x,y} = \langle T c_x(\tau_1) c_y^\dagger(\tau_2) \rangle_{\vec{s}} \tag{77}$$

where T corresponds to the time ordering. Thus for $\tau_1 > \tau_2$ $G_{\vec{s}}(\tau_1, \tau_2)_{x,y}$ reduces to

$$\langle c_x(\tau_1) c_y^\dagger(\tau_2) \rangle_{\vec{s}} = \frac{\text{Tr}\left[U_{\vec{s}}(\beta, \tau_1) c_x U_{\vec{s}}(\tau_1, \tau_2) c_y^\dagger U_{\vec{s}}(\tau_2, 0) \right]}{\text{Tr}\left[U_{\vec{s}}(\beta, 0) \right]}$$

$$= \frac{\text{Tr}\left[U_{\vec{s}}(\beta, \tau_2) U_{\vec{s}}^{-1}(\tau_1, \tau_2) c_x U_{\vec{s}}(\tau_1, \tau_2) c_y^\dagger U_{\vec{s}}(\tau_2, 0) \right]}{\text{Tr}\left[U_{\vec{s}}(\beta, 0) \right]} \tag{78}$$

Evaluating $U^{-1}(\tau_1, \tau_2) c_x U_{\vec{s}}(\tau_1, \tau_2)$ boils down to the calculation of

$$c_x(\tau) = e^{\tau \vec{c}^\dagger A \vec{c}} c_x e^{-\tau \vec{c}^\dagger A \vec{c}}$$

where A is an arbitrary matrix. Differentiating the above with respect to τ yields

$$\frac{\partial c_x(\tau)}{\partial \tau} = e^{\tau \vec{c}^\dagger A \vec{c}} \left[\vec{c}^\dagger A \vec{c}, c_x \right] e^{-\tau \vec{c}^\dagger A \vec{c}} = -\sum_z A_{x,z} c_z(\tau).$$

Thus,

$$c_x(\tau) = \left(e^{-A} \vec{c} \right)_x \quad \text{and similarly} \quad c_x^\dagger(\tau) = \left(\vec{c}^\dagger e^A \right)_x. \tag{79}$$

123

We can use the above equation successively to obtain:

$$U_{\vec{s}}^{-1}(\tau_1, \tau_2) c_x U_{\vec{s}}(\tau_1, \tau_2) = (B_{\vec{s}}(\tau_1, \tau_2)\vec{c})_x$$
$$U_{\vec{s}}^{-1}(\tau_1, \tau_2) c_x^\dagger U_{\vec{s}}(\tau_1, \tau_2) = \left(\vec{c}^\dagger B_{\vec{s}}^{-1}(\tau_1, \tau_2)\right)_x \quad (80)$$

Since B is a matrix and not an operator, we can pull it out of the trace in Eq. (78). Note that the above equation automatically leads to a Wick's theorem for time displaced Green function since the theorem holds for equal time quantities. Thus, we obtain the result:

$$G_{\vec{s}}(\tau_1, \tau_2)_{x,y} = \langle c_x(\tau_1) c_y^\dagger(\tau_2) \rangle_{\vec{s}} = B_{\vec{s}}(\tau_1, \tau_2) G_{\vec{s}}(\tau_2) \quad \tau_1 > \tau_2 \quad (81)$$

where $G_{\vec{s}}(\tau_1)$ is the equal time Green function computed previously. A similar calculation will yield for $\tau_2 > \tau_1$

$$G_{\vec{s}}(\tau_1, \tau_2)_{x,y} = -\langle c_y^\dagger(\tau_2) c_x(\tau_1) \rangle_{\vec{s}} = -\left(1 - G_{\vec{s}}(\tau_1)\right) B_{\vec{s}}^{-1}(\tau_2, \tau_1). \quad (82)$$

Returning to Eq. (73) we see that we have already computed the time displaced Green functions $G_{\vec{s}}(0, \tau)$ and $G_{\vec{s}}(\tau, 0)$ when discussing a stabilization scheme for the equal time Green functions. However, this calculation is expensive and is done only at times $\tau = n\tau_1$ where τ_1 is time scale on which all energy scales fit well on finite precision machines. To obtain the Green functions for arbitrary values of τ one uses the relations:

$$G_{\vec{s}}(0, \tau + \tau_2) = G_{\vec{s}}(0, \tau) B_{\vec{s}}^{-1}(\tau_2, \tau)$$
$$G_{\vec{s}}(\tau + \tau_2, 0) = B_{\vec{s}}(\tau_2, \tau) G_{\vec{s}}(\tau, 0) \quad (83)$$

where $\tau_2 < \tau_1$.

With the above method, we have access to all time displaced Green functions $G_{\vec{s}}(0, \tau)$ and $G_{\vec{s}}(\tau, 0)$. However, we do not use translation invariance in imaginary time. Clearly, using this symmetry in the calculation of time displaced quantities will reduce the fluctuations which may sometimes be desirable. A numerically expensive but elegant way of producing all time displaced Green functions has been proposed by Hirsch[32]. Let β be a multiple of τ_1, $l\tau_1 = \beta$ and τ_1 small enough so that the scales involved in $B_s(\tau + \tau_1, \tau)$ fit on finite precision machines. Using the definition $\tau_i = i\tau_1$ with $i = 1 \cdots l$ one can show:

$$\begin{pmatrix} 1 & 0 & . & 0 & B_{\vec{s}}(\tau_1, 0) \\ -B_{\vec{s}}(\tau_2, \tau_1) & 1 & 0 & . & 0 \\ 0 & -B_{\vec{s}}(\tau_3, \tau_2) & 1 & . & 0 \\ . & 0 & -B_{\vec{s}}(\tau_4, \tau_3) & . & . \\ . & . & 0 & . & . \\ . & . & . & . & \\ 0 & . & 0 & -B_{\vec{s}}(\tau_l, \tau_{l-1}) & 1 \end{pmatrix}^{-1} =$$

$$\begin{pmatrix} G_{\vec{s}}(\tau_1, \tau_1) & G_{\vec{s}}(\tau_1, \tau_2) & .. & G_{\vec{s}}(\tau_1, \tau_l) \\ G_{\vec{s}}(\tau_2, \tau_1) & G_{\vec{s}}(\tau_2, \tau_2) & .. & G_{\vec{s}}(\tau_2, \tau_l) \\ . & . & .. & . \\ G_{\vec{s}}(\tau_l, \tau_1) & G_{\vec{s}}(\tau_l, \tau_2) & .. & G_{\vec{s}}(\tau_l, \tau_l) \end{pmatrix} \quad (84)$$

The matrix to inverse is l times the size of the B matrices, and hence expensing to compute. It is worth noting that on vector machines the performance grows with growing vector size so that the above method can become attractive. Having computed the Green functions $G_{\vec{s}}(\tau_i, \tau_j)$ we can obtain Green functions on any two time slices by using equations of the type (83).

3.5.2 PQMC

Zero temperature time displaced Green functions are given by:

$$G_s \left(\Theta + \frac{\tau}{2}, \Theta - \frac{\tau}{2} \right)_{x,y} \tag{85}$$

$$= \frac{\langle \Psi_T | U_{\vec{s}} \left(2\Theta, \Theta + \frac{\tau}{2} \right) c_x U_{\vec{s}} \left(\Theta + \frac{\tau}{2}, \Theta - \frac{\tau}{2} \right) c_y^\dagger U_{\vec{s}}(\Theta - \frac{\tau}{2}, 0) | \Psi_T \rangle}{\langle \Psi_T | U_{\vec{s}}(2\Theta, 0) | \Psi_T \rangle}$$

$$= \left[B_{\vec{s}} \left(\Theta + \frac{\tau}{2}, \Theta - \frac{\tau}{2} \right) G_{\vec{s}} \left(\Theta - \frac{\tau}{2} \right) \right]_{x,y}$$

and

$$G_s \left(\Theta - \frac{\tau}{2}, \Theta + \frac{\tau}{2} \right)_{x,y} \tag{86}$$

$$= - \frac{\langle \Psi_T | U_{\vec{s}}(2\Theta, \Theta + \frac{\tau}{2}) c_y^\dagger U_{\vec{s}}(\Theta + \frac{\tau}{2}, \Theta - \frac{\tau}{2}) c_x U_{\vec{s}}(\Theta - \frac{\tau}{2}, 0) | \Psi_T \rangle}{\langle \Psi_T | U_{\vec{s}}(2\Theta, 0) | \Psi_T \rangle}$$

$$= - \left[\left(1 - G_{\vec{s}} \left(\Theta - \frac{\tau}{2} \right) \right) B_{\vec{s}}^{-1} \left(\Theta + \frac{\tau}{2}, \Theta - \frac{\tau}{2} \right) \right]_{x,y}.$$

Here $\tau > 0$ and we have used Eq. (80), as well as the equal time Green function (Eq. (39)). Two comments are in order. (i) For a given value of τ the effective projection parameter is $\Theta - \tau$. Thus, before starting a simulation, one has to set the maximal value of τ which will be considered, τ_M and the effective projection parameter $\Theta - \tau_M$ should be large enough to yield the ground state within the desired precision. (ii) In a canonical ensemble, the chemical potential is meaningless. However, when single particle Green functions are computed it is required to set the reference energy with regards to which a particle will be added or removed. In other words, it is the chemical potential which delimits photoemission from inverse photoemission. Thus, it is useful to have an estimate of this quantity if single particle or pairing correlations are under investigation. For observable such as spin-spin or charge- charge time displaced correlations this complication does not come into play since they are in the particle-hole channel.

We are now left with the problem of computing the Green functions. A direct multiplication of the equal time Green function with B matrices is unstable for larger values of τ. This can be understood in the framework of free electrons on a two-dimensional square lattice:

$$H = -t \sum_{<\vec{i},\vec{j}>} c_{\vec{i}}^\dagger c_{\vec{j}}, \tag{87}$$

where the sum runs over nearest-neighbors. For this Hamiltonian one has:

$$\langle \Psi_0 | c_{\vec{k}}^\dagger(\tau) c_{\vec{k}} | \Psi_0 \rangle = \exp \left(\tau (\epsilon_{\vec{k}} - \mu) \right) \langle \Psi_0 | c_{\vec{k}}^\dagger c_{\vec{k}} | \Psi_0 \rangle, \tag{88}$$

where $\epsilon_{\vec{k}} = -2t(\cos(\vec{k}\vec{a}_x) + \cos(\vec{k}\vec{a}_y))$, $\vec{a}_x$, $\vec{a}_y$ being the lattice constants. We will assume $|\Psi_0\rangle$ to be non-degenerate. In a numerical calculation the eigenvalues and eigenvectors of the above Hamiltonian will be known up to machine precision, ϵ. In the case $\epsilon_{\vec{k}} - \mu > 0$, $\langle \Psi_0 | c_{\vec{k}}^\dagger c_{\vec{k}} | \Psi_0 \rangle \equiv 0$. However, on a finite precision machine the later quantity will take a value of the order of ϵ. When calculating $\langle \Psi_0 | c_{\vec{k}}^\dagger(\tau) c_{\vec{k}} | \Psi_0 \rangle$ this roundoff error will be

blown up exponentially and the result for large values of τ will be unreliable. In Eq. (86) the B matrices play the role of the exponential factor $\exp\left(\tau(\epsilon_{\vec{k}} - \mu)\right)$ and the equal time Green functions correspond to $\langle \Psi_0 | c_{\vec{k}}^\dagger c_{\vec{k}} | \Psi_0 \rangle$. In the PQMC, the stability problem is much more severe than for free electrons since the presence of the time dependent HS field mixes different scales.

We present two methods to circumvent this problem. The first method is numerically expensive but has been used extensively and hence tested for many models[28]. The second method has recently been developed, is elegant, simple to implement and very cheap in CPU time[33].

The first method lies on the observation that introducing a large but finite temperature $T = 1/\beta$ stabilizes the calculation. For the free electrons:

$$\langle \Psi_0 | c_{\vec{k}}^\dagger(\tau) c_{\vec{k}} | \Psi_0 \rangle = \lim_{\beta \to \infty} \frac{\exp\left(\tau(\epsilon_{\vec{k}} - \mu)\right)}{1 + \exp\left(\beta(\epsilon_{\vec{k}} - \mu)\right)}. \tag{89}$$

Even if the eigenvalues are known only up to machine precision, the right hand side of the above equation for large but finite values of β is a numerically stable operation. To implement this idea in the PQMC, we use the fact that the trial wave function is a single Slater determinant. Thus, we can find a single particle Hamiltonian, $H_0 = \sum_{x,y} c_x^\dagger (h_0)_{x,y} c_y$, which has $|\Psi_T\rangle$ as a non-degenerate ground state. Hence the equation

$$
\begin{aligned}
G_{\vec{s}}\left(\Theta - \frac{\tau}{2}\right) &\equiv \frac{\langle \Psi_T | U_{\vec{s}}(2\Theta, \Theta - \frac{\tau}{2}) c_x c_y^\dagger U_{\vec{s}}(\Theta - \frac{\tau}{2}, 0) | \Psi_T \rangle}{\langle \Psi_T | U_{\vec{s}}(2\Theta, 0) | \Psi_T \rangle} \\
&= \lim_{\beta \to \infty} \frac{\mathrm{Tr}\left[e^{-\beta H_O} U_{\vec{s}}(2\Theta, \Theta - \frac{\tau}{2}) c_x c_y^\dagger U_{\vec{s}}(\Theta - \frac{\tau}{2}, 0) \right]}{\mathrm{Tr}\left[e^{-\beta H_O} U_{\vec{s}}(2\Theta, 0) \right]} \\
&= \lim_{\beta \to \infty} \left[1 + B_{\vec{s}}\left(\Theta - \frac{\tau}{2}, 0\right) e^{-\beta h_O} B_{\vec{s}}\left(2\Theta, \Theta - \frac{\tau}{2}\right) \right]_{x,y} \quad (90)
\end{aligned}
$$

is valid and yields a link between the FTQMC and PQMC, so that at finite but large values of β we can use the methods introduced for the FTQMC to compute time displaced Green functions. In particular, we can use the relation

$$
\lim_{\beta \to \infty} \begin{pmatrix} I & B_{\vec{s}}(\Theta - \frac{\tau}{2}, 0) e^{-\beta h_0} B_{\vec{s}}(2\Theta, \Theta + \frac{\tau}{2}) \\ -B_{\vec{s}}(\Theta + \frac{\tau}{2}, \Theta - \frac{\tau}{2}) & I \end{pmatrix}^{-1} =
$$

$$
\begin{pmatrix} G_{\vec{s}}(\Theta - \frac{\tau}{2}) & G_{\vec{s}}(\Theta - \frac{\tau}{2}, \Theta + \frac{\tau}{2}) \\ G_{\vec{s}}(\Theta + \frac{\tau}{2}, \Theta - \frac{\tau}{2}) & G_{\vec{s}}(\Theta + \frac{\tau}{2}) \end{pmatrix} \tag{91}
$$

where the Green functions refer to the PQMC Green functions of Eq. (86). To compute in a numerically stable way, similar methods to those applied for the FTQMC are used (see Eq. (75)). A convenient choice of H_0 is obtained in a basis where the trial wave function may be written as:

$$|\Psi_T\rangle = \prod_{n=1}^{N_p} \gamma_n^\dagger |0\rangle. \tag{92}$$

In this basis, we define H_0 through

$$H_0 \gamma_n^\dagger |0\rangle = \begin{cases} -\gamma_n^\dagger |0\rangle & \text{if } \gamma_n^\dagger \gamma_n |\Psi_T\rangle = |\Psi_T\rangle \\ +\gamma_n^\dagger |0\rangle & \text{if } \gamma_n^\dagger \gamma_n |\Psi_T\rangle = 0 \end{cases} \tag{93}$$

For the specific case of the Hubbard model and with the above choice of H_0 values of $\beta t \sim 40$ were well sufficient to satisfy Eq. (90) up to an average precision of 10^{-11}. Clearly this method is ad-hoc since it requires adding a *fictitious* temperature. Furthermore, since the upgrading is done with the PQMC, every time one wishes to compute time displaced correlation function all required quantities have to be computed from scratch.

A more elegant and efficient method rests on the observation that in the PQMC the Green function is a projector. Consider again the free electron case. For a non-degenerate Ground state, $\langle \Psi_0 | c_{\vec{k}}^\dagger c_{\vec{k}} | \Psi_0 \rangle = 0, 1$ so that

$$\langle \Psi_0 | c_{\vec{k}}^\dagger (\tau) c_{\vec{k}} | \Psi_0 \rangle = \left(\langle \Psi_0 | c_{\vec{k}}^\dagger c_{\vec{k}} | \Psi_0 \rangle \exp \left((\epsilon_{\vec{k}} - \mu) \right) \right)^\tau . \tag{94}$$

The above involves only well defined numerical manipulations even in the large τ limit provided that all scales fit onto finite precision machines for a unit time interval.

The implementation of this idea in the QMC algorithm is as follows. First, one has to notice that the Green function $G_{\vec{s}}(\tau)$ is a projector:

$$G_{\vec{s}}(\tau)^2 = G_{\vec{s}}(\tau). \tag{95}$$

We have already seen that for $P^\dagger B_{\vec{s}}(2\Theta, \tau) = V_L D_L U^\langle$ and $B_{\vec{s}}(\tau, 0) = U^\rangle D_R U_R$, $G_{\vec{s}}(\tau) = 1 - U^\rangle (U^\langle U^\rangle)^{-1} U^\langle$. Since

$$\left[U^\rangle (U^\langle U^\rangle)^{-1} U^\langle \right]^2 = U^\rangle (U^\langle U^\rangle)^{-1} U^\langle$$

we have:

$$G_{\vec{s}}^2(\tau) = G_{\vec{s}}(\tau) \text{ and } (1 - G_{\vec{s}}(\tau))^2 = 1 - G_{\vec{s}}(\tau). \tag{97}$$

This property implies that $G_{\vec{s}}(\tau_1, \tau_3)$ obeys a simple composition identity

$$G_{\vec{s}}(\tau_1, \tau_3) = G_{\vec{s}}(\tau_1, \tau_2) G_{\vec{s}}(\tau_2, \tau_1). \tag{98}$$

In particular for $\tau_1 > \tau_2 > \tau_3$

$$G_{\vec{s}}(\tau_1, \tau_3) = B_{\vec{s}}(\tau_1, \tau_3) G_{\vec{s}}^2(\tau_3) = G_{\vec{s}}(\tau_1, \tau_3) G_{\vec{s}}(\tau_3)$$
$$= \underbrace{G_{\vec{s}}(\tau_1, \tau_3) B_{\vec{s}}^{-1}(\tau_2, \tau_3)}_{G_{\vec{s}}(\tau_1, \tau_2)} \underbrace{B_{\vec{s}}(\tau_2, \tau_3) G_{\vec{s}}(\tau_3)}_{G_{\vec{s}}(\tau_2, \tau_3)}$$

A similar proof is valid for $\tau_3 > \tau_2 > \tau_1$

Using this composition property (98) we can break up a large τ interval into a set of smaller intervals of length $\tau = N \tau_1$ so that

$$G_{\vec{s}}\left(\Theta + \frac{\tau}{2}, \Theta - \frac{\tau}{2} \right) = \prod_{n=0}^{N-1} G_{\vec{s}}\left(\Theta - \frac{\tau}{2} + [n+1]\tau_1, \Theta - \frac{\tau}{2} + n\tau_1 \right) \tag{99}$$

The above equation is the generalization of Eq. (94). If τ_1 is *small* enough each Green function in the above product is accurate and has matrix elements bounded by order unity. The matrix multiplication is then numerically well defined.
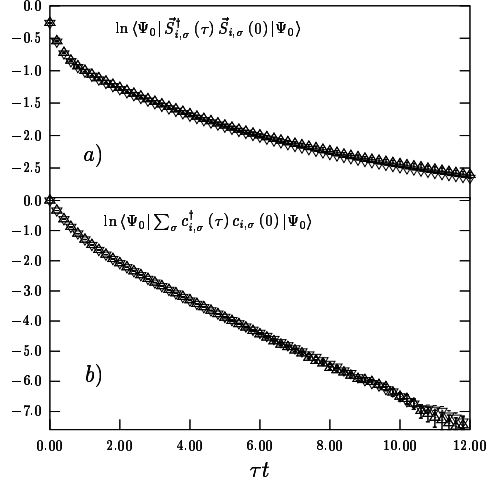
Figure 8. Imaginary time displaced on-site spin-spin (a) and Green function (b) correlation function. We consider a 6×6 lattice at half-filling and $J/t = 1.2$. In both (a) and (b) results obtained form Eq. (99) ($\triangle$) and (91) ($\bigtriangledown$) are plotted.

We conclude this section by comparing both presented approaches for the calculation of time displaced correlation functions in the PQMC. We consider the special case of the Kondo lattice model (see Fig. 8). As apparent the results are identical within error-bars. The important point however, is that the method based on Eq. (99) is for the considered case an order of magnitude quicker in CPU time than the method based on Eq. (91).

3.6 The Sign Problem

The sign problem remains the central challenge in QMC simulations of correlated electron systems. We have shown how it apears in the framework of the World Line algorithm for the case of free fermions with nearest and next nearest neighbor hopping. Since in the PQMC and FTQMC the one body terms are treated exactly the sign problem does not occur in this simple example. However, interactions will in many cases lead to a sign problem. Insight into the origin of the sign problem in the PQMC and FTQMC is obtained through the work of Fahy and Hamann[34, 35] which we will briefly review.

The starting point is to rewrite the imaginary time propagation of the trial wave function as diffusion equation in the space of Slater determinants:

$$\sum_{\vec{s}} U_{\vec{s}}(2\Theta, 0)|\Psi_T\rangle = \int \mathrm{d}\Psi f(\Psi, 2\Theta)|\Psi\rangle \qquad (100)$$

Since $U_{\vec{s}}(2\Theta, 0)$ is a one-body propagator in a time dependent external field, $U_{\vec{s}}(2\Theta, 0)|\Psi_T\rangle$ is a single Slater determinant (See Eq. (33)) so that the sum over the HS fields may be replaced by a weighted average over normalized Slater determinants $|\Psi\rangle$. Fahy and Hamann[34, 35], have shown that $f(\Psi, \tau)$ satisfies a diffusion type equation in the space of Slater determinants which is invariant under parity $|\Psi\rangle \rightarrow -|\Psi\rangle$. Thus, the solutions of the diffusion equations may be classified according to this symmetry:

$f^+(\Psi, \tau) = f^+(-\Psi, \tau)$ and $f^-(\Psi, \tau) = -f^-(-\Psi, \tau)$. The reader will convince himself that only f^- solutions contribute to the integral over Slater determinants. However, the integrand, $f(\Psi, \tau)$, is exponentially dominated by the even parity solutions $f^+(\Psi, \tau)$ of the diffusion equation[34,35]. Hence, the relevant odd parity solutions are exponentially damped in comparison to the even parity solutions. This leads to exponential increase of the signal to noise ratio.

Based on the above analysis, Fahy and Hamann have proposed a solution to the sign problem, which is referred to as positive projection[34]. Let us start the diffusion process with the trial wave function $|\Psi_T\rangle$ which we require - without loss of generality - to have positive overlap with the ground state: $\langle\Psi_0|\Psi_T\rangle > 0$. At infinitesimal time $\tau = \epsilon$ a population of Slater determinants $\{f(\Psi, \epsilon)|\Psi\rangle\}$ with $f(\Psi, 0) = \delta(\Psi - \Psi_T)$ is obtained. If one of those Slater determinants, $|\Psi_1\rangle$ at time $\tau = \epsilon$, is orthogonal to the ground state, $\langle\Psi_0|\Psi_1\rangle = 0$, it may be discarded since it will provide no information on the ground state at all times $\tau > \epsilon$. This may easily be seen since starting from $|\Psi_1\rangle$ the population of Slater determinants generated by the diffusion equation has zero overlap with the ground state:

$$\langle\Psi_0| \int d\Psi f(\Psi, \tau)|\Psi\rangle = \langle\Psi_0|e^{-(\tau-\epsilon)H}|\Psi_1\rangle = 0, \tag{101}$$

since $f(\Psi, \tau = \epsilon) = \delta(\Psi - \Psi_1)$ and $\langle\Psi_0|\Psi_1\rangle = 0$. The important point is that computed analytically the ensemble of Slater determinants originating from Ψ_1 cancel. It is the stochastic cancellation of those Slater determinants which lies at the origin of the sign problem. The above procedure is repeated iteratively and at each infinitesimal time step Slater determinants with $\langle\Psi_0|\Psi\rangle = 0$ are discarded. This procedure eliminates the exponential growth of the signal to noise ratio.

The above procedure is exact provided we know a-priori the surface $\mathcal{N}$ defined by: $\langle\Psi_0|\Psi\rangle = 0$. This information is in general not available. Thus, the positive projection scheme has to be implemented based on an approximate knowledge of $\mathcal{N}$. An implementation of this scheme has been carried out by[36,37] in an algorithm which is referred to as the constrained path QMC (CPQMC). However, a major drawback is that the surface $\mathcal{N}$ in the CPQMC is approximated by a single Slater determinant corresponding to a mean-field solution of the model under consideration. In contrast, the Green function method has the ability to incorporate optimized correlated wave functions as starting point for the fixed-node approximation.

There are nevertheless a set of problems where the sign problem may be avoided in FTQMC and PQMC. As we will see in the subsequent section, particle-hole symmetry allows us to avoid the sign problem. Furthermore, models with attractive interactions which couple independently to an internal symmetry with an even number of states lead to weights, for a given HS configuration, which are an even power of a single determinant. If the determinant itself is real (i.e. absence of magnetic fields), the overall weight will be positive. An example is the attractive Hubbard model.

4   Application of the Auxiliary Field QMC to Specific Hamiltonians

In this section, we will concentrate on applications of the FTQMC and PQMC. Both approaches involve a computational effort which scales as the cubed of the volume. This makes it hard to achieve very large lattice sizes. Hence the importance of reducing finite

size effects. Below we will describe a method which turns out to be extremely efficient for the case of free electrons where size effects are know to be severe[38]. We then show how to apply the FTQMC and PQMC to the attractive and repulsive Hubbard models, the Kondo-lattice model, hard core bosons and the Heisenberg model. It is beyond the scope of this article to review in detail the physics related to the models. We will concentrate primarily on the technical aspects. In most cases we have the two-dimensional case in mind, the generalization to higher or lower dimensions being straightforward.

4.1   Size Effects

Size effects become particularly severe when the ground state turns out to be a metallic state with large coherence temperature. On the other hand, insulators are characterized by the localization of the wave function and are hence rather insensitive to boundary conditions on finite sized systems. It thus becomes apparent, that the worst case scenario for severe size effects are just free electrons in a tight binding approximation:

$$H = -t \sum_{\langle \vec{i}, \vec{j} \rangle} c_{\vec{i}}^{\dagger} c_j + \text{H.c..} \tag{102}$$

In many cases before turning on the interaction which will automatically restrict the size of the lattice under consideration it is important to control size effects for this simple case. We will concentrate on the two dimensional case on a torus geometry which for the above model reduces to imposing periodic boundary conditions: $c_{\vec{i}+L\vec{e}_x}^{\dagger} = c_{\vec{i}}^{\dagger}, c_{\vec{i}+L\vec{e}_y}^{\dagger} = c_{\vec{i}}^{\dagger}$ where L is the linear length of the lattice lying in the $\vec{e}_x, \vec{e}_y$ plane.

To reduce size effects on thermodynamic quantities one may in principle consider the Hamiltonian:

$$H(L) = \sum_{\langle \vec{i}, \vec{j} \rangle} t_{\vec{i}, \vec{j}}(L) c_{\vec{i}}^{\dagger} c_j + \text{H.c.} \tag{103}$$

where $t_{\vec{i}, \vec{j}}(L)$ are arbitrary hopping parameters which have to satisfy

$$\lim_{L \to \infty} t_{\vec{i}, \vec{j}}(L) = -t. \tag{104}$$

Clearly this choice of hopping matrix elements on finite lattices will break the lattice symmetry. This is a price we are willing to pay provided that the convergence as a function of system size of thermodynamics quantities is greatly improved. Eq. (104) nevertheless guarantees that in the thermodynamic limit this symmetry is restored. To determine the hopping matrix elements $t_{\vec{i}, \vec{j}}(L)$ so as to reduce size effects on say the specific heat, $C_v(L, T) = \frac{\partial E(L)}{\partial T}$, one may minimize

$$\chi^2 = \sum_{T} [C_v(L, T) - C_v(L = \infty, T)]^2 \tag{105}$$

where the sum extends over a given range of temperatures. Taking into account only amplitude modulations of the hopping matrix elements leads already to a cumbersome minimization problem which does not provide satisfactory results.

Instead of carrying out a complicated minimization problem we can try to guess which matrix elements $t_{\vec{i}, \vec{j}}(L)$ will minimize size effects. It turns out that introducing a magnetic

field produces remarkable results. The magnetic field is introduced via the Peirls phase factors:

$$H(L) = -t \sum_{\langle \vec{i}, \vec{j} \rangle} e^{\frac{2\pi i}{\Phi_0} \int_{\vec{i}}^{\vec{j}} \vec{A}_L(\vec{l}) \cdot d\vec{l}} c_{\vec{i}}^{\dagger} c_j + \text{H.c.} \tag{106}$$

with $\vec{B}_L(\vec{x}) = \vec{\nabla} \times \vec{A}_L(\vec{x})$ and Φ_0 the flux quanta. The torus geometry imposes restrictions on the $\vec{B}_L$ field. Since, a translation in the argument of the vector potential may be absorbed in a gauge transformation:

$$\vec{A}_L(\vec{x} + L\vec{e}_x) = \vec{A}_L(\vec{x}) + \vec{\nabla}\chi_x(\vec{x}),$$
$$\vec{A}_L(\vec{x} + L\vec{e}_y) = \vec{A}_L(\vec{x}) + \vec{\nabla}\chi_y(\vec{x}), \tag{107}$$

we chose, the boundary condition

$$c_{\vec{i}+L\vec{e}_x}^{\dagger} = e^{\frac{2\pi i}{\Phi_0} \chi_x(\vec{i})} c_{\vec{i}}^{\dagger}, \quad c_{\vec{i}+L\vec{e}_y}^{\dagger} = e^{\frac{2\pi i}{\Phi_0} \chi_y(\vec{i})} c_{\vec{i}}^{\dagger} \tag{108}$$

to satisfy the requirement:

$$[H(L), T_{L\vec{e}_x}] = [H(L), T_{L\vec{e}_y}] = 0. \tag{109}$$

Here, $T_{\vec{x}}$ corresponds to a translation by $\vec{x}$. However, magnetic translation operators belong to the magnetic algebra[39]:

$$T_{L\vec{e}_x} T_{L\vec{e}_y} = e^{-i2\pi \frac{(L\vec{e}_x \times L\vec{e}_y) \cdot \vec{B}}{\Phi_0}} T_{L\vec{e}_y} T_{L\vec{e}_x}. \tag{110}$$

Thus, to obtain a single valued wave function the condition of flux quantization has to be satisfied: $\frac{(L\vec{e}_x \times L\vec{e}_y) \cdot \vec{B}}{\Phi_0} = n$ where n is an integer. Here, we consider a static magnetic field running along the z-axis perpendicular to the x, y plane in which the lattice lies. Hence, the smallest magnetic field which we can consider on a given lattice size satisfies:

$$\frac{BL^2}{\Phi_0} = 1. \tag{111}$$

With this choice of magnetic field and associated vector potential Eq. (104) holds.

To illustrate the reduction of size effects caused by the inclusion of the magnetic field, we first consider the single particle density of states. In a basis where $H(L)$ is diagonal, $H(L) = \sum_{n=1}^{N} \epsilon_n \gamma_n^{\dagger} \gamma_n$ with $c_n^{\dagger} = \sum_m \gamma_m^{\dagger} U_{m,n}^{\dagger}$ and $U^{\dagger} U = I$, the local density of states reads:

$$N(r, \omega) = \text{Im} \sum_n^N \frac{|U_{n,r}|^2}{\epsilon_n - \omega - i\delta} \tag{112}$$

where δ is a positive infinitesimal and N the total number of sites. Since the magnetic field breaks translation invariance (it is the site dependent vector potential which enters the Hamiltonian) $N(r, \omega)$ is site dependent. Averaging over sites yields the density of states $N(\omega)$ plotted in Fig. 9. As apparent, without the magnetic field and up to $L = 32$, $N(\omega)$ is dominated by size effects for the considered value of $\delta = 0.01t$. In contrast, the presence of the magnetic field provides remarkable improvements. In particular the van-Hove singularity is well reproduced already on $L = 16$ lattices and at $L = 32$ the result is next to exact for the considered value of δ. It is instructive to look at the $L = 8$ case
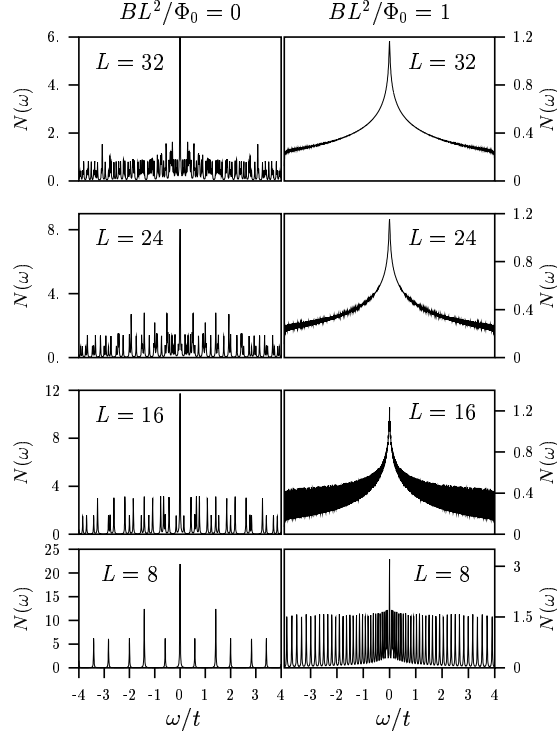
Figure 9. Density of states $N(\omega) = \frac{1}{N} \sum_r N(r, \omega)$ with (right column) and without (left column) magnetic field. Here, we consider $\delta = 0.01t$.

with and without magnetic fields. When B is turned on, the degeneracy of levels is lifted. Each level - apart from the $\epsilon_n = 0$ level which is two fold degenerate - is nondegenerate. This is precisely what one expects for Landau levels which have degeneracy $L^2 B/\Phi_0$ which is unity in our case. This provides an intuitive understanding of why the method works so well. Since each level becomes singly degenerate, the single particle states cover homogeneously the the energy range of the band-width. Clearly this can only be achieved by breaking the lattice symmetry on finite sized systems.

We now turn our attention to the specific heat coefficient $\gamma = C_v/T$ (see Fig. 10 a, b). As apparent, for a given system size, the inclusion of the magnetic field provides a gain of more than one order of magnitude in the temperature scale at which size effects set in. In particular the $\ln(1/T)$ behavior of γ due the the van-Hove singularity becomes apparent already on $L = 6$ lattices.

Upon inspection a similar improvement is obtained for the spin susceptibility (see Fig. 10 c, d). Note that since we are dealing with free electrons the charge and spin susceptibilities are identical.

One crucial question is whether the magnetic field will introduce a sign problem in the numerical simulations. It turns out that in some non-trivial cases is does not and we can hence benefit from the observed dramatic reduction in size effects. This method has been
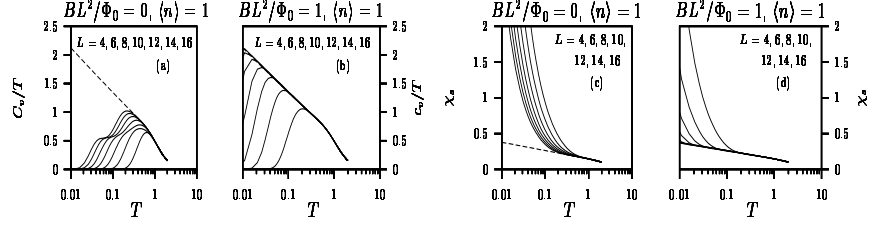
Figure 10. Specific and spin susceptibility versus temperature without (a,c) and with (b,d) magnetic field. The curves from right to left correspond to increasingly large lattices as denoted in the figure. The dashed line corresponds to the exact result.

used successfully in a depleted Kondo lattice model and has opened a whole temperature range where coherence effects may me studied without suffering from size effects[38].

Other schemes have been proposed to reduce size effects. In particular, averaging over boundary conditions has been suggested[40, 41]. This method has the advantage of not breaking translation symmetry. However, the averaging requires several simulations and is hence computationally expensive. In contrast with the presented method the improvement in reduction of size effects is obtained within a single simulation.

4.2 The Hubbard Model

The Hubbard model in a magnetic field is given by:

$$
H_U = -t \underbrace{\sum_{\langle \vec{i},\vec{j} \rangle,\sigma} e^{\frac{2\pi i}{\Phi_0} \int_{\vec{i}}^{\vec{j}} \vec{A}\cdot d\vec{l}} c_{\vec{i},\sigma}^\dagger c_{\vec{j},\sigma}}_{=\sum_{\vec{i},\vec{j},\sigma} c_{\vec{i},\sigma}^\dagger h_t(\vec{A})_{\vec{i},\vec{j}} c_{\vec{j},\sigma}} + U \sum_{\vec{i}} \left(n_{\vec{i},\uparrow} - 1/2 \right)\left(n_{\vec{i},\downarrow} - 1/2 \right) - \mu \sum_{\vec{i}} n_{\vec{i}}.
$$
(113)

We start by considering the $SU(2)$ invariant HS decoupling of Eq. (25). Since the HS field couples equivalently to up and down spins we obtain for the FTQMC:

$$
\text{Tr}\left[e^{-\beta(H-\mu N)} \right] = \sum_{\vec{s}} C_{\vec{s}} \det\left(1 + B_{\vec{s}}(\beta,0) \right)^2 \quad \text{with}
$$
(114)

$$
C_{\vec{s}} = \frac{1}{2^N} e^{\beta U N/4 - i\alpha \sum_{\vec{i},n} s_{\vec{i},n}}, \quad B(\beta,0) = \prod_{n=1}^{m} e^{h_I(\vec{s}_n)} e^{-\Delta\tau(h_t(\vec{A})-\mu)}.
$$

Here, $h_I(\vec{s}_n)_{\vec{i},\vec{j}} = \delta_{\vec{i},\vec{j}} i\alpha s_{\vec{i},n}$ and $\cos(\alpha) = \exp(-\Delta\tau U/2)$.

For the PQMC a trial wave function which factorizes in spin up and down sectors is usually chosen:

$$
|\Psi_T\rangle = |\Psi_T^\uparrow\rangle \otimes |\Psi_T^\downarrow\rangle, \quad |\Psi_T^\sigma\rangle = \prod_{y=1}^{N_p^\sigma} (\vec{c}_\sigma^\dagger P^\sigma)_y |0\rangle.
$$
(115)

Here, $N_p^\uparrow = N_p^\downarrow$ are the number of particles in the spin up and down sectors. Typically, the trial wave function is chosen to be the solution of the non-interacting system. Hence,

$$
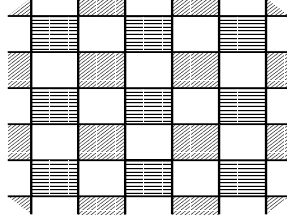P^\uparrow = P^\downarrow = P
$$
(116)

133

Figure 11. Checkerboard decomposition for the two dimensional square lattice with nearest neighbor hopping. $h_t^{(1)}$ ($h_t^{(2)}$) contains hopping processes along the boundaries of the horizontally (diagonally) shaded squares.

so that:

$$\langle \Psi_T | e^{2\Theta H} | \Psi_T \rangle = \sum_{\vec{s}} C_{\vec{s}} \det \left(P^\dagger B_{\vec{s}}(2\Theta, 0) P \right)^2 . \tag{117}$$

Replacing β by 2Θ and setting $\mu = 0$ in the above definitions of $B_{\vec{s}}(2\Theta, 0)$ and $C_{\vec{s}}$ yields the form of those quantities for the PQMC.

Before discussing separately the attractive ($U < 0$) and repulsive case ($U > 0$) let us comment on the matrix multiplication $e^{-\Delta \tau h_t(\vec{A})} C$ where C is an $N \times N$ matrix. A straightforward multiplication yields a computational cost scaling as N^3. To reduce this cost the checkerboard decomposition is often used. The matrix h_t is written as $h_t = h_t^{(1)} + h_t^{(2)}$ where $h_t^{(1)}$ and $h_t^{(2)}$ are sums of commuting four site hopping matrices: $h_t^{(1,2)} = \sum_{j=1}^{N/4} (h_t^{(1,2)})_j$ (See Fig. 11). Thus the the multiplication

$$e^{-\Delta \tau h_t} A = e^{-\Delta \tau h_t^{(1)}} e^{-\Delta \tau h_t^{(2)}} A + \mathcal{O}(\Delta \tau^2) \tag{118}$$

$$= \prod_{i=1}^{N/4} e^{-\Delta \tau (h_t^{(1)})_i} \prod_{j=1}^{N/4} e^{-\Delta \tau (h_t^{(2)})_j} A + \mathcal{O}(\Delta \tau^2)$$

Since $(h_t^{(1,2)})_j$ involves hopping on four sites irrespective of the lattice size, the matrix multiplication $e^{-\Delta \tau (h_t^{(1,2)})_j} A$ scales as N. Hence the overall matrix multiplication scales as N_s^2. Since the systematic error involved in the Trotter decomposition is already of order $\Delta \tau^2$ the above checkerboard decomposition does not introduce a new source of errors. However we have gained a power in the computational cost.

4.2.1 $U < 0$

The attractive Hubbard model has generated considerable interest since i) in two dimensions it shows a Kosterlitz-Thouless transition to an s-wave superconducting state[42, 43] and ii) in the strong coupling limit pairs form at a temperature scale roughly set by U whereas the Kosterlitz-Thouless transition is expected to scale as t^2/U. Hence, the model offers the possibility of studying the physics of a metallic state whith preformed pairs, a subject of interest in the context of high T_c superconductivity[44].

When $U < 0$, α in Eq. (114) is a pure imaginary number so that in the absence of magnetic fields, the determinant is real. Since the weight is the square of a real number it
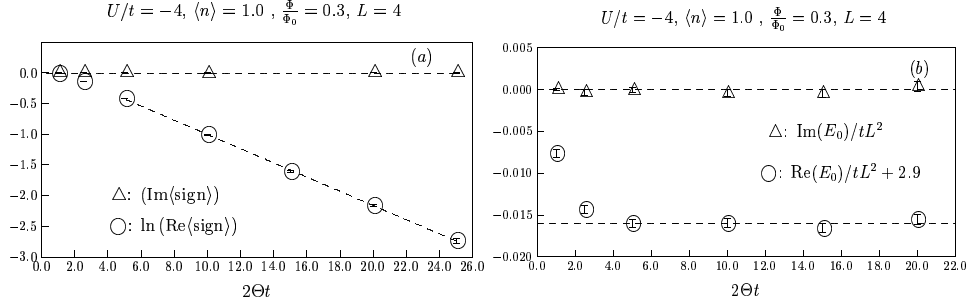
Figure 12. (a) Real and imaginary part of the average sign. Within the error-bars the imaginary part vanishes and the real part decays exponentially with the projection parameter Θ. (b) Real and imaginary part of the energy as a function of Θ. For a single HS configuration, the imaginary part of the energy is non-zero. Only after averaging does it vanish. In this case, the sign problem is not severe, since convergence to the ground state is achieved before the average sign becomes prohibitly small.

is positive and hence no sign problem occurs. In the weak coupling limit or BCS regime, the simulations perform well. However, in the strong coupling limit the method suffers from long autocorrelation times.

In the presence of a magnetic field, a sign problem occurs since the determinant becomes complex. We illustrate this point as well as the behavior of the sign problem when the product of determinants is complex by considering a vector potential $\vec{A}(\vec{x}) = \Phi \vec{e}_x / L$ at $\Phi = 0.3\Phi_0$. Such a vector potential introduces a twist in the boundary conditions which corresponds to nothing but threading a magnetic field with flux Φ through the torus on which lies the electronic system. This may be used to probe for flux quantization as well as a Kosterlitz-Thouless transition[43]. Note that insulating states may equally be determined by such a construction[45,25]. For this choice of $\vec{A}$, the fermionic determinant is complex. Hence in the framework of the PQMC and following Eq. (13), observables are evaluated with:

$$\langle O \rangle = \frac{\sum_{\vec{s}} \overline{\mathrm{Pr}}_{\vec{s}} \mathrm{sign}(\vec{s}) \langle O \rangle_{\vec{s}}}{\sum_{\vec{s}} \overline{\mathrm{Pr}}_{\vec{s}} \mathrm{sign}(\vec{s})} \qquad \text{where} \tag{119}$$

$$\mathrm{sign}(\vec{s}) = \frac{\det \left(P^\dagger B_{\vec{s}}(2\Theta, 0) P \right)^2}{|\det \left(P^\dagger B_{\vec{s}}(2\Theta, 0) P \right)^2 |}, \quad \overline{\mathrm{Pr}}_{\vec{s}} = \frac{|\det \left(P^\dagger B_{\vec{s}}(2\Theta, 0) P \right)^2 |}{\sum_{\vec{s}} |\det \left(P^\dagger B_{\vec{s}}(2\Theta, 0) P \right)^2 |}.$$

For a given HS configuration $\mathrm{sign}(\vec{s}) = e^{-i\phi(\vec{s})}$. After summation over the HS fields, the average sign, $\langle \mathrm{sign} \rangle = \sum_{\vec{s}} \overline{\mathrm{Pr}}_{\vec{s}} \mathrm{sign}(\vec{s})$ is a real quantity. This follows from

$$\langle \mathrm{sign} \rangle = \frac{\langle \Psi_T | e^{-2\Theta H} | \Psi_T \rangle}{\sum_{\vec{s}} |\det \left(P^\dagger B_{\vec{s}}(2\Theta, 0) P \right)^2 |} + \mathcal{O}(\Delta\tau^2) \tag{120}$$

and the fact that H is hermitian so that the numerator is a real quantity. [e] This property gives us a nice internal check for the validity of Monte Carlo sampling. As shown in Fig. (12) the real part of the average sign decays exponentially with the projection parameter Θ.

---

[e]This property equally holds for finite values of $\Delta\tau$ since the kinetic and potential terms in H as well as the trial wave function are real representable in Fourier space.

4.2.2 $U > 0$

The repulsive Hubbard model is given by Eq. (113) with $U > 0$. At half-filling the Hubbard model describes a Mott insulator with long range antiferromagnetic order. The nature of the metallic state in the vicinity of the Mott insulator as well as the metal-insulator transition as a function of doping has attracted considerable recent interest in particular in conjunction with high T_c superconductors[46].

For $U > 0$, α in Eq. (114) is a real number so that the determinant is a complex quantity and hence a sign problem occurs. In the special case of half-filling, $\mu = 0$ in Eq. (113), the model is particle-hole symmetric. This symmetry allows us to avoid the sign-problem. The particle-hole transformation reads.

$$\mathcal{P}^{-1} c^{\dagger}_{\vec{i},\sigma} \mathcal{P} = (-1)^{i_x + i_y} c^{\dagger}_{\vec{i},\sigma}. \tag{121}$$

where $\vec{i} = (i_x, i_y)$. Note that the Hamiltonian (113) at $\mu = 0$ is invariant under a combined time reversal and particle-hole transform due to the presence of the vector potential. Using the notation of Eq. (114):

$$\mathcal{P}^{-1} H_t \mathcal{P} \equiv \mathcal{P}^{-1} \vec{c}^{\dagger}_{\sigma} h_t(\vec{A}) \vec{c}_{\sigma} \mathcal{P} = \vec{c}^{\dagger}_{\sigma} \overline{h_t(\vec{A})} \vec{c}_{\sigma} \quad \text{and} \tag{122}$$
$$\mathcal{P}^{-1} H_I(\vec{s}_n) \mathcal{P} \equiv \mathcal{P}^{-1} \vec{c}^{\dagger}_{\sigma} h_I(\vec{s}_n) \vec{c}_{\sigma} \mathcal{P} = \sum_{\vec{i}} i\alpha s_{\vec{i},n} + \vec{c}^{\dagger}_{\sigma} \overline{h_I(\vec{s}_n)} \vec{c}_{\sigma}.$$

Thus

$$\det(1 + B_{\vec{s}}(\beta, 0)) = \text{Tr}\left[\prod_{n=1}^{m} e^{H_I(\vec{s}_n)} e^{-\Delta\tau H_t} \right]$$

$$= \text{Tr}\left[\prod_{n=1}^{m} e^{\mathcal{P}^{-1} H_I(\vec{s}_n)\mathcal{P}} e^{-\Delta\tau \mathcal{P}^{-1} H_t \mathcal{P}} \right]$$

$$= e^{\sum_{\vec{i},n} i\alpha s_{\vec{i},n}} \det(1 + \prod_{n=1}^{m} e^{\overline{h_I(\vec{s}_n)}} e^{-\Delta\tau \overline{h_t(\vec{A})}})$$

$$= e^{\sum_{\vec{i}} i\alpha s_{\vec{i},n}} \overline{\det(1 + B_{\vec{s}}(\beta, 0))} \tag{123}$$

and hence $C_{\vec{s}} \det\left(1 + B_{\vec{s}}(\beta, 0)\right)^2$ (see Eq. (114)) is a positive quantity even in the presence of a magnetic field. More generally, the above is valid for a half-filled Hubbard model on bipartite lattice [f] with inter-sublattice single-electron hopping. Thus, and for example, simulations on a half-filled honnneycomb lattice are sign free and show Mott semi-metal-insulator transitions[47].

Away from half-filling the sign problem sets in and turns out to be rather severe with the use of the HS transformation of Eq. (25). It is then more efficient to consider the HS which couples to the magnetization (24) to obtain:

$$\text{Tr} e^{-\beta(H - \mu N)} = C \sum_{\vec{s}} \det\left(1 + B^{\uparrow}_{\vec{s}}(\beta, 0)\right) \det\left(1 + B^{\downarrow}_{\vec{s}}(\beta, 0)\right) \quad \text{with}$$

$$C = e^{\beta U N/4} 2^N, \quad B^{\sigma}_{\vec{s}}(\beta, 0) = \prod_{n=1}^{m} e^{h^{\sigma}_I(\vec{s}_n)} e^{-\Delta\tau(h_t(\vec{A}) - \mu)} \tag{124}$$

---

[f] The lattice sites of a bipartite lattice may be split into two sublattices, A and B such that the nearest neighbors of any site in A belong to B.
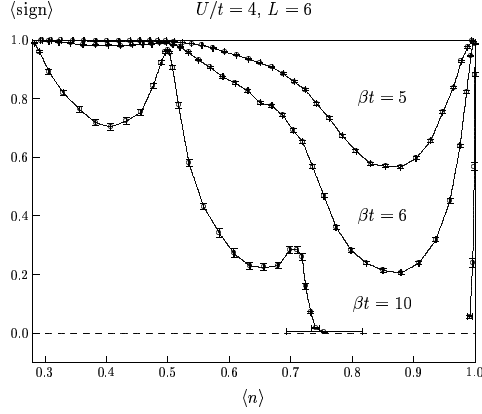
Figure 13. Average sign versus band filling $\langle n \rangle$ on a 6×6 lattice at $U/t = 4$. Filled shells are present at $\langle n \rangle = 26/36$ and $\langle n \rangle = 18/36$. As apparent for those band fillings, the decay of the average sign is slow.

with $(h_I^\sigma(\vec{s}_n))_{\vec{i},\vec{j}} = \delta_{\vec{i},\vec{j}} \sigma \tilde{\alpha} s_{\vec{i},n}$. In a very similar manner as above, one will show that for the particle-hole symmetric case the sign problem does not occur since: $\det(1 + B_{\vec{s}}^\uparrow(\beta, 0)) = e^{\sum_{\vec{i}, \sigma \tilde{\alpha} s_{\vec{i},n}}} \overline{\det(1 + B_{\vec{s}}^\downarrow(\beta, 0))}$. Fig. 13 plots the average sign as a function of electronic density for the HS transformation (24). As apparent, it is most severe at low dopings. In general, when the average sign drops below 0.1 accurate simulations become prohibitly expensive. One will notice that the average sign decays more slowly for special band fillings. Those band fillings corresponds to filled shells for which the solution of the non-interacting system is non-degenerate. The dependence of the average sign on different choices of the HS decoupling has been considered in[48].

For the PQMC, we again assume that the trial wave function factorizes in spin up and spin down sectors (115). With the HS transformation (24) we obtain:

$$\langle \Psi_T | e^{-2\Theta H} | \Psi_T \rangle = C \sum_{\vec{s}} \prod_\sigma \det \left(P^{\sigma,\dagger} B_{\vec{s}}^\sigma(2\Theta, 0) P^\sigma \right) \qquad (125)$$

with similar definitions for $B_{\vec{s}}^\sigma$ as for the FTQMC. At half-filling, the sign problem may again be avoided provided that the trial wave function is appropriately chosen. It is convenient to require the trial wave function to be a non-degenerate ground state of a given single-particle Hamiltonian $H_0 = H_0^\uparrow + H_0^\downarrow$ with,

$$H_0^\sigma = \sum_\sigma \vec{c}_\sigma^\dagger T_0^\sigma \vec{c}_\sigma. \qquad (126)$$

Using Eq. (90) to relate the PQMC to the FTQMC and following Eq. (123) the sign problem is absent provided that:

$$P^{-1} \vec{c}_\uparrow^\dagger T_0^\uparrow c_\uparrow P = \vec{c}_\uparrow^\dagger \overline{T_0^\downarrow} \vec{c}_\uparrow + C \qquad (127)$$

where C is a constant.

The choice of the trial wave function is important. Quick convergence as a function of projection parameter Θ is the measure for the quality of the trial wave function. Away from half-band filling when the sign problem sets in, it is important to reach convergence

quickly before the average sign becomes prohibitively small. In the PQMC, different symmetry sectors may be probed independently by judiciously choosing the trial wave function. An example where symmetry considerations are important is the half-filled Hubbard model. The ground state at this band-filling has long-range antiferromagnetic order. This continuous symmetry breaking is accompanied by gapless spin excitations: spin waves. On finite size lattices, however, spin symmetry is not broken, and the ground state is a spin singlet with an energy gap to spin excitations set by v_s/L where v_s is the spin-wave velocity and L the linear size of the lattice. Choosing a spin-singlet trial wave function is a good starting point since it is orthogonal to the low lying spin excitations. Hence, they do not have to be filtered out at great cost (see Fig. 14). To generate a spin singlet trail wave function we consider the non-interacting Hamiltonian:

$$H_0 = \sum_{\langle \vec{i}, \vec{j} \rangle, \sigma} \left(t_{\vec{i}, \vec{j}} c_{\vec{i}, \sigma}^{\dagger} c_{\vec{j}, \sigma} + \text{H.c.} \right) \tag{128}$$

where $\langle \vec{i}, \vec{j} \rangle$ is a sum over nearest neighbors and

$$t_{\vec{i}, \vec{i}+\vec{a}_x} = \left\{ \begin{array}{ll} -t(1+\delta) & \text{if } i_x = 2n+1 \\ -t(1-\delta) & \text{if } i_x = 2n \end{array} \right. , \quad t_{\vec{i}, \vec{i}+\vec{a}_y} = -t(1+\delta) \tag{129}$$

with $\delta << t$. The dimerization δ leads to a non-degenerate ground state at half band-filling and hence to a spin singlet ground state which we use as trial wave function $|\Psi_T\rangle$:

$$\vec{S}^2 |\psi_T\rangle = 0, \quad \text{with} \quad \vec{S} = \sum_{\vec{i}} \vec{S}_{\vec{i}} \tag{130}$$

and $\vec{S}_{\vec{i}}$ is the spin operator on site $\vec{i}$. This trial wave function was used to produce the data of Fig. 6.

Unrestricted Hartree Fock solutions may be used as trial wave functions. In contrast to the above, those trial wave functions have overlaps with all symmetry sectors. However, this choice of trial wave function optimizes the overlap with the ground state. At finite dopings, those trial wave functions have been discussed in[49].

4.3 Periodic Anderson and Kondo Lattice Models

The Kondo lattice model (KLM) as well as the periodic Anderson model (PAM) are the prototype Hamiltonians to describe heavy fermion materials[50] and Kondo insulators[51]. The physics under investigation is that of a lattice of magnetic impurities embedded in a metallic host. The symmetric PAM reads:

$$H_{PAM} = \sum_{\vec{k}, \sigma} \varepsilon(\vec{k}) c_{\vec{k}, \sigma}^{\dagger} c_{\vec{k}, \sigma} - V \sum_{\vec{i}, \sigma} \left(c_{\vec{i}, \sigma}^{\dagger} f_{\vec{i}, \sigma} + f_{\vec{i}, \sigma}^{\dagger} c_{\vec{i}, \sigma} \right)$$
$$+ U_f \sum_{\vec{i}} \left(n_{\vec{i}, \uparrow}^{f} - 1/2 \right) \left(n_{\vec{i}, \downarrow}^{f} - 1/2 \right). \tag{131}$$

The unit cell, denoted by $\vec{i}$, contains an extended and a localized orbitals. The fermionic operators $c_{\vec{k}, \sigma}^{\dagger}$ ($f_{\vec{k}, \sigma}^{\dagger}$) create electrons on extended (localized) orbitals with wave vector $\vec{k}$ and $z-$component of spin σ. The overlap between extended orbitals generates a conduction

band with dispersion relation $\varepsilon(\vec{k})$. There is a hybridization matrix element, V, between both orbitals in the unit-cell and the Coulomb repulsion- modeled by a Hubbard U_f- is taken into account on the localized orbitals. In the limit of large U_f, charge fluctuations on the localized orbitals are suppressed and the PAM maps onto the KLM[52]:

$$H_{KLM} = \sum_{\vec{k},\sigma} \varepsilon(\vec{k}) c^{\dagger}_{\vec{k},\sigma} c_{\vec{k},\sigma} + J \sum_{\vec{i}} \vec{S}^c_{\vec{i}} \cdot \vec{S}^f_{\vec{i}}. \tag{132}$$

Here $\vec{S}^c_{\vec{i}} = \frac{1}{2} \sum_{s,s'} c^{\dagger}_{\vec{i},s} \vec{\sigma}_{s,s'} c_{\vec{i},s'}$, where $\vec{\sigma}$ are the Pauli $s = 1/2$ matrices. A similar definition holds for $\vec{S}^f_{\vec{i}}$. A magnetic energy scale $J = 8V^2/U$ emerges and there is a constraint of one electron per localized orbital.

It is beyond the scope of this review to discuss the physics of the PAM and KLM. The interested reader is referred to[53]. Here we concentrate only on the technical aspects involved in the simulations. Simulations of the PAM are identical to those for the repulsive Hubbard model[54]. Again, at half-filling, the sign problem is absent due to the underlying particle-hole symmetry.

Simulation of the KLM on the other hand have up to recently been plagued by the sign-problem even in the case of half-filling where the model is invariant under particle-hole transformation[55,56]. To achieve a sign-free formulation of the problem[29] in the half-filled case we first consider the Hamiltonian:

$$H = \sum_{\vec{k},\sigma} \varepsilon(\vec{k}) c^{\dagger}_{\vec{k},\sigma} c_{\vec{k},\sigma} - \frac{J}{4} \sum_{\vec{i}} \left[\sum_{\sigma} c^{\dagger}_{\vec{i},\sigma} f_{\vec{i},\sigma} + f^{\dagger}_{\vec{i},\sigma} c_{\vec{i},\sigma} \right]^2. \tag{133}$$

With the use of the HS transformation of Eq. (25) to decouple the perfect square term a QMC algorithm may readily be formulated for the above model. Without constraints on the Hilbert space, the reader will easily persuade himself that the sign problem does not occur since we are dealing with an attractive interaction ($J > 0$) which couples to an internal symmetry – the spin – with an even number of states. We will see that the constraint of single occupancy on f-sites leads to a sign problem away from half-filling.

To see how H relates to H_{KLM} we compute the square in Eq. (133) to obtain:

$$H = \sum_{\vec{k},\sigma} \varepsilon(\vec{k}) c^{\dagger}_{\vec{k},\sigma} c_{\vec{k},\sigma} + J \sum_{\vec{i}} \vec{S}^c_{\vec{i}} \cdot \vec{S}^f_{\vec{i}} \tag{134}$$

$$- \frac{J}{4} \sum_{\vec{i},\sigma} \left(c^{\dagger}_{\vec{i},\sigma} c^{\dagger}_{\vec{i},-\sigma} f_{\vec{i},-\sigma} f_{\vec{i},\sigma} + \text{H.c.} \right) + \frac{J}{4} \sum_{\vec{i}} \left(n^c_{\vec{i}} n^f_{\vec{i}} - n^c_{\vec{i}} - n^f_{\vec{i}} \right).$$

As apparent, there are only pair-hopping processes between the f- and c-sites. Thus the total number of doubly occupied and empty f-sites is a conserved quantity:

$$[H, \sum_{\vec{i}} (1 - n^f_{\vec{i},\uparrow})(1 - n^f_{\vec{i},\downarrow}) + n^f_{\vec{i},\uparrow} n^f_{\vec{i},\downarrow}] = 0. \tag{135}$$

If we denote by Q_n the projection onto the Hilbert space with $\sum_{\vec{i}} (1 - n^f_{\vec{i},\uparrow})(1 - n^f_{\vec{i},\downarrow}) + n^f_{\vec{i},\uparrow} n^f_{\vec{i},\downarrow} = n$ then:

$$H Q_0 = H_{KLM} + \frac{JN}{4} \tag{136}$$

since in the Q_0 subspace the f-sites are singly occupied and hence the pair-hopping term vanishes. Thus, it suffices to choose

$$Q_0|\Psi_T\rangle = |\Psi_T\rangle \qquad (137)$$

to ensure that

$$\frac{\langle\Psi_T|e^{-\Theta H}Oe^{-\Theta H}|\Psi_T\rangle}{\langle\Psi_T|e^{-2\Theta H}|\Psi_T\rangle} = \frac{\langle\Psi_T|e^{-\Theta H_{KLM}}Oe^{-\Theta H_{KLM}}|\Psi_T\rangle}{\langle\Psi_T|e^{-2\Theta H_{KLM}}|\Psi_T\rangle}. \qquad (138)$$

To obtain a trial wave function which satisfies the requirements $Q_0|\Psi_T\rangle = |\Psi_T\rangle$ we are forced to choose H_0 of the form:

$$H_0 = \sum_{\langle \vec{i},\vec{j}\rangle,\sigma} \left(t_{\vec{i},\vec{j}} c_{\vec{i},\sigma}^\dagger c_{\vec{j},\sigma} + \text{H.c.} \right) + h_z \sum_{\vec{i}} e^{i\vec{Q}\cdot\vec{i}} \left(f_{\vec{i},\uparrow}^\dagger f_{\vec{j},\uparrow} - f_{\vec{i},\downarrow}^\dagger f_{\vec{j},\downarrow} \right) \qquad (139)$$

which generates a Néel state ($\vec{Q} = (\pi,\pi)$) on the localized orbitals. and the hopping matrix elements satisfy Eq. (129). With this choice of the trial wave function and the definition of the particle-hole transformation

$$\mathcal{P}^{-1} c_{\vec{i},\sigma}^\dagger \mathcal{P} = (-1)^{i_x+i_y} c_{\vec{i},\sigma}^\dagger$$

$$\mathcal{P}^{-1} f_{\vec{i},\sigma}^\dagger \mathcal{P} = -(-1)^{i_x+i_y} f_{\vec{i},\sigma}^\dagger$$

one may readily show the absence of sign problem at half-filling.

Although attractive, the above approach turns out to be (i) numerically inefficient and (ii) restricted to the PQMC. In the half-filled case, the principle source of inefficiency lies in the coupled constraints, $Q_0|\Psi_T\rangle = |\Psi_T\rangle$ and $|\Psi_T\rangle$ is a Slater determinant factorizable in the spin indices which inhibits the choice of a spin singlet trial wave function. Since the ground state is known to be a spin singlet on finite lattices[57,58] convergence is bad especially in the small J/t limit for which the ground state has long-range antiferromagnetic order, with small spin-wave velocity.

To alleviate both problems we relax the constraint $Q_0|\Psi_T\rangle = |\Psi_T\rangle$ and add a Hubbard term on the f-sites to the Hamiltonian:

$$H = \sum_{\vec{k},\sigma} \varepsilon(\vec{k}) c_{\vec{k},\sigma}^\dagger c_{\vec{k},\sigma} - \frac{J}{4} \sum_{\vec{i}} \left[\sum_\sigma c_{\vec{i},\sigma}^\dagger f_{\vec{i},\sigma} + f_{\vec{i},\sigma}^\dagger c_{\vec{i},\sigma} \right]^2$$

$$+ U_f \sum_{\vec{i}} (n_{\vec{i},\uparrow}^f - 1/2)(n_{\vec{i},\downarrow}^f - 1/2) \qquad (140)$$

This Hamiltonian is again block diagonal in the Q_n subspaces. During the imaginary time propagation, the components $Q_n|\Psi_T\rangle$ of the trial wave function will be suppressed by a factor $e^{-\Theta U_f n/2}$ in comparison to the component $Q_0|\Psi_T\rangle$.

To incorporate the Hubbard term in the QMC simulation the HS transformation of Eq. (25) is recommended at least for the half filled case. Having relaxed the constraint $Q_0|\Psi_T\rangle = |\Psi_T\rangle$ we are now free to choose a spin singlet trial wave function which we generate from:

$$H_0 = \sum_{\vec{k},\sigma} \varepsilon(\vec{k}) c_{\vec{k},\sigma}^\dagger c_{\vec{k},\sigma} - \frac{J}{4} \sum_{\vec{i},\sigma} (c_{\vec{i},\sigma}^\dagger f_{\vec{i},\sigma} + f_{\vec{i},\sigma}^\dagger c_{\vec{i},\sigma}) \qquad (141)$$
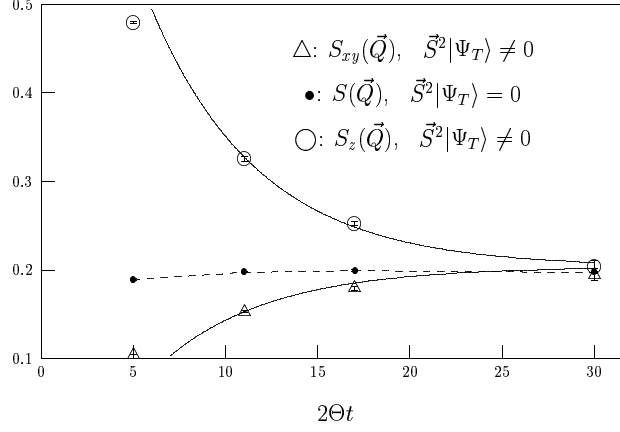
$$L = 4,\ J/t = 1.6$$

Figure 14. Spin-spin correlations as a function of the projection parameter Θ. Here, $S(\vec{Q}) = \frac{4}{3}\langle \vec{S}^f(\vec{Q}) \cdot \vec{S}^f(-\vec{Q})\rangle$, $S_z^f(\vec{Q}) = 4\langle \vec{S}_z^f(\vec{Q}) \cdot \vec{S}_z^f(-\vec{Q})\rangle$, and $S_{xy}^f(\vec{Q}) = 2\left(\langle \vec{S}_x^f(\vec{Q}) \cdot \vec{S}_x^f(-\vec{Q})\rangle + \langle \vec{S}_y^f(\vec{Q}) \cdot \vec{S}_y^f(-\vec{Q})\rangle\right)$. The trial wave function with $\vec{S}^2|\Psi_T\rangle \neq 0$ ($\vec{S}^2|\Psi_T\rangle = 0$) corresponds to the ground state of the Hamiltonian in Eq. (141) (Eq. (139)). In the *large* Θ limit, the results are independent on the choice of the trial wave function. In particular, starting from a broken symmetry state the symmetry is restored at *large* values of Θt. For this system, the spin gap is given by $\Delta_{sp} = 0.169 \pm 0.004$[29]. Starting with a trial wave function with $\vec{S}^2|\Psi_T\rangle \neq 0$, convergence to the ground state follows approximatively the form: $a + be^{-\Delta_{sp}2\Theta}$. The solid lines correspond to a least square fit to this form.

which is nothing but the non-interacting PAM with hybridization $V = J/4$. The ground state at half-filling is clearly a spin singlet. With this choice of the trial wave function, HS transformations of Eqn. (25), (28) as well as the particle-hole transformation of Eq. (140) the absence of sign problem in the half-filled case is readily shown for $J > 0$.

Fig. 14 demonstrates the importance of using a spin singlet trial wave function. Starting from a Néel order for the f-electrons (See Eq. (139)) convergence to the ground state follows approximatively $e^{-\Delta_{sp}2\Theta}$ where Δ_{sp} corresponds to the spin-gap. When the spin gap is small, convergence is poor and the remedy is to consider a spin singlet trial wave function.

It is equally possible to consider the ferromagnetic exchange $J < 0$. To achieve a sign free simulation at least at half-filling we define the particle hole transformation as

$$\mathcal{P}^{-1}c_{\vec{i},\sigma}^{\dagger}\mathcal{P} = (-1)^{i_1+i_2}c_{\vec{i},\sigma}^{\dagger}$$
$$\mathcal{P}^{-1}f_{\vec{i},\sigma}^{\dagger}\mathcal{P} = (-1)^{i_1+i_2}f_{\vec{i},\sigma}^{\dagger}$$

in conjunction with a trial wave function generated by the non-interacting Hamiltonian

$$H_0 = \sum_{\vec{k},\sigma}\varepsilon(\vec{k})c_{\vec{k},\sigma}^{\dagger}c_{\vec{k},\sigma} - \frac{J}{4}\sum_{\langle \vec{i},\vec{j}\rangle,\sigma}(c_{\vec{i},\sigma}^{\dagger}f_{\vec{j},\sigma} + f_{\vec{j},\sigma}^{\dagger}c_{\vec{i},\sigma}) \tag{142}$$

leads to a sign free simulation for the ferromagnetic half-filled case.

Having introduced the Hubbard term on the f-sites, the FTQMC may be formulated. For a given temperature U_f has to be large enough so as to eliminate double occupancy on the f-sites and hence ensure projection onto the Q_0 subspace. At this point, it is very convenient to choose the $SU(2)$-invariant HS decomposition of Eq. (25) since one can take the limit $U_f \to \infty$ by setting $\alpha = \pi/2$. Hence irrespective of the considered temperature, we are guaranteed to be in the correct Hilbert space. Note that since the Hubbard U_f term commutes with the Hamiltonian of Eq. (133) no uncontrolled Trotter error is involved in taking the limit $U_f \to \infty$.

It is beyond the scope of this review to describe the results obtained with the above algorithm for the Kondo Lattice model and the reader is referred to the Refs.[29,59,38].

4.4 Hard-Core Boson Systems and the Heisenberg Hamiltonian

The spin $1/2$ Heisenberg model is defined by the Hamiltonian

$$H = J \sum_{\langle \vec{i}, \vec{j} \rangle} \vec{S}_{\vec{i}} \vec{S}_{\vec{j}}, \tag{143}$$

where the spin operator, $\vec{S}_{\vec{i}} = (1/2) \sum_{\sigma, \sigma'} c_{\vec{i}, \sigma}^{\dagger} \vec{\sigma}_{\sigma, \sigma'} c_{\vec{i}, \sigma'}$ act on the states, $| \uparrow \rangle, | \downarrow \rangle$ and $\vec{\sigma}$ are the Pauli spin $1/2$ matrices. Defining the raising and lowering spin operators,

$$S_{\vec{i}}^{+} = S_{\vec{i}}^{x} + i S_{\vec{i}}^{y} \quad S_{\vec{i}}^{-} = S_{\vec{i}}^{x} - i S_{\vec{i}}^{y} \tag{144}$$

transforms the Heisenberg model to:

$$H = J \sum_{\langle \vec{i}, \vec{j} \rangle} \frac{1}{2} \left(S_{\vec{i}}^{+} S_{\vec{j}}^{-} + S_{\vec{i}}^{-} S_{\vec{j}}^{+} \right) + S_{\vec{i}}^{z} S_{\vec{j}}^{z}. \tag{145}$$

The raising and lowering operators satisfy the commutation relations:

$$\left[S_{\vec{i}}^{+}, S_{\vec{j}}^{-} \right] = \delta_{\vec{i}, \vec{j}} 2 S_{\vec{i}}^{z}. \tag{146}$$

The mapping onto hard core bosons follows from the identification

$$| \uparrow \rangle \to |1\rangle, \quad | \downarrow \rangle \to |0\rangle \tag{147}$$

Hard core boson operators, $b^{\dagger}$ acting on the states $|1\rangle$ and $|0\rangle$ satisfy the commutation rules:

$$\left[b_{\vec{i}}^{\dagger}, b_{\vec{j}} \right] = \delta_{\vec{i}, \vec{j}} 2 \left(b_{\vec{i}}^{\dagger} b_{\vec{i}} - \frac{1}{2} \right) \tag{148}$$

which follows from the usual bosonic commutation rules with constraint of no double occupancy: $b_{\vec{i}}^{\dagger} b_{\vec{i}}^{\dagger} = 0$. The identification of states (147) leads to:

$$S_{\vec{i}}^{+} \to b_{\vec{i}}^{\dagger}, \ S_{\vec{i}}^{-} \to b_{\vec{i}}, \text{ and } S_{\vec{i}}^{z} \to \left(b_{\vec{i}}^{\dagger} b_{\vec{i}} - \frac{1}{2} \right). \tag{149}$$

Since both the S and b operators satisfy identical commutation rules on their respective Hilbert spaces (Eqn. (146) and (148)), the Heisenberg model may be written in it's hard core boson form:

$$H = J \sum_{\langle \vec{i}, \vec{j} \rangle} \frac{1}{2} \left(b_{\vec{i}}^{\dagger} b_{\vec{j}} + b_{\vec{j}}^{\dagger} b_{\vec{i}} \right) + \left(b_{\vec{i}}^{\dagger} b_{\vec{i}} - \frac{1}{2} \right) \left(b_{\vec{j}}^{\dagger} b_{\vec{j}} - \frac{1}{2} \right) \tag{150}$$

To carry out simulations of hard core boson Hamiltonians such as the Heisenberg model within the framework of the FTQMC of PQMC, we have to explicitly build the hard core bosons from fermions ($b_{\vec{i}}^{\dagger} = c_{\vec{i},\uparrow}^{\dagger} c_{\vec{i},\downarrow}^{\dagger}$) and restrict the Hilbert space to doubly or empty occupied sites in terms of fermions. One can achieve this goal by considering the Hamiltonian

$$H = -t \sum_{\langle i,j \rangle} \left(\sum_{\sigma} c_{\vec{i},\sigma}^{\dagger} c_{\vec{j},\sigma} + H.c. \right)^2 - V \sum_{\langle i,j \rangle} \left(n_{\vec{i}} \pm n_{\vec{j}} \right)^2$$
$$-U \sum_{i} n_{\vec{i},\uparrow} n_{\vec{i},\downarrow}. \tag{151}$$

Here, $n_{\vec{i}} = n_{\vec{i},\uparrow} + n_{\vec{i},\downarrow}$ and $n_{\vec{i},\sigma} = c_{\vec{i},\sigma}^{\dagger} c_{\vec{i},\sigma}$. At first glance, we can see that for $t, U, V > 0$ and with the use of the HS transformations (25),(28), the sign is absent since the weight for a given configuration of HS fields is a product of two identical real determinants.

To see how the above Hamiltonian relates to that of hard core boson systems, we expand the squares to obtain (up to a chemical potential term):

$$H = -2t \sum_{\langle i,j \rangle} \left(c_{\vec{i},\uparrow}^{\dagger} c_{\vec{i},\downarrow}^{\dagger} c_{\vec{j},\downarrow} c_{\vec{j},\uparrow} + H.c. \right) + (t \mp 2V) \sum_{\langle i,j \rangle} n_{\vec{i}} n_{\vec{j}}$$
$$+4t \sum_{\langle i,j \rangle} \vec{S}_{\vec{i}} \vec{S}_{\vec{j}} - (U + 8V) \sum_{i} n_{\vec{i},\uparrow} n_{\vec{i},\downarrow}. \tag{152}$$

As apparent, the Hamiltonian conserves the number of singly occupied sites. That is, the operator

$$P = \sum_{\vec{i}} n_{\vec{i}} (2 - n_{\vec{i}}). \tag{153}$$

which counts the singly occupied sites is a conserved quantity:

$$[P, H] = 0. \tag{154}$$

In particular, if one projects onto the subspace with $P = 0$ (P_0) then in this subspace the spin-spin term as well as the Hubbard interaction vanish:

$$HP_0 = -2t \sum_{\langle i,j \rangle} \left(c_{\vec{i},\uparrow}^{\dagger} c_{\vec{i},\downarrow}^{\dagger} c_{\vec{j},\downarrow} c_{\vec{j},\uparrow} + H.c. \right)$$
$$+(t \mp 2V) \sum_{\langle i,j \rangle} n_{\vec{i}} n_{\vec{j}} - 3(t + V) \sum_{\vec{i}} n_{\vec{i}} \tag{155}$$

To enforce this constraint (i.e. projection on the P_0 subspace on the imaginary time propagation) within the PQMC one just has to appropriately choose the trial wave function:

$$P_0 | \Psi_T \rangle = | \Psi_T \rangle \tag{156}$$

A possible choice is:

$$| \Psi_T \rangle = | \Psi_T^{\uparrow} \rangle \otimes | \Psi_T^{\downarrow} \rangle, \quad | \Psi_T^{\sigma} \rangle = \prod_{n=1}^{N_p^{\sigma}} c_{\vec{i}_n,\sigma}^{\dagger} | 0 \rangle \tag{157}$$
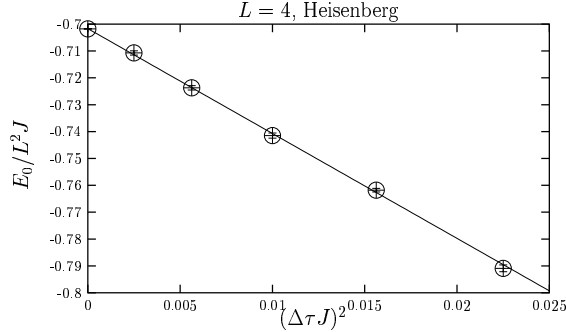
Figure 15. Ground state energy of the Heisenberg model on a 4×4 lattice as a function of the imaginary time discretization $\Delta\tau$. The data point at $\Delta\tau = 0$ corresponds to the exact result for this lattice size.

where $N_p^\uparrow = N_p^\downarrow$ corresponds to the number of electrons in the spin σ sector. Alternatively and in analogy to the Kondo lattice model, the constraint may be imposed with the attractive U term. The inclusion of this term allows the use of the FTQMC.

In the P_0 subspace

$$b_{\vec{i}}^\dagger = c_{\vec{i},\uparrow}^\dagger c_{\vec{i},\downarrow}^\dagger \text{ and } n_i = 2 b_{\vec{i}}^\dagger b_{\vec{i}}. \tag{158}$$

where $b_{\vec{i}}^\dagger$ are the desired hard-core bosons. Thus,

$$HP_0 = -2t \sum_{\langle i,j \rangle} \left(b_{\vec{i}}^\dagger b_{\vec{j}} + H.c. \right) + 4(t \mp 2V) \sum_{\langle i,j \rangle} b_{\vec{i}}^\dagger b_{\vec{i}} b_{\vec{j}}^\dagger b_{\vec{j}}$$
$$-6(t+V) \sum_{\vec{i}} b_{\vec{i}}^\dagger b_{\vec{i}} \tag{159}$$

which is nothing but a model of hard core bosons with nearest neighbor density-density interaction of arbitrary sign.

We can test the method at the Heisenberg point: $V = 0$. (The explicit mapping, up to a chemical potential term, to Eq. (150) is achieved after the canonical transformation: $b_{\vec{i}}^\dagger \to (-1)^{i_x+i_y} b_{\vec{i}}^\dagger$.) Fig. 15 plots the ground state energy as a function of $\Delta\tau$. As apparent, the QMC converges to the exact result. In this formulation, frustrating interactions would amount in inserting terms of the form $t \left(c_{\vec{i}}^\dagger c_{\vec{j}} + \text{H.c.} \right)^2$ for $\vec{i}, \vec{j}$ within the same sublattice and with $t > 0$. The reader will easily convince himself that this leads to a sign problem. Finally we note that the use of the auxiliary field QMC for non-frustrated Heisenberg models should be seen as an amusing curiosity since it is not competitive with the loop algorithm approach.

5 The Hirsch-Fye Impurity Algorithm

A very much related algorithm to the FTQMC and PQMC is the Hirsch-Fye impurity algorithm[60] which is extensively used in the framework of dynamical mean field theories[15,16]. As it's name suggests, this algorithm is triggered at solving impurity problems and allows

simulations directly in the *thermodynamic* limit. However as will be apparent below the CPU time scales as the third power of the inverse temperature β. For simplicity we will consider the single impurity Anderson model for the formulation of the problem and the Kondo model for the example applications.

The Anderson impurity model reads:

$$H = \overbrace{\sum_{\vec{k},\sigma} \epsilon(\vec{k}) c^{\dagger}_{\vec{k},\sigma} c_{\vec{k},\sigma} + V \sum_{\vec{k},\sigma} c^{\dagger}_{\vec{k},\sigma} f_{\sigma} + f^{\dagger}_{\sigma} c_{\vec{k},\sigma} + \epsilon_f \sum_{\sigma} f^{\dagger}_{\sigma} f_{\sigma}}^{\equiv H_0}$$
$$+ U \left(f^{\dagger}_{\uparrow} f_{\uparrow} - 1/2 \right) \left(f^{\dagger}_{\downarrow} f_{\downarrow} - 1/2 \right). \tag{160}$$

Following the procedure introduced for the Hubbard model, the partition function is given by:

$$Z \equiv \text{Tr} \left[e^{-\beta(H-\mu N)} \right] = \sum_{\vec{s}} \left[\prod_{\sigma} \det \left[1 + B^{\sigma}_m B^{\sigma}_{m-1} \cdots B^{\sigma}_1 \right] \right]. \tag{161}$$

With the notation

$$H_0 = \sum_{\sigma,\vec{i}} a^{\dagger}_{\vec{i},\sigma} (h_0)_{\vec{i},\vec{j}} a_{\vec{j},\sigma} \tag{162}$$

where $a_{\vec{j},\sigma}$ denotes c- of f-operators, $\vec{i}, \vec{j}$ running over all orbitals, and the HS transformation of Eq. (24),

$$B^{\sigma}_n = e^{-\Delta\tau h_0} e^{V^{\sigma}_n}$$
$$(V^{\sigma}_n)_{i,j} = \delta_{i,j} \begin{cases} 0 & \text{if } \vec{i} \neq \text{impurity site} \\ \tilde{\alpha}\sigma s_n & \text{if } \vec{i} = \text{impurity site} \end{cases} \tag{163}$$

Note that since we are considering a single impurity, we require only a single Hubbard Stratonovich field per time slice, s_n. Finally, $m\Delta\tau = \beta$.

The determinant in a given spin sector may be written as

$$\det \left[1 + B^{\sigma}_m B^{\sigma}_{m-1} \cdots B^{\sigma}_1 \right] = \det O^{\sigma} \quad \text{with} \tag{164}$$

$$O^{\sigma} = \begin{pmatrix} 1 & 0 & . & . & 0 & B^{\sigma}_1 \\ -B^{\sigma}_2 & 1 & 0 & . & . & 0 \\ 0 & -B^{\sigma}_3 & 1 & . & . & 0 \\ . & 0 & -B^{\sigma}_4 & . & . & . \\ . & . & 0 & . & . & . \\ . & . & . & . & . & . \\ 0 & . & . & 0 & -B^{\sigma}_m & 1 \end{pmatrix}. \tag{165}$$

From Eq. (84) we identify:

$$(O^{\sigma})^{-1} \equiv g^{\sigma} = \begin{pmatrix} G^{\sigma}(1,1) & G^{\sigma}(1,2) & .. & G^{\sigma}(1,m) \\ G^{\sigma}(2,1) & G^{\sigma}(2,2) & .. & G^{\sigma}(2,m) \\ . & . & .. & . \\ G^{\sigma}(m,1) & G^{\sigma}(m,2) & .. & G^{\sigma}(m,m) \end{pmatrix} \tag{166}$$

where $G^\sigma(n_1, n_2)$ are the time displaced Green functions as defined in Eqn. (81) and (82). Given a HS configuration $\vec{s}$ and $\vec{s}'$ and associated matrices V and V' the Green functions g and g' satisfy the following Dyson equation.

$$g' = g + (g - 1)(e^{V' - V} - 1)g' \tag{167}$$

To demonstrate the above, we consider

$$\tilde{O}^\sigma = O^\sigma e^{-V^\sigma} = \begin{pmatrix} e^{-V_1^\sigma} & 0 & . & . & 0 & e^{-\Delta\tau h_0} \\ e^{-\Delta\tau h_0} & e^{-V_2^\sigma} & 0 & . & . & 0 \\ 0 & e^{-\Delta\tau h_0} & e^{-V_3^\sigma} & . & . & 0 \\ . & 0 & e^{-\Delta\tau h_0} & . & . & . \\ . & . & 0 & . & . & . \\ . & . & . & . & . & . \\ 0 & . & . & 0 & e^{-\Delta\tau h_0} & e^{-V_m^\sigma} \end{pmatrix} \tag{168}$$

so that (omitting the spin index σ)

$$\tilde{g}' \equiv \tilde{O}'^{-1} = [\tilde{O} + \underbrace{\tilde{O}' - \tilde{O}}_{\equiv e^{-V'} - e^{-V}}]^{-1} = \tilde{g} - \tilde{g}\left(e^{-V'} - e^{-V}\right)\tilde{g}'. \tag{169}$$

Substitution, $\tilde{g} = e^V g$, leads to the Dyson Eq. (167).

The Green function matrix has dimensions $mN \times mN$ where N is the total number of orbitals and m the number of Trotter slices. Let $x = (\tau_x, i_x)$ with Trotter slice τ_x and orbital i_x, and the site index of the impurity to 0. Since

$$(e^{V' - V} - 1)_{x,y} = (e^{V' - V} - 1)_{x,x}\delta_{x,y}\delta_{i_x,0} \tag{170}$$

we can use the Dyson equation only for the impurity Green function:

$$g'_{f,f'} = g_{f,f'} + \sum_{f''}(g - 1)_{f,f''}(e^{V' - V} - 1)_{f'',f''}g'_{f'',f'} \tag{171}$$

with indices $f \equiv (\tau, 0)$ running from $1 \cdots m$.

We now have all the ingredients to carry out a simulation. (Note that the algorithm is free of numerical instabilities.) Let us start from a random HS configuration $\vec{s}'$. For this configuration, we have to compute the impurity Green function. From the $U = 0$ solution, g_0^f (which can be obtained analytically[61]), we compute the impurity Green function for the HS fields $\vec{s}'$ with the use of Eq. (171). This is readily achieved at the cost of an $m \times m$ matrix inversion.

To upgrade a single HS field with the Metropolis method, we have to calculate the ratio of the determinants (see Eq. (161)) as shown in section 3.3. This ratio only requires the knowledge of the equal time impurity Green function which is already at hand. If the proposed spin-flip is accepted the impurity Green function may readily be upgraded with the use of Eq. (171). Note that since we are considering a single spin flip, sum over f'' in Eq. (171) has only one non-vanishing contribution.

The attractive feature of the Hirsch-Fye impurity algorithm is that the conduction electrons may be considered directly in the thermodynamic limit. This is not be possible within the previously discussed FTQMC since the dimension of the matrices involved scale as the total number of orbitals. The Hirsch-Fye algorithm is not limited to impurity models. However, when applied to lattice models it is less efficient than the FTQMC and PQMC.
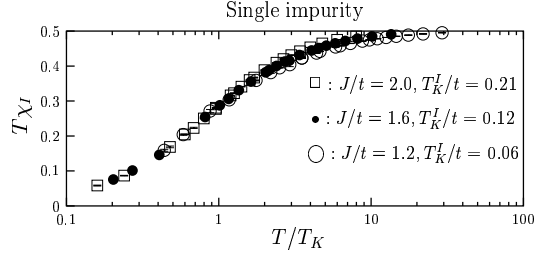
Figure 16. Impurity spin susceptibility of the Kondo model as computed with the Hirsch-Fye impurity algorithm.[38]

The Hirsch-Fye impurity algorithm may equally be applied to the Kondo model,

$$H = \sum_{\vec{k},\sigma} \varepsilon(\vec{k}) c^{\dagger}_{\vec{k},\sigma} c_{\vec{k},\sigma} + J \vec{S}^c_{\vec{I}} \cdot \vec{S}^f_{\vec{I}} \tag{172}$$

where the same formulation as for the lattice problem is used. Fig. 16 plots the impurity spin susceptibility

$$\chi_I = \int_0^\beta \langle \vec{S}^f_{\vec{I}}(\tau) \cdot \vec{S}^f_{\vec{I}} \rangle \tag{173}$$

for various values of J/t for a half-filled conduction band. As apparent and at low energies the data collapse to the universal form $\chi_I = \frac{1}{T} f\left(T/T_K^I\right)$ where T_K^I is the Kondo temperature.

6 Conclusion

We have presented in all details the auxiliary field (or determinantal) Quantum Monte Carlo method for lattice problems. The ground state, finite temperature as well as Hirsch-Fye impurity algorithms were considered. The formulation of these algorithms for a range of fermionic as well as bosonic models was discussed. When the sign problem is avoidable the computational effort scales as the volume to the cubed times inverse temperature. For the Hirsch-Fye impurity algorithm – formulated directly in the thermodynamic limit – the computational cost scales as the cubed of the inverse temperature. The algorithms produce thermodynamic, dynamical -in conjunction with the Maximum Entropy method- as well as ground state properties of the model under consideration. They are unique in the sense that the sign problem turns out to be avoidable for particle-hole symmetric models as well as for models with attractive interactions which couple independently to an internal symmetry with an even number of states. It is not clear at present if other symmetries may be put to use so as to avoid the sign problem. Clearly, the sign problem remains the central issue and calls for new numerical approaches to the correlated electron problem.

147

Appendix

A The Monte Carlo Method

In this appendix, we briefly outline the Monte Carlo method. Our aim is to compute:

$$\langle O \rangle_P = \int_\Omega d\vec{x} P(\vec{x}) O(\vec{x}) \tag{174}$$

where Ω denotes the integration space, and $P(\vec{x})$ is a probability distribution,

$$\int_\Omega d\vec{x} P(\vec{x}) = 1 \ \ \text{and} \ \ P(\vec{x}) \geq 0 \ \ \forall \ \ \vec{x}\epsilon\Omega. \tag{175}$$

For simplicity, we will assume Ω to be a subspace of $\mathcal{R}^d$ with volume V. Here, d is the dimension. In practice, one does not have access to P, but to the unnormalized probability distribution $g(\vec{x})$ which satisfies

$$P(\vec{x}) = \frac{g(\vec{x})}{Z}, \ \ Z = \int_\Omega d\vec{x} g(\vec{x}). \tag{176}$$

In the terminology of statistical mechanics, $g(\vec{x})$ corresponds to the Boltzmann weight and Z to the partition function. Hence the evaluation of Eq. (174) boils down to the calculating the quotient of two integrals. One may break up Ω into hypercubes of linear dimension h and approximate the integrals by sums. Depending upon the method used the systematic error will be proportional to h^k. The required number of function evaluations N is of the order V/h^d so that the systematic error scales a $N^{-k/d}$. Clearly, when d is large poor results are obtained. As we will now see, in the large d limit, the Monte Carlo method becomes attractive.

A.1 The Central Limit Theorem

Suppose that we have a set of independent points $\{\vec{x}_i\}$, $i : 1 \cdots N$ distributed according to the probability distribution $P(\vec{x})$ we can approximate $\langle O \rangle_P$ by:

$$\langle O \rangle_P \sim \frac{1}{N} \sum_{\substack{i=1 \\ \vec{x}_i \epsilon P}}^{N} O(\vec{x}_i) = X. \tag{177}$$

Clearly, X will depend upon the chosen series of $\{\vec{x}_i\}$. The central limit theorem, tells us that in the large N limit the probability of obtaining a given value of X, $\mathcal{P}(X)$ reads

$$\mathcal{P}(X) = \frac{1}{\sqrt{2\pi}} \frac{1}{\sigma} \exp\left[-\frac{(X - \langle O \rangle_P)^2}{2\sigma^2} \right] \ \ \text{with} \ \ \sigma^2 = \frac{1}{N} \left(\langle O^2 \rangle_P - \langle O \rangle_P^2 \right). \tag{178}$$

Thus independently of the dimension d, the convergence to the exact result scales as $1/\sqrt{N}$. The width of the above normal distribution, σ, corresponds to the statistical error. For practical purposes, one estimates σ by

$$\sigma^2 \approx \frac{1}{N} \left(\frac{1}{N} \sum_{\substack{i=1 \\ \vec{x}_i \epsilon P}} O(\vec{x}_i)^2 - \left(\frac{1}{N} \sum_{\substack{i=1 \\ \vec{x}_i \epsilon P}} O(\vec{x}_i) \right)^2 \right) \tag{179}$$
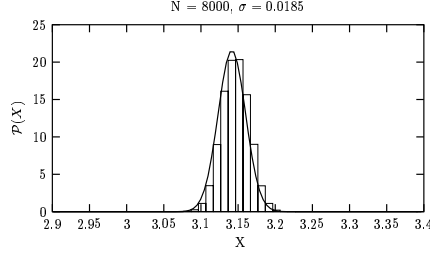
Figure 17. Boxes correspond to the distribution results obtained after 10000 simulations. For each simulation we draw $N = 8000$ points. For a single simulation, we obtain $\sigma = 0.0185$. The solid line corresponds to the result of central limit theorem with above value of σ.

Instead of demonstrating the central limit theorem, we give a simple example: the evaluation of the number π obtained via:

$$\pi = 4 \int_0^1 \mathrm{d}x \int_0^1 \mathrm{d}y \Theta(1 - x^2 + y^2), \tag{180}$$

where Θ is the Heavyside function, $\Theta(x) = 1$ for $x > 0$ and vanishes otherwise. In this example we $P(x, y) \equiv 1$. To generate the a sequence of N points $(x, y)_i$ from this probability distribution, we draw random numbers, x, y, in the interval $[0, 1]$. For $N = 8000$ we obtain an error $\sigma = 0.0185$ with the use of Eq. (179). To check the central limit theorem, we repeat the simulation 10000 times with different random numbers. Fig. (17) shows the thus obtained distribution which compares well to the result of the central limit theorem.

The jackknife and bootstrap methods[62] provide alternative ways of estimating the error (179). These methods become particularly useful, if not essential, when one wishes to estimate the error on $f(\langle O_1 \rangle, \cdots, \langle O_1 \rangle)$ where f is an arbitrary function of n variables. For a given sequence $\vec{x}_i \epsilon P(\vec{x})$, $i : 1 \cdots N$, the jackknife focuses on the samples that leaves out one configuration at a time:

$$f_i^J = f\left(\frac{1}{N-1} \sum_{j \neq i} O_1(\vec{x_j}), \cdots, \frac{1}{N-1} \sum_{j \neq i} O_n(\vec{x_j}) \right). \tag{181}$$

The error estimate on f is then given by:

$$\left(\sigma_f^J\right)^2 \approx N \left(\frac{1}{N} \sum_{i=1}^N (f_i^J)^2 - \left(\frac{1}{N} \sum_{i=1}^N f_i^J \right)^2 \right) \tag{182}$$

One may verify explicitly that for $n = 1$ and $f(x) = x$ Eq. (182) reduces to Eq. (179) up to a factor $(N/(N-1))^2$ which tends to unity in the large N limit.

An alternative method for determining errors of f is the bootstrap algorithm. For a given sample of N configurations $\{\vec{x}_1 \cdots \vec{x}_N\}$ drawn from the probability distribution $P(\vec{x})$, we can construct N^N sets of N configurations, $\{\vec{x}_{i_1} \cdots \vec{x}_{i_N}\}$ with $i_1 : 1 \cdots N$, $i_2 : 1 \cdots N, \cdots, i_N : 1 \cdots N$, which correspond to the ideal bootstrap samples. For a

given bootstrap sample, defined by the vector $\vec{i} = (i_1, \cdots, i_N)$,

$$f_{\vec{i}}^B = f\left(\frac{1}{N}\sum_{k=1}^N O_1(\vec{x}_{i_k}), \cdots, \frac{1}{N}\sum_{k=1}^N O_n(\vec{x}_{i_k})\right). \tag{183}$$

The bootstrap estimate of the error is given by:

$$\left(\sigma_f^B\right)^2 \approx \frac{1}{N^N}\sum_{i_1,\cdots 1_N=1}^N (f_{\vec{i}}^B)^2 - \left(\frac{1}{N^N}\sum_{i_1,\cdots,i_N=1}^N f_{\vec{i}}^B\right)^2. \tag{184}$$

Again, one may check that for the special case, $n = 1$ and $f(x) = x$ Eq. (184) reduces to Eq. (179). Clearly, when N is large, it is numerically out of reach to generate all of the N^N bootstrap samples. Typically, to estimate the right hand side of Eq. (184) 200 or more bootstrap samples are generated stochastically. Since each bootstrap sample is equally probable we can generate them with: $i_k = \mathrm{trunc}\,(N * \xi_k + 1)$ where ξ_k is a random number in the interval $[0, 1]$ and the function trunc returns an integer by truncating the numbers after the decimal point.

A.2   Generating Markov Chains

Our task is now to generate a set of points $\vec{x}$ distributed according to $P(x)$. We introduce a Monte-Carlo time t, and a time dependent probability distribution $P_t(\vec{x})$ which evolves in time according to a Markov process: the future $(t + 1)$ depends only on the present (t). Our aim is to obtain: $P_{t\to\infty}(\vec{x}) = P(\vec{x})$. To define the Markov chain, we introduce a matrix $T_{\vec{y},\vec{x}}$ which corresponds to the probability of going from $\vec{x}$ to $\vec{y}$. The time evolution of $P_t(\vec{x})$ is given by:

$$P_{t+1}(\vec{y}) = \sum_x T_{\vec{y},\vec{x}} P_t(\vec{x}) \tag{185}$$

T has to satisfy the following properties.

$$\sum_x T_{\vec{y},\vec{x}} = \sum_y T_{\vec{y},\vec{x}} = 1, \;\; T_{\vec{y},\vec{x}} \geq 0 \tag{186}$$

That is, the probability of reaching a given $\vec{y}$ from any $\vec{x}$ or of landing anywhere in Ω given a initial $\vec{x}$ is of unit. T has to be ergodic:

$$\forall \vec{x}, \vec{y} \epsilon \Omega \exists s | \left(T^s\right)_{\vec{y},\vec{x}} > 0. \tag{187}$$

Thus, we are assured to sample the whole phase space provided the above is satisfied. Lastly, the requirement of stationarity:

$$\sum_{\vec{x}} T_{\vec{y},\vec{x}} P(\vec{x}) = P(\vec{y}). \tag{188}$$

Once we have reached the desired distribution, $P(\vec{x})$, we wish to to stay there. Stationarity is automatically satisfied if

$$T_{\vec{y},\vec{x}} P(\vec{x}) = T_{\vec{x},\vec{y}} P(\vec{y}) \tag{189}$$

as may be seen by summing on sides over $\vec{y}$ or $\vec{x}$. This relation is referred to as detailed balance or microreversibility. However, one has to keep in mind that stationarity and not detailed balance is essential.

That $P_t(\vec{x})$ approaches the equilibrium distribution $P(\vec{x})$ may be seen with:

$$
\begin{aligned}
||P_{t+1} - P|| &\equiv \sum_{\vec{y}} |P_{t+1}(\vec{y}) - P(\vec{y})| \\
&= \sum_{\vec{y}} |\sum_{\vec{y}} T_{\vec{y},\vec{x}} P_t(\vec{x}) - \sum_{\vec{x}} T_{\vec{y},\vec{x}} P(\vec{x})| \\
&\leq \sum_{\vec{y}} \sum_{\vec{x}} T_{\vec{y},\vec{x}} |P_t(\vec{x}) - P(\vec{x})| \\
&= \sum_{\vec{x}} |P_t(\vec{x}) - P(\vec{x})| \equiv ||P_t - P||.
\end{aligned}
\tag{190}
$$

Under the assumption of ergodicity, the strict equality holds only when $P_t = P$. Due to Eq. (186), the right eigenvectors of T have eigenvalues $|\lambda| \leq 1$, $\lambda = 1$ corresponding to the stationary distribution P. Starting with an arbitrary distribution $P_0(\vec{x})$ convergence to P will be determined by the eigenvalue of T with second largest absolute value, λ_1. The rate of convergence of $P_t(\vec{x})$ to $P(\vec{x})$ will then scale as $\exp -t/\tau$ where $\tau = -1/\log(|\lambda_1|) > 0$.

Having defined T, we now have to construct it explicitly. Let $T_{\vec{y},\vec{x}}^0$ the probability of proposing a move from $\vec{x}$ to $\vec{y}$ and $a_{\vec{y},\vec{x}}$ the probability of accepting it. $1 - a_{\vec{y},\vec{x}}$ corresponds to the probability of rejecting the move. T_0 is required to satisfy Eq. (186). Since in general we want to propose moves which change the initial configuration, $T_{x,x}^0 = 0$. With $a_{\vec{y},\vec{x}}$ and $T_{\vec{y},\vec{x}}^0$ we build $T_{\vec{y},\vec{x}}$ with:

$$
T_{\vec{y},\vec{x}} = \begin{cases} T_{\vec{y},\vec{x}}^0 a_{\vec{y},\vec{x}} & \text{if } \vec{y} \neq \vec{x} \\ \sum_{\vec{y} \neq \vec{x}} T_{\vec{y},\vec{x}}^0 (1 - a_{\vec{y},\vec{x}}) & \text{if } \vec{y} = \vec{x} \end{cases}
\tag{191}
$$

Clearly $T_{\vec{y},\vec{x}}$ satisfies Eq. (186). To satisfy the stationarity, we impose the detailed balance condition to obtain the equality:

$$
T_{\vec{y},\vec{x}}^0 a_{\vec{y},\vec{x}} P_{\vec{x}} = T_{\vec{x},\vec{y}}^0 a_{\vec{x},\vec{y}} P_{\vec{y}}.
\tag{192}
$$

Let us set:

$$
a_{\vec{y},\vec{x}} = \mathcal{F}(Z) \quad \text{with } Z = \frac{T_{\vec{x},\vec{y}}^0 P_{\vec{y}}}{T_{\vec{y},\vec{x}}^0 P_{\vec{x}}}
\tag{193}
$$

with $\mathcal{F}(Z) :]0 : \infty[\rightarrow [0,1]$. Since $a_{\vec{x},\vec{y}} = \mathcal{F}(1/Z)$, $\mathcal{F}$ has to satisfy:

$$
\frac{\mathcal{F}(Z)}{\mathcal{F}(1/Z)} = Z.
\tag{194}
$$

There are many possible choices. The Metropolis algorithm is based on the choice:

$$
\mathcal{F}(Z) = \min(Z, 1).
\tag{195}
$$

Thus, one proposes a move from $\vec{x}$ to $\vec{y}$ and accepts it with probability $Z = \frac{T_{\vec{x},\vec{y}}^0 P_{\vec{y}}}{T_{\vec{y},\vec{x}}^0 P_{\vec{x}}}$. In the practical implementation, one picks a random number r in the interval $[0 : 1]$. If $r < Z$

$(r > Z)$ one accepts (rejects) the move. Alternative choices of $\mathcal{F}(Z)$ are for example:

$$\mathcal{F}(Z) = \frac{Z}{1+Z} \tag{196}$$

which is referred to as the Heat bath method.

That the so constructed T matrix is ergodic depends upon the choice of T^0. In many cases, one will wish to combine different types of moves to achieve ergodicity. For a specific move, i we construct $T^{(i)}$ as shown above so that $T^{(i)}$ conditions (186) and (189). The moves may be combined in two ways:

$$T = \sum_i \lambda_i T^{(i)}, \quad \sum_i \lambda_i = 1 \tag{197}$$

which is referred to as random upgrading since one picks with probability λ_i the move $T^{(i)}$. Clearly, T equally satisfies (186), (189) and if the moves have to be chosen appropriately to satisfy the ergodicity condition. Another choice is sequential upgrading. A deterministic ordering of the moves is chosen to obtain:

$$T = \prod_i T^{(i)}. \tag{198}$$

This choice does not satisfy detailed balance condition, but does satisfy stationarity (188) as well as (186). Again ergodicity has to be *checked* on a case to case basis.

In principle, we could now start with an arbitrary probability distribution $P_0(\vec{x})$ and propagate it along Monte Carlo time t ($P_{t+1} = TP_t$). Convergence to the equilibrium distribution will occur on time scales set by τ. This procedure involves handling many configurations $\vec{x}$ at a given time t. Alternatively one can start with a single configuration $\vec{x}$ and propagate it according to T. That is the probability of having the configuration $\vec{y}$ at the next MC time is given by $T_{\vec{y},\vec{x}}$. This procedure generates a sequence of configuration in MC time. For *large* values of N (see below) $\vec{x}_{t=1} \cdots \vec{x}_{t=N}$ will be distributed according to P. The observable O may now be estimated with:

$$\langle O \rangle_P \approx \frac{1}{N} \sum_{t=1}^N O(\vec{x}_t). \tag{199}$$

The required value of N depends autocorrelation time of the observable O:

$$C_O(t) = \frac{\frac{1}{N}\sum_{s=1}^N O(\vec{x}_s)O(\vec{x}_{s+t}) - \left(\frac{1}{N}\sum_{s=1}^N O(\vec{x}_s)\right)^2}{\frac{1}{N}\sum_{s=1}^N O(\vec{x}_s)^2 - \left(\frac{1}{N}\sum_{s=1}^N O(\vec{x}_s)\right)^2} \tag{200}$$

One expects $C_O(t) \sim e^{-t/\tau_O}$ where τ_O corresponds to the MC time scale on which memory of the initial configuration is lost. Hence, to obtain meaningful results, $N >> \tau_O$. Note that one should equally take into account a *warm up* time by discarding at least the first τ_O configurations in the MC sequence. Naively, one would expect $\tau_O = \tau$. However, this depends on the overlap of the observable with the slowest mode in the MC dynamics which relaxes as $e^{-t/\tau}$. In particular in a model with spin rotation symmetry the slowest mode may correspond to the rotation of the total spin. In this case, observables which are invariant under a spin rotation will not be effected by the slowest mode of the MC dynamics. Hence in this case $\tau_O < \tau$.

We now consider the estimation of the error. To apply the central limit theorem, we need a set of independent estimates of $\langle O \rangle_P$. This may be done by regrouping the data into *bins* of size $n\tau_O$.

$$\tilde{O}_n(t) = \frac{1}{n\tau_O} \sum_{s=1}^{n\tau_O} O(\vec{x}_{(t-1)n\tau_O+s}) \tag{201}$$

with $t = 1 \cdots N/(n\tau_O)$. If n is large enough (i.e. $n \approx 10 - 20$) then $\tilde{O}_n(t)$ may be considered as an independent estimate, and the error is given by:

$$\sigma_n = \sqrt{\frac{1}{M}\left(\frac{1}{M}\sum_{t=1}^{M}\tilde{O}_n(t)^2 - \left(\frac{1}{M}\sum_{i=1}^{M}\tilde{O}_n(t)\right)^2\right)} \tag{202}$$

where $M = N/(n\tau_O)$. If n is large enough the error σ_n should be n independent.

We conclude this section with an example of error analysis for the one-dimensional Ising model:

$$H(\{\sigma\}) = -J \sum_{i=1}^{L} \sigma_i \sigma_{i+1} \quad \sigma_{L+1} = \sigma i \tag{203}$$

where $\sigma_i = \pm 1$. This model may easily be solved exactly with the transfer matrix method and thus produces a useful testing ground for the MC approach. In particular at zero temperature, $T = 0$, a phase transition to a ferromagnetically ordered phase ($J > 0$) occurs[7]. Spin-spin correlations are given by:

$$g(r) = \frac{1}{L}\sum_{i=1}^{L}\langle\sigma_i\sigma_{i+r}\rangle \text{ with } \langle\sigma_i\sigma_{i+r}\rangle = \frac{\sum_{\{\sigma\}} e^{-\beta H(\{\sigma\})}\sigma_i\sigma_{i+r}}{\sum_{\{\sigma\}} e^{-\beta H(\{\sigma\})}} \tag{204}$$

where β corresponds to the inverse temperature. To simulate the model, we use a simple random site upgrading method: a site (i) is randomly chosen, and the spin is flipped ($\sigma_i \rightarrow -\sigma_i$) with the heat bath algorithm. The MC time unit corresponds to a single sweep meaning that L sites are randomly chosen before a measurement is carried out.
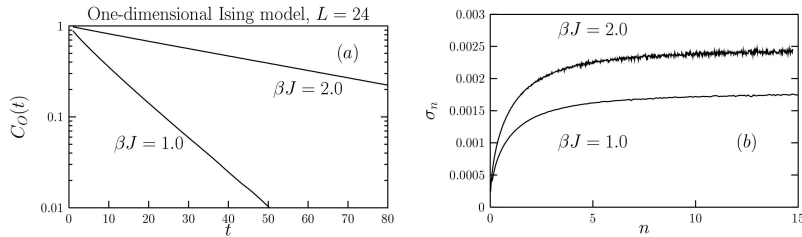

Figure 18. One dimensional Ising model on an L=24 site lattice. (a) Autocorrelation time (see Eq. (200)) for $g(r = L/2)$. The time unit is corresponds to a single sweep. (b) Estimate of the error (see Eq. (202)). Here, n corresponds to the size of the bins in units of the autocorrelation time. As apparent $n \sim 10$ is sufficient to obtain a reliable estimate of the error. After 2×10^6 sweeps, our results yield $g(r = L/2) = 0.076 \pm 0.0018$ and 0.909 ± 0.0025 for $\beta t = 1$ and 2 respectively. The exact result reads $g(r = L/2) = 0.0760$ and 0.9106 at $\beta t = 1$ and 2 respectively.

Fig. 18 plots the autocorrelation time for $g(r = L/2)$ on an $L = 24$ site lattice at $\beta J = 1$ and $\beta J = 2$. From Fig. 18a one can extract the autocorrelation time: $\tau_O \approx 11, 54$ for for $\beta J = 1, 2$ respectively. Fig. 18b plots the error as function of bin size in units of the τ_O (see Eq. (202)). As apparent, $n \approx 10$ is sufficient to get a reliable estimate of the error.

References

1. S. R. White. *Physics Reports*, 301:187, 1998.
2. H. G. Evertz, G. Lana, and M. Marcu. *Phys. Rev. Lett.*, 70:875, 1993.
3. R. Blankenbecler, D. J. Scalapino, and R. L. Sugar. *Phys. Rev. D*, 24:2278, 1981.
4. J. E. Hirsch, D. J. Scalapino, R. L. Sugar, and R. Blankenbecler. *Phys. Rev. B*, 26:5033, 1981.
5. M. Barma and B. S. Shastry. *Phys. Rev. B*, 18:3351, 1978.
6. F. F. Assaad and D. Würtz. *Phys. Rev. B*, 44:2681, 1991.
7. R. J. Baxter. *Exactly solved models in statistical mechanics*. Academic Press Limited, London, 1989.
8. M. Troyer, M. Imada, and K. Ueda. *J. Phys. Soc. Jpn.*, 66:2957, 1997.
9. J. E. Hirsch. *Phys. Rev. B*, 31:4403, 1985.
10. S. R. White, D. J. Scalapino, R. L. Sugar, E. Y. Loh, J. E. Gubernatis, and R. T. Scalettar. *Phys. Rev. B*, 40:506, 1989.
11. E. Loh and J. Gubernatis. In W. Hanke and Y. V. Kopaev, editors, *Modern Problems of Condensed Matter Physics*, volume 32, page 177. North Holland, Amsterdam, 1992.
12. G. Sugiyama and S.E. Koonin. *Anals of Phys.*, 168:1, 1986.
13. S. Sorella, S. Baroni, R. Car, and M. Parrinello. *Europhys. Lett.*, 8:663, 1989.
14. S. Sorella, E. Tosatti, S. Baroni, R. Car, and M. Parrinello. *Int. J. Mod. Phys. B*, 1:993, 1989.
15. M. Jarrell. *Phys. Rev. Lett.*, 69:168, 1992.
16. A. Georges, G. Kotliar, W. Krauth, and M. J. Rozenberg. *Rev. of. Mod. Phys.*, 68:13, 1996.
17. R. M. Fye. *Phys. Rev. B*, 33:6271, 1986.
18. B.B. Beard and U.J. Wiese. *Phys. Rev. Lett.*, 77:5130, 1996.
19. H. G. Evertz. The loop algorithm. *cond-mat/9707221*, 1997.
20. M. Brunner, F. F. Assaad, and A. Muramatsu. *Phys. Rev. B*, 62:12395, 2000.
21. M. Brunner, S. Capponi, F. F. Assaad, and A. Muramatsu. *Phys. Rev. B*, 63:R180511, 2001.
22. M. Troyer, F. F. Assaad, and D. Würtz. *Helv. Phys. Acta.*, 64:942, 1991.
23. J. E. Hirsch. *Phys. Rev. B*, 28:4059, 1983.
24. F. F. Assaad. In E. Krause and W. Jäger, editors, *High performance computing in science and engineering*, page 105. Springer, Berlin, 1998. [cond-mat/9806307].
25. F. F. Assaad, M. Imada, and D. J. Scalapino. *Phys. Rev. B*, 56:15001, 1997.
26. F. F. Assaad, M. Imada, and D. J. Scalapino. *Phys. Rev. Lett*, 77:4592, 1996.
27. W. H. Press, S. A. Teukolsky, W. T. Vetterling, and B. P. Flannery. *Numerical Recipes in C*. Cambridge University Press, Cambridge, 1992.
28. F. F. Assaad and M. Imada. *J. Phys. Soc. Jpn.*, 65:189, 1996.
29. F. F. Assaad. *Phys. Rev. Lett.*, 83:796, 1999.

30. M. Jarrell and J.E. Gubernatis. *Physics Reports*, 269:133, 1996.

31. W. von der Linden. *Applied Physics A*, 60:155, 1995.

32. J. E. Hirsch. *Phys. Rev. B*, 38:12023, 1988.

33. M. Feldbacher and F. F. Assaad. *Phys. Rev. B*, 63:73105, 2001.

34. S. Fahy and D. R. Hamann. *Phys. Rev. Lett.*, 65:3437, 1990.

35. S. Fahy and D. R. Hamann. *Phys. Rev. B*, 43:765, 1991.

36. S. Zhang, J. Carlson, and J. E. Gubernatis. *Phys. Rev. Lett.*, 74:3652, 1995.

37. S. Zhang, J. Carlson, and J. E. Gubernatis. *Phys. Rev. B*, 55:7464, 1997.

38. F. F. Assaad. Depleted kondo lattices: mean-field and Quantum Monte Carlo calculations. *cond-mat/0104126, to appear in Phys. Rev. B*.

39. E. Fradkin. *Field Theories of condensed matter systems*. Frontiers in Physics. Addison-Wesley Publishing Company, Redwood City, 1991.

40. D. Poilblanc. *Phys. Rev. B*, 44:9562, 1991.

41. C. Gross. *Z. Phys. B*, 86:359, 1992.

42. R. T. Scalettar, E. Y. Loh, J. E. Gubernatis, A. Moreo, S. R. White, D. J. Scalapino, and R. L. Sugar. *Phys. Rev. Lett.*, 62:1407, 1989.

43. F. F. Assaad, W. Hanke, and D. J. Scalapino. *Phys. Rev. B*, 50:12835, 1994.

44. N. Trivedi and M. Randeria. *Phys. Rev. Lett.*, 75:312, 1995.

45. W. Kohn. *Phys. Rev. A*, 133:171, 1964.

46. M. Imada, A. Fujimori, and Y. Tokura. *Rev. Mod. Phys.*, 70:1039, 1998.

47. S. Sorella and E. Tosatti. *Europhys. Lett.*, 19:699, 1992.

48. G. G. Batrouni and R. T. Scalettar. *Phys. Rev. B*, 42:2282, 1990.

49. N. Furukawa and M. Imada. *J. Phys. Soc. Jpn.*, 60:3669, 1991.

50. P. A. Lee, T. M. Rice, J. W. Serene, L. J. Sham, and J. W. Wilkins. *Comm. Condens. Matter Phys.*, 12:99, 1986.

51. G. Aeppli and Z. Fisk. *Comm. Condens Matter Phys.*, 16:155, 1992.

52. J. R. Schrieffer and P. A. Wolff. *Phys. Rev.*, 149:491, 1966.

53. H. Tsunetsugu, M. Sigrist, and K. Ueda. *Rev. Mod. Phys.*, 69:809, 1997.

54. M. Vekic, J. W. Cannon, D. J. Scalapino, R. T. Scalettar, and R. L. Sugar. *Phys. Rev. Lett.*, 74:2367, 1995.

55. R. M. Fye and D. J. Scalapino. *Phys. Rev. Lett.*, 65:3177, 1990.

56. R. M. Fye and D. J. Scalapino. *Phys. Rev. B*, 44:7486, 1991.

57. S. Q. Shen. *Phys. Rev. B*, 53:14252, 1996.

58. H. Tsunetsugu. *Phys. Rev. B*, 55:3042, 1997.

59. S. Capponi and F. F. Assaad. *Phs. Rev. B*, 63:155113, 2001.

60. J. E. Hirsch and R. M. Fye. *Phys. Rev. Lett.*, 56:2521, 1986.

61. A. C. Hewson. *The Kondo Problem to Heavy Fermions*. Cambridge Studies in Magnetism. Cambridge Universiy Press, Cambridge, 1997.

62. B. Efron. *The jackknife, the bootsrap and other resampling plans.* CBMS-NSF conference series in applied mathematics. J. W. Arrowsmith Ltd., Bristol, England, 1982.